12-2016

Characterization and Modeling of Bond-Loss Behavior in Pretensioned Concrete I-Girders

Behnam Naji
Clemson University, behnam.naji@gmail.com

CHARACTERIZATION AND MODELING OF BOND-LOSS BEHAVIOR IN PRETENSIONED CONCRETE I-GIRDERS

A Dissertation
Presented to
the Graduate School of
Clemson University

In Partial Fulfillment
of the Requirements for the Degree
Doctor of Philosophy
Civil Engineering

---

by
Behnam Naji
December 2016

Accepted by:
Dr. Brandon E. Ross, Committee Chair
Dr. Thomas E. Cousins
Dr. Amin Khademi
Dr. Bryant G. Nielson

ABSTRACT

Bond-loss failures have been widely observed in load tests of precast-pretensioned concrete I-girders. This type of failure is associated with shear cracking near the support that interrupts anchorage of the strands, leading to loss of bond and slipping of the strands relative to the concrete. It has been experimentally demonstrated that this failure type can occur at load levels that are lower than the nominal shear and flexural capacities. Because bond loss can be the controlling factor for structural capacity, it is critical that strand anchorage be considered when detailing and calculating the capacity of I-girder end regions.

This dissertation makes four contributions. First, a consistent terminology and characterization scheme for bond-loss behavior is presented. A review of 22 different test programs revealed that fifteen different terminologies were used to describe failures associated with bond loss. In response to these wide ranging terminologies, the different types of failure involving strand-concrete bond loss are characterized and a consistent labeling scheme is proposed. The fifteen different labels are condensed into four primary bond-loss behaviors. A flowchart is presented for assisting future researchers in characterizing and labeling bond-loss failures.

Second, a bond-loss database is presented. The database was constructed in two phases. During the first phase of data gathering, 84 specimens were added from ten different test programs. During the second phase of data collecting, 36 more specimens from eleven different test programs were added. The database forms a basis for developing and testing quantitative models of bond-loss behavior.

Third, models for calculating bond-loss resistance of pretensioned concrete I-girders were proposed. The initial model was developed and compared to the phase-one database of 84 experimental specimens. A refined model was also proposed. The accuracy of the refined model is examined by comparing the refined model to the expanded database with 120 specimens. The refined model improves the initial model by by using statistical linear regression analysis and the least squares method to identify best-fit equations with the experimental data. The refined model also has the advantage of being developed using a larger database.

For the fourth contribution, the proposed bond loss model is used to evaluate the conservativeness of the strand debonding limitations in the current AASHTO LRFD Bridge Design Specifications. Debonding of select strands is an effective means of controlling stresses and cracking at the ends of pretensioned concrete girders, but can also have adverse effect on capacity due to loss of strand bond. The debonding limitations are evaluated by calculating the bond-loss capacity of six in-service bridge girders from different states. Capacities associated with varying levels of strand debonding are compared to the factored shear loads on each bridge. Calculations of bond-loss capacity are based on the initial model which was created as part of the third contribution.

DEDICATION

Dedicated to my beloved parents

ACKNOWLEDGMENTS

I would like to express my deepest gratitude to my advisor, Dr. Brandon E. Ross, for his excellent guidance, persistent help, patience, and for directing this dissertation and bringing it to its conclusion with expertise. Without his thoughtful encouragement and careful supervision this dissertation would never have been possible.

My thanks also go out to my PhD committee members: Dr. Thomas Cousins, Dr. Amin Khademi, and Dr. Bryant Nielson for their helpful comments and motivations.

I would also like to thank my parents, brother and sister. They were always supporting me and encouraging me with their best wishes. I do not have words to adequately describe my appreciation for all they have provided me.

TABLE OF CONTENTS

Table of Contents (Continued) Page

LIST OF TABLES

LIST OF FIGURES

Chapter 1 Page

Chapter 2

Chapter 3

List of Figures (Continued) Page

Chapter 4

List of Figures (Continued) Page

Chapter 5

Chapter 6

CHAPTER ONE

INTRODUCTION

The overall objective of this dissertation is to compile and create the evidence, tools, and knowledge needed to control and mitigate end region cracks in pretensioned concrete I-girders while also ensuring sufficient capacity; specifically the research advances strand debonding as a method for crack control, by creating an accurate model for calculating bond-loss resistance of pretensioned concrete I-girders. Methods used in this research include creation and analysis of empirical databases, analysis using fundamental concepts in the mechanics of concrete structures, and rigorous statistical analysis. Success in meeting the objectives will facilitate durable concrete bridge members that also have sufficient strength and serviceability.

End region cracks are horizontal and diagonal web cracks that form at the ends of pretensioned concrete I-girders during or immediately following prestress transfer. AASHTO LRFD specifications currently refer to this phenomenon as "splitting" (AASHTO 2014). With increasing use of deep girders, thin webs, and high prestress forces, these cracks are apparently becoming more common and sometimes larger (Gamble 2014). Types of end region cracking are shown in **Fig. 1**.

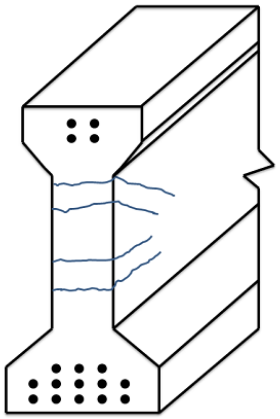

Figure 1. End-region cracking of I-girder

Concrete cracks when tensile stresses exceed tensile capacity of the concrete. End-region splitting cracks form due to vertical and inclined tensile stresses caused from the distribution of eccentric prestressing force from the bottom flange to the rest of the cross section (**Fig. 2**). End region cracks are of concern primarily due to their influence on the durability of concrete girders. These cracks expose strand and reinforcing steel, and allow for the ingress of chlorides and other corrosives. Also, visible cracks can be unpleasant to pedestrians and other transit system users. Thus control and prevention of end region cracks are concerns for durability and serviceability more than for strength.

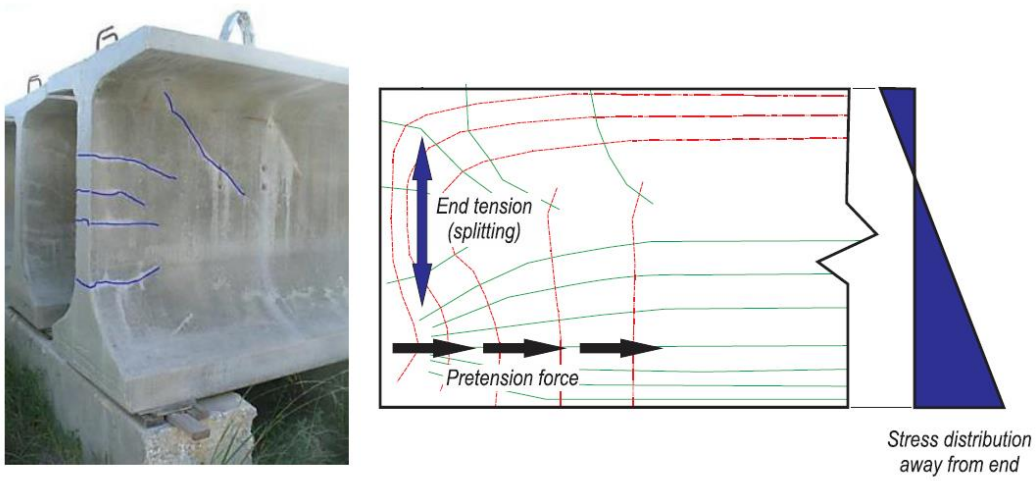

Figure 2. Vertical tensile stresses induced from distribution of prestressing force (Willis 2014)

End region cracking of I-girders has been the focus of researchers for decades (Kaar and Magura 1965; Dane and Bruce 1975). Investigations into web-splitting cracks have been conducted using two distinct approaches. First, many researchers (Rabbat et al. 1979; Russel and Burns 1993) have investigated reduction in end region cracks by controlling concrete stresses. Harped strand and strand debonding (**Fig. 3**) are the primary strategies that have been studied for controlling stresses. The second approach has focused on controlling the cracks through optimization of end-region reinforcement (Marshall and Mattock 1962; Tadros et al. 2010).

While debonding is beneficial for controlling end stresses and cracking, it can also compromise the shear capacity of the end region (Abdalla et al. 1993; Burgeno and Sun 2011; Ross et al. 2014a). In particular, debonding limits the resistance to bond-loss failures. The current research study aims to create an accurate model to calculate nominal capacity of a pretensioned I-girder end region against bond-loss failure. In this

dissertation, bond-loss resistance is defined as the shear force corresponding to loss of strand-concrete bond, and consequently, loss of shear resistance of the end region. Once bond-loss capacity can be accurately assessed, then strand debonding can be more utilized as a method to control and mitigate end region splitting stresses and cracking. The remainder of this chapter will describe the fundamental concepts, current state-of-the-art, and research plan associated with these objectives.

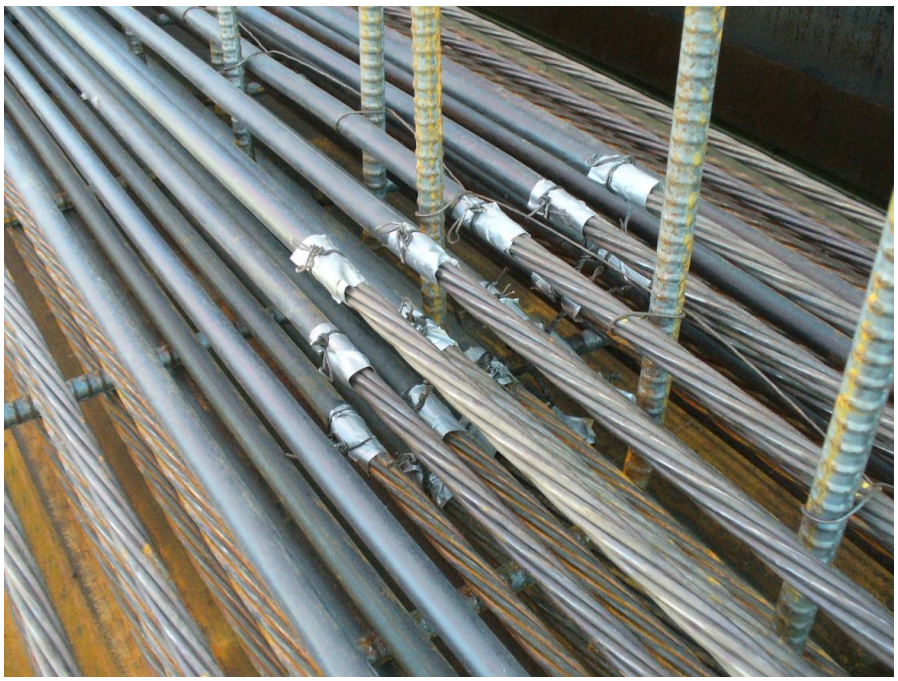

Figure 3. Strand debonding to reduce the stresses in the end-region of concrete girder (Willis 2014)

Background

The end-region of a pretensioned girder must satisfy two critical functions. It must facilitate transfer of prestress forces from the prestressing strands to the concrete element and, at the same time, carry shear forces from the girder to the support. The following sections describe the concepts and code provisions associated with these two

functions. Background information presented in this section provides a basis for this research study.

Strand-Concrete Bond Behavior

Mechanical interlock, adhesion, and the Hoyer effect are three distinct phenomena that contribute to bond between concrete and pretensioned strands. Bond stresses are not easy to represent mathematically (Russel and Burns 1993). Russel and Burns (1993) suggested that a conceptual understanding of elements of bond, as described below, is a sufficient way to explain the bond behavior of pretensioned seven-wire strand. They defined adhesion as a tendency of the strand and concrete surfaces to stick together. Adhesion can be loosely thought of as the "glue" between the concrete and steel.

The Hoyer effect is named after Hoyer, a German Engineer who was one the pioneers of prestressed concrete in the early 1950s (Hoyer 1939). Hoyer observed that the diameter of the strand reduces as it is elongated due to the prestressing force (Poisson's effect). After release of prestressing force, strands expand laterally, seeking to return to their original shape. However in strands that are surrounded by concrete the expansion is restrained. Resistance to the lateral expansion creates normal and frictional forces at the strand-concrete interface. These friction forces resist movement of strand with respect to the concrete thus adding to bond and force transfer.

The third bond mechanism is mechanical interlock. Prestressing strands are made of seven wires in which six outer wires are twisted around the center one. This configuration leads to normal forces between the wires when the strand is loaded in tension. When concrete is cast around strands, it forms a surface in the shape of the

seven-wire strand. When embedded strand moves relative to the surrounding concrete it must untwist, which movement is resisted by concrete, thus creating force transfer between the strands and concrete (Russel and Burns 1993).

Bond and force transfer mainly develop from a combination of Hoyer's effect and mechanical interlocking (Russell and Burns 1993). Most of the transfer bond is expected to come from Hoyer's effect because twist restraint should occur first for the mechanical interlocking to be fully effective. **Figure 4** shows the relative contributions from two main elements of bond in transfer zone. Note that adhesion does not contribute to bond once slip has occurred.

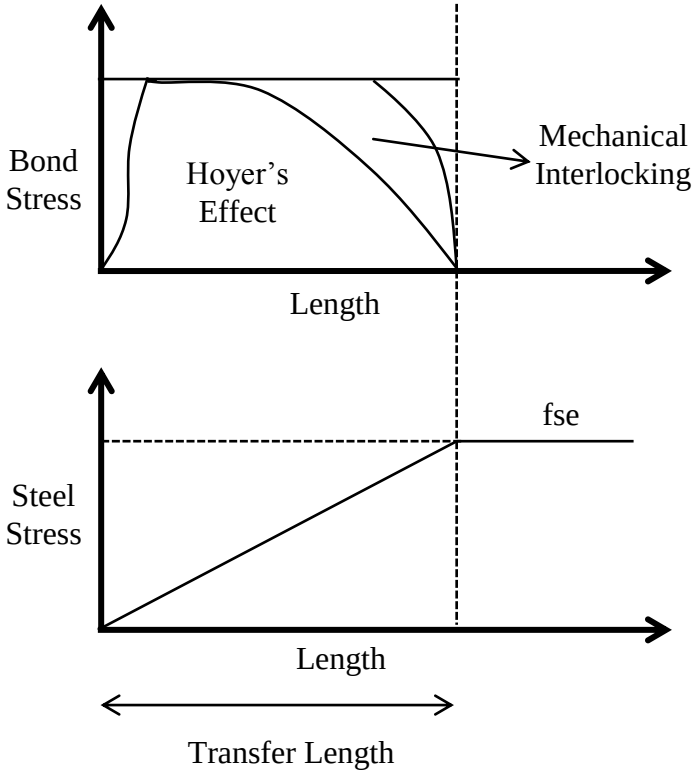

Figure 4. Bond mechanics in transfer zone (Based on Russell and Burns 1993)

Bond-loss Failure

Bond-loss failure has been extensively observed in load tests of I-girder end region capacity (Shahawy and Batchelor 1996; Deatherage et al. 1994). Bond-loss failure is characterized by the formation of cracks in the end region due to applied loads (**Fig. 5_left**). These cracks interrupt anchorage of strands, leading to loss of bond and slipping of strands relative to the concrete (**Fig. 5_right**). Strand slip allows the crack to open wider and causes rotation about the crack tip. Once the slip and resulting rotation are sufficient, then the beam will fail as the compression zone crushes under a combination of shear and flexural actions. The specifics of bond-loss behavior can vary from specimen to specimen; the terminology and mechanics associated with different types of bond-loss failures are described in detail in chapter 2.

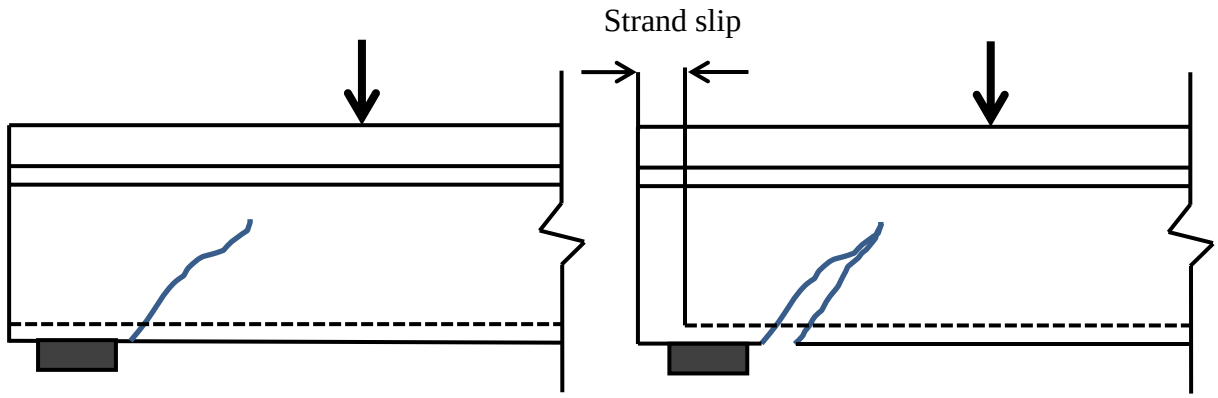

Figure 5. Basic description of bond-loss failure; crack forms near support (left) and crack leads to bond loss and strand slip (right)

Strand-concrete bond-loss failure occurs when external loads result in increasing strand tension within the transfer zone. Strand diameter reduces and results in loss of bond (reversal of Hoyer's effect). Strands also lose their twist restraint since Hoyer's

effect is damaged. Strands are allowed to twist and consequently bond strength from mechanical interlocking becomes ineffective. It is important to recognize that adhesion does not contribute to bond once slip has occurred. The result is an anchorage failure with possible collapse of the whole pretensioned member. For purpose of this research, bond-loss failure is characterized by the formation of cracks within the end region, slipping of strands relative to the concrete, and failure of a member to reach nominal shear or flexural capacity.

AASHTO LRFD End-Region Model

The capacity of end-regions to carry shear forces is addressed in LRFD section 5.8.3.5-2. This section presents Equation (1) for proportioning end region reinforcement based on the end-region free body diagram shown in **Fig. 6**.

$$A_s f_y + A_{ps} f_{ps} \geq \left(\frac{V_u}{\phi_v} - 0.5V_s - V_p\right) cot\theta \qquad (1)$$

where

A_s = area of non-prestressing tension steel

f_y = specified yield strength of reinforcement bars

A_{ps} = area of prestressing steel

f_{ps} = average stress in prestressing steel coincident with V_u

V_u = factored shear force

ϕ_v = resistance factor for shear

V_s = resistance provided by the vertical reinforcement

V_p = component of prestressing in direction of the shear force

θ = angle of inclination of diagonal compressive stresses

C = force in compression zone

d_v = effective shear depth

T = longitudinal tie force in flexural reinforcement

V_a = force along crack interface

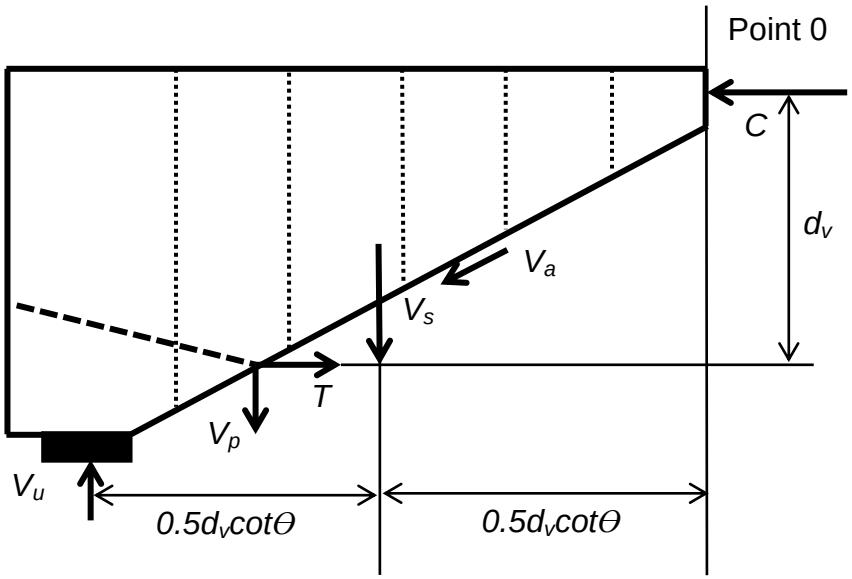

Figure 6. Free body diagram of end region (based on AASHTO LRFD 2014)

Equation (1) was derived by moment equilibrium of the end region about 'point 0', as shown in Fig. 6. The intent of the code provision is to ensure that sufficient transverse and flexural reinforcement are present to carry the shear force in the end region. Bond-loss failure is implicitly addressed in LRFD section 5.8.3.5, which requires that "any lack of full development length [of the longitudinal tie] shall be accounted for" when using Equation (1). However, instructions are not explicitly given for how to account for lack of full development. An important feature of the LRFD approach is that

it assumes yielding of the transverse reinforcement. This feature will be scrutinized in subsequent chapters.

Assuming that bond-loss of the flexural reinforcement controls end region capacity, Equation (1) can be rearranged to the form shown in Equation (2) to calculate nominal bond-loss capacity. This approach has been used by multiple authors (Ross et al. 2011; Garber et al. 2016) in order to modify the LRFD equation for use in calculating bond-loss capacity.

$$\frac{V_u}{\phi_v} \leq V_{nb} = \frac{A_s f_y + A_{ps} f_{psb}}{cot\theta} + 0.5V_s + V_p \quad (2)$$

where

V_{nb} = nominal bond capacity

f_{psb} = stress in prestressing strand coincident with bond-loss failure

Similar to the provisions of LRFD section 5.8.3.5, proposed bond-loss resistance models (presented in chapters 3 and 5) are also based on moment equilibrium of the end region; however, the models rely on fewer simplifications and are consequently applicable to a wider range of girders.

Strand Debonding

The transfer of stresses from strands to concrete at the end region of prestressed beam results in a complex stress state that can lead to concrete cracking as discussed in the introduction and shown in Fig. 2. This stress state includes vertical tension (splitting) action at the end of the web, which occurs as eccentric pretension forces are transferred into the bottom flange then distributed to the rest of the cross-section.

Strand debonding is a common procedure used in prestressed concrete members to reduce tensile stresses in the end region. The approach is to move the stress transfer in the end region between select prestressing strands and concrete by placing plastic sheathing (Fig. 3) around the strands. Since stress transfer between debonded strands and concrete initiates away from the member end, the stresses at the end region are reduced (**Fig. 7**).

While the use of debonded strands has been found effective in reducing cracking, debonding of prestressing strands can have negative impact on the shear capacity of the pretensioned girders (Abdalla et al. 1993; Burgeno and Sun 2011; Ross et al. 2014a). In particular, strand debonding affects a reduction in bond-loss capacity. Strands that are debonded cannot contribute to the longitudinal tie force and end region capacity (See Fig. 6). Therefore, the benefits of strand debonding must be balanced with the requirement to provide sufficient strength against bond-loss failure. Balancing these objectives is the subject of chapter 4.

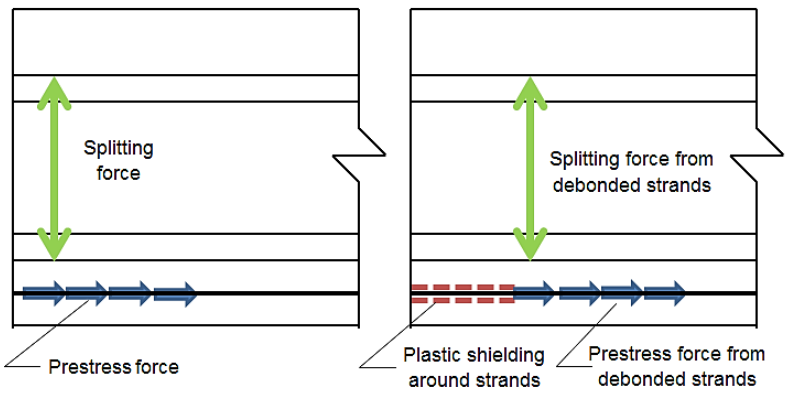

Figure 7. Splitting force in end-region from fully bonded strands (left) and partially debonded strands (right)

AASHTO LRFD Strand Debonding Limits

Bond-loss failure is tacitly addressed in provisions of LRFD section 5.11.4.3 governing partial strand debonding. While strand debonding has been used with relative success in reducing end region cracks (Okumus and Oliva 2013; Ross et al. 2014b), end region cracking continues to be a problem in the production of pretensioned concrete girders. With regards to strand debonding, the AASHTO-LRFD specifications provide the following requirements.

- Not more than 40 % of the strands at any one horizontal row shall be debonded
- The number of partially debonded strands should not exceed 25 percent of the total number of strands.
- The exterior strands of each horizontal row shall be fully bonded
- Debonded strands shall be symmetrically distributed about the centerline of the member.
- Debonded lengths of pairs of strands that are symmetrically positioned about the centerline of the member shall be equal.
- Not more than 40 % of the debonded strands, or four strands, whichever is greater, shall have the debonding terminated at any section

Commentary to LRFD 5.11.4.3 says that shear resistance should be "thoroughly investigated" when strands are debonded in excess of the stated limitations. Because there is correlation between bond-loss capacity and partial strand debonding, LRFD limits the percentage of partially debonded strands to 25% -as stated above- of the total strand. The recommended limit of 25 percent of debonded strands is derived from tests

conducted by the Florida Department of Transportation (Shahawy and Batchelor 1991; Shahawy et al. 1993) which indicate that the anchored strength of the strands was found to be one of the primary contributors to the shear resistance of prestressed concrete beams in their end zones (AASHTO 2014).Thus the limitation addresses the reduction of shear capacity due to the debonding of strands. To express differently, it is generally accepted that partial strand debonding has serviceability benefits because of reduced end region stresses and cracking. However, the trade-off is that debonding limits the number of strands available to act as a tie in the end region, and thereby reduces resistance to bond-loss failure.

Organization of the Dissertation

This dissertation is written in 6 chapters. Chapter one describes background and introduction. Chapters two through five consist of four research papers, which have been either published or submitted to the peer-reviewed journals. Chapter six presents conclusion of this dissertation.

Chapter one is an introduction to this research study and provides a brief background about strand-concrete bond behavior, bond-loss failure, and end-region strand debonding. Additionally, this chapter explains the research problem to be addressed and significance of this research study.

Characterization of different types of failure involving strand-concrete bond loss is discussed in chapter 2. A consistent labeling scheme is proposed by condensing fifteen different labels found in the referenced test programs into four primary behaviors. Additionally, a flowchart is presented for assisting researchers in characterizing and

labeling bond-loss failures. Chapter 2 has been accepted for publication in ASCE Journal of Bridge Engineering. Co-authors include Brandon Ross and Royce Floyd.

A new model for calculating nominal capacity of a pretensioned I-girder end region against bond-loss failure is presented in chapter 3. A database consisting of 84 specimens failed in bond-loss failure, from 10 different experimental test programs, is also constructed, and the accurateness of the proposed model is investigated by comparing the model to the database. Chapter 3 has been published in Transportation Research Record: Journal of the Transportation Research Board. Co-author includes Brandon Ross.

The conservatism of the AASHTO LRFD 25% debonding limitation with respect to shear failures involving loss of strand-concrete bond is evaluated in chapter 4. This is accomplished by calculating the bond-loss capacity of six in-service girders from different states and for different levels of strand debonding, and comparing the results with factored shear force on the in-service bridges. Calculations of the bond-loss capacity are based on the model presented in chapter 3. Chapter 4 has been submitted for publication to a peer-reviewed journal. Co-author includes Brandon Ross.

Chapter 5 introduces a refined model for calculating bond-loss resistance of pretensioned I-girders. The refined model presented in chapter 5 is created through linear regression and least squares analyses. Additionally, the bond-loss database is also expanded by adding 36 more specimens from 11 experimental test programs, resulting in 120 specimens having some type of bond-loss failure. The database and model in chapter 5 are expansions and refinements of those presented in chapter 3. The refined model is

also compared to LRFD end-region model described in the introduction chapter, and as will be shown, the refined model is more accurate than LRFD model. Chapter 5 has been submitted to a peer-reviewed journal. Co-authors include Brandon Ross and Amin Khademi.

Chapter 6 summarizes the contributions of this research study.

The overall objective of this dissertation is to control and mitigate end region cracks in pretensioned concrete I-girders by advancing strand debonding as a method for crack control. Since strand debonding affects a reduction in bond-loss resistance of the end region, research studies presented in chapter 2, 3 and 5 aim to create an accurate model to calculate nominal capacity of a pretensioned I-girder end region against bond-loss failure. Once bond-loss capacity is accurately assessed, then durability and serviceability benefits of strand debonding can be balanced with the need for sufficient resistance to bond-loss failure; and hence, strand debonding can be more utilized as a method to control and mitigate end region splitting stresses and cracking as described in chapter 4.

References:

AASHTO. (2014). *AASHTO LRFD bridge design specifications*, 7th Ed., Washington, DC.

Abdalla, O. A., Ramirez, J. A., and Lee, R. H. (1993). "Strand debonding in pretensioned beams-precast prestressed concrete bridge girders with debonded strands-continuity issues." *Rep. No. FHWA/INDOT/JHRP-92*, Indiana DOT, Indianapolis, IN.

Burgueño, R., and Sun, Y. (2011). "Effects of debonded strands on the production and performance of prestressed concrete beams." *Rep. No. CEE-RR–2011/01*, Michigan DOT, Lansing, MI.

Dane III, J., and Bruce, R. N. J. (1975). "Elimination of draped strands in prestressed concrete girders." *Rep. No. FHWA-RD-75-S0399*, New Orleans, LA.

Deatherage, J. H., Burdette, E. G., and Chew C. K. (1994). "Development length and lateral spacing requirements of prestressing strand for prestressed concrete bridge girders." *PCI J.*, 39(1), 70-83.

Gamble, W. L. (2014). "Discussion on comparison of details for controlling end-region cracks in precast, pretensioned concrete I-girders." *PCI J.*, 134-136.

Garber, D. B., Gallardo, J. M., Deschenes, D. J., and Bayrak, O. (2016). "Nontraditional shear failures in bulb-t prestressed concrete bridge girders." *J. Bridge Eng.*, 10.1061/(ASCE)BE.1943-5592.0000890.

Hoyer, E. (1939). "Der Stahlasitenbenton [Piano-String-Concrete]", Otto Elsner, Berlin. [In German].

Kaar, P. H., and Magura, D. D. (1965). "Effect of strand blanketing on performance of pretensioned girders." *PCI J.*, 10(6), 20-34.

Marshall, W. T., and Mattock, A. H. (1962). “Control of horizontal cracking in the ends of pretensioned prestressed concrete girders.” *PCI J.*, *7*(5), 56–74.

Okumus, P., and Oliva, M. G. (2013). “Evaluation of crack control methods for end zone cracking in prestressed concrete bridge girders.” *PCI J.*, 58(2), 91-105.

Rabbat, B. G., Kaar, P. H., Russell, H. G., and Bruce, R. N. J. (1979). “Fatigue tests of pretensioned girders with blanketed and draped strands.” *PCI J.*, 24(4), 88-114.

Ross, B. E., Ansley, M., and Hamilton, H. R. (2011). “Load testing of 30-year-old AASHTO type III highway bridge girders.” *PCI J.*, 56(4), 152-163.

Ross, B. E., Hamilton, H. R., and Consolazio, G. R. (2014a). “Experimental study of end region detailing and shear behavior of concrete I-girders.” *J. Bridge Eng.*, 10.1061/(ASCE)BE.1943-5592.0000676.

Ross, B. E., Willis, M. D., Hamilton, H. R., and Consolazio, G. R. (2014b). “Comparison of details for controlling end-region cracks in precast, pretensioned concrete I-girders.” *PCI J.*, 59(2), 96-108.

Russell, B. W., and Burns, N. H. (1993). “Design guidelines for transfer, development and debonding of large diameter seven wire strands in pretensioned concrete girders.” *Rep. No. FHWA/TX-93+1210-5F*, Texas DOT, Austin, TX.

Shahawy, M. A., and Batchelor, B. (1991). “Bond and shear behavior of prestressed AASHTO type II beams.” Florida DOT, Tallahassee, FL.

Shahway, M. A., and Batchelor, B. (1996). “Shear behavior of full-scale prestressed concrete girders: comparison between AASHTO specifications and LRFD code.” *PCI J.*, 41(3), 48-62.

Shahawy, M. A., Robinson, B., and Batchelor, B. (1993). “An investigation of shear strength of prestressed concrete AASHTO type II girders.” Florida DOT, Tallahassee, FL.

Tadros, M. K., Badie, S. S., and Tuan, C. Y. (2010). “Evaluation and repair procedures for precast/prestressed concrete girders with longitudinal cracking in the web.” *NCHRP Rep. No.* 654, Transportation Research Board, Washington, DC.

Willis, M. D. (2014). “Post-tensioning to prevent end-region cracks in pretensioned concrete girders.” MS thesis, Clemson University, Clemson, SC.

CHAPTER TWO

CHARACTERIZATION OF BOND-LOSS FAILURES IN PRETENSIONED CONCRETE GIRDERS

Abstract: Failures of strand-concrete bond have been widely observed in load tests of precast-pretensioned concrete I-girders. Through a review of 22 different test programs, fifteen different terminologies were identified to describe failures associated with bond loss. In many cases, previous researchers used different terms to describe the same failure behavior. In response to the wide ranging and sometimes inconsistent terminologies used in the literature, this technical note makes two contributions. First, the different types of failure involving strand-concrete bond loss are characterized and a consistent labeling scheme is proposed. The fifteen different labels given in the referenced test programs are condensed into four primary behaviors. Second, a flowchart is presented for assisting future researchers in characterizing and labeling bond-loss failures. Decision points in the flowchart are based on a synthesis of the reviewed test programs, which included 120 unique load tests having some type of bond-loss failure.

Introduction

Failures involving strand-concrete bond have been extensively observed in load tests of precast pretensioned concrete I-girders (Table 1). This research focuses on bond-loss failure due to cracking that interrupts anchorage of the strands (Figure 1a), leading to loss of bond and slipping of the strands relative to the concrete (Figure 1b). While this paper focuses on failures having shear cracks near the support, bond-loss failures have

also been observed in load tests without such cracks (Dang et al. 2016). The characterization methods discussed in this paper can be applied whenever cracks form within the strand development length.

Table 1. Labels Given to Failures with Loss of Strand-Concrete Bond

Failure Label	Author(s)
Bond-shear	Deatherage et al. 1994, Tawfiq 1995, Shahawy and Batchelor 1996, Ma et al. 2000, Kahn et al. 2002, Jongpitaksseel 2003, Ross et al. 2011a, Ross et al. 2013,
Slip-compression	Ross et al. 2011b
Shear-tension	Kaufman and Ramirez 1988
Flexure-bond	Deatherage et al. 1994, Shahawy and Batchelor 1996,
Bond-flexure	Deatherage et al. 1994
Bond	Kahn et al. 2002, Burkett and Kose 1999
Flexure w/ slip	Barnes et al. 1999
Hybrid	Burkett and Kose 1999
Shear-slip	Meyer et al. 2002
Flexure/shear-slip	Meyer et al. 2002
Shear-slip/flexure	Meyer et al. 2002
Strand slip	Hartmann et al. 1988, Labonte and Hamilton 2005, Kuchma et al. 2008
Strand anchorage	Abdalla et al. 1993
Bond/flexure-shear	Tawfiq 1995
Anchorage zone distress	Garber et al. 2016
Described, not named	Maruyama and Rizkalla 1988, Alshegir and Ramirez 1992, Raymond et al. 2005

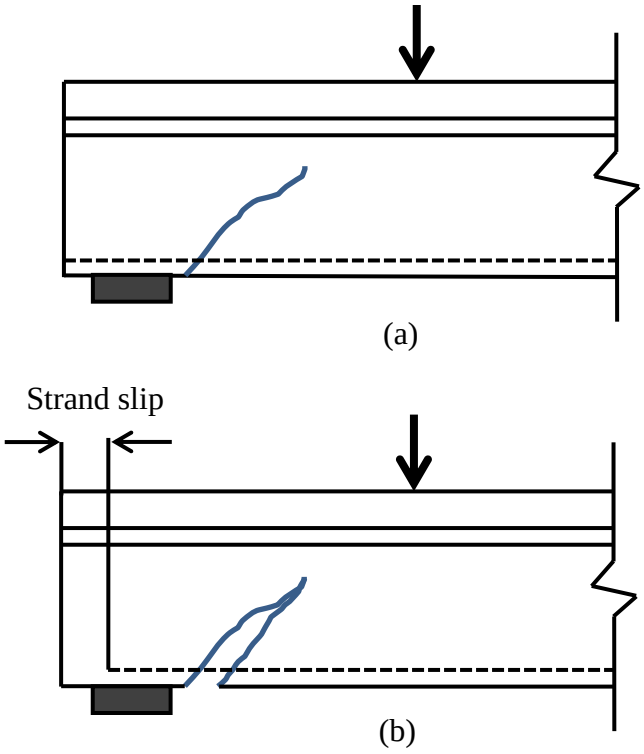

Fig. 1. Basic description of bond-loss failure; a) crack forms near support; b) crack leads to bond loss and strand slip

There are multiple sub-categories of bond-loss failure; these sub-categories and their attendant behaviors are described later in this technical note. It has been experimentally demonstrated (Shahawy and Batchelor 1996) that failure due to loss of strand-concrete bond can occur at load levels that are lower than the nominal shear and flexural capacities. In one example, bond-loss failure resulted in an experimental capacity that was approximately10% less than the nominal shear strength (Ross et al. 2011a). Because bond loss can be the controlling factor for structural capacity (Ross et al. 2014; Garber et al. 2016), it is critical that strand anchorage be considered when detailing and calculating the capacity of I-girder end regions.

Many different terminologies have been used to describe failures that occur due to loss of strand-concrete bond. Table 1 presents fifteen different terminologies that were identified through a review of 22 different test programs. Also listed in the Table 1 are researchers who described failures occurring due to loss of bond, but did not use a specific label to describe the failure. Through a review of these programs, it has been recognized that some identical bond-loss behavior has been labeled differently by different researchers (e.g. strand slip and strand anchorage). These programs included load tests of 327 different pretensioned girders, of which 120 resulted in some type of bond-loss failure. These 120 specimens do not include tests wherein lack of cover, spacing, or confinement was listed as a primary factor for failure.

The inconsistent terminology in the literature makes it challenging to compare results between different test programs. In response, this technical note proposes a consistent scheme for labeling and characterizing bond-loss failures. To that end, the first part of this note describes the mechanics associated with four different types of bond-loss failures. The descriptions and categories are largely based on the work by Deatherage et al. (1994), but draw on each of the references listed in Table 1. The second part of this note presents a flowchart to assist future researchers in categorizing bond-loss failures. Decision points in the flowchart are based on a synthesis of the experimental results from the reviewed test programs.

Development of the labeling scheme and flowchart were focused on bond loss of fully bonded (i.e. not shielded) strands. For example, test results from Barnes et al. (1999) and Burkett and Kose (1999) included specimens for which the shielded strands

slipped but the fully bonded strands did not. Failures involving bond loss and slipping of fully bonded strands are the primary focus of this technical note.

Types of bond-loss failure

The proposed labeling convention contains two parts and follows this format: "primary failure mode-secondary or contributing failure mode." For example, the label "bond-shear" is given when bond loss is the primary cause of failure and shear failure results from bond-loss. Labels for three other failure types are also given using the same format.

Each of the test programs reviewed in preparation of this technical note used hydraulic jacks to load the girders. The failure descriptions, crack patterns, typical load-displacement, and typical load-strand slip responses presented in the following sections are based on progression of events as load is applied using a hydraulic system. Consistent with the vast majority of the reviewed tests, the descriptions presented below are also based on simple-span boundary conditions and a single point load located near one support.

Bond-Shear

Figure 2a shows a representative crack pattern, load-displacement relationship, and load-strand slip relationship for a specimen that fails in bond-shear. Information in the figure is based on crack patterns and structural behavior reported in the literature, such as examples listed in Table 2. Bond-shear failure initiates with the formation of inclined cracks in the web and bottom flange near the girder end. These cracks disturb anchorage of the prestressing strands, leading to loss of strand-concrete bond and slipping

of the strands relative to the concrete (Abdalla et al. 1993). The primary cracks occurring with bond-shear failures are inclined cracks, however, flexural cracks have also been observed in some cases. As load is increased, the displacement, slip, and crack size also increase, and eventually lead to shear failure. Peak load is limited by a reduced available tension force due to bond loss, which precedes and leads to the eventual shear failure. In contrast with other failure types that will be discussed, the compression zone does not crush in specimens that fail in bond-shear.

The shear failure portion of a bond-shear failure can take different forms. Web-shear and flexural-shear failures have both been observed in test girders following bond loss (Tawfiq 1995). For simplicity, however, these distinctions are not considered in the proposed classification scheme. Failures are simply labeled as "bond-shear" when bond loss precedes and leads to shear failure, regardless of the shear behavior.

Bond-shear failure was the most commonly observed failure type in the reviewed test programs, accounting for 81 out of 120 bond-loss failures. In the database, 88% (71 out of 81) of the bond-shear failures occurred when the shear span-to-depth ratio (*a/d*) was less than 3, the remaining 12% of bond-shear failure occurred when the *a/d* ratio was greater than 3.

Failures with bond-shear characteristics have been referred to as "bond" , "shear tension" , "shear-slip", "strand anchorage", "bond/flexure-shear", "strand-slip", and " anchorage zone distress" failures (Kaufman and Ramirez 1988; Hartmann et al. 1988; Abdalla et al. 1993; Tawfiq 1995; Meyer et al. 2002; Kahn et al. 2002; Labonte and Hamilton 2005; Garber et al. 2016).

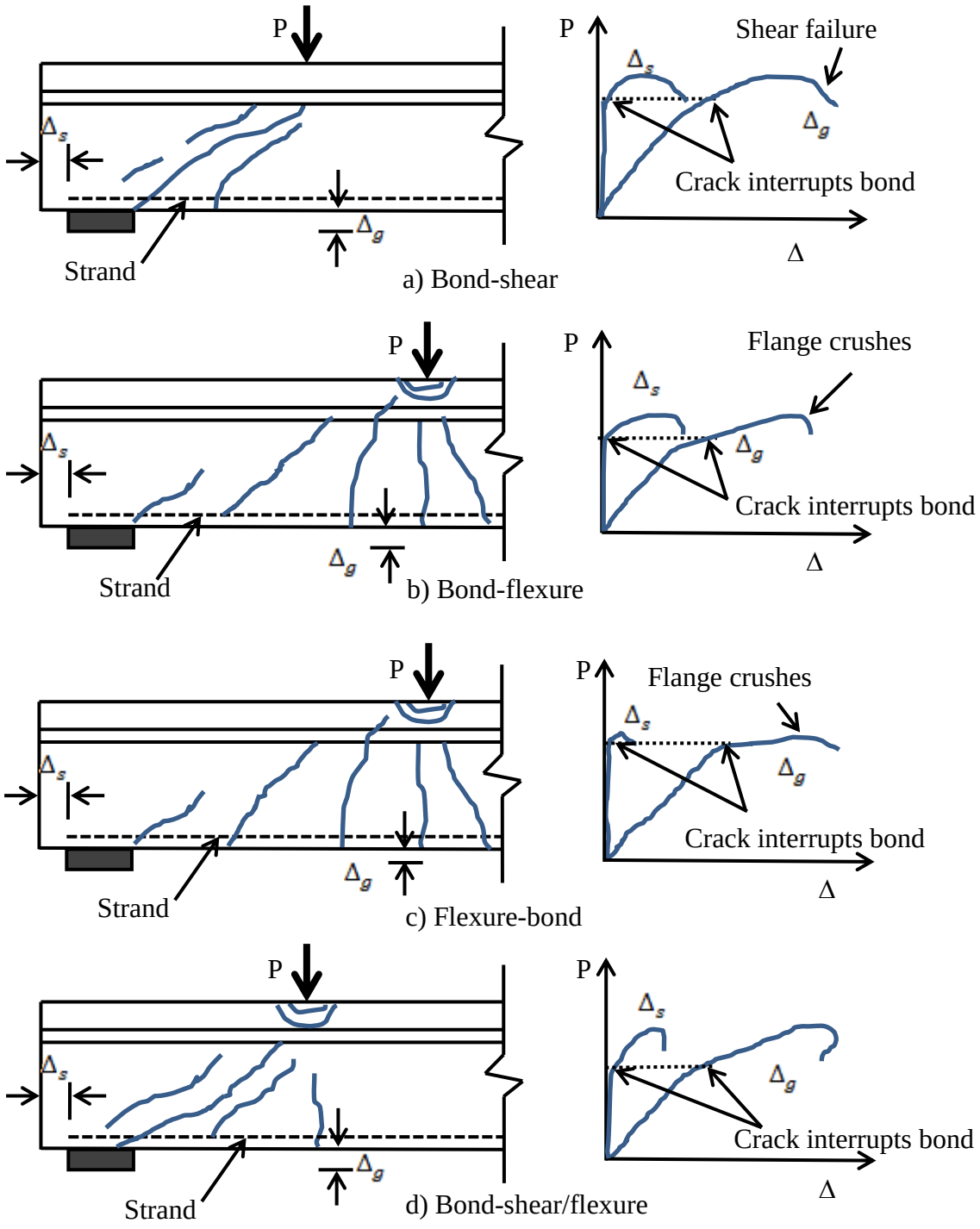

Fig. 2. Typical crack pattern and structural behavior; a) bond-shear; b) bond-flexure; c) flexure-bond; d) bond-shear/flexure (Δ_s: Strand slip, and Δ_g: Girder displacement)

For the representative behavior shown in Figure 2a, loss of stiffness of the girder is shown to occur prior to slipping of the strands. To express it differently, the first crack typically occurs in the web of the girder end; and hence, doesn't disturb anchorage of the prestressing strands. Loss of stiffness prior to loss of anchorage is common throughout bond-shear and other failure modes. In some instances, however, strand slip occurs approximately simultaneously with loss of stiffness. Examples of both conditions are shown in Shahawy and Batchelor (1996). In the proposed characterization scheme, the time of slip relative to the loss of stiffness is not considered as a factor when determining failure type.

Table 2. Examples of Bond-Shear Failures

Reference	Specimen ID	Failure label in original reference
Kaufman and Ramirez (1988)	1-3, 1-4	Shear tension
Ross et al. (2011a)	G1, G2	Bond-shear

Bond-flexure

Like all of the girder specimens in the references, those failing in bond-flexure behave approximately linear-elastically up to the cracking load (Figure 2b). The initial cracks do not necessarily cause slip, however, after cracking, the girders lose stiffness and the load-displacement response becomes nonlinear. As load increases, the cracks grow in quantity and size. Bond loss and strand slip occur after cracks intersect with strands in the end region. Shear cracking adjacent to the support has been reported in specimens exhibiting bond-flexure failure (e.g. Specimens F8N and F12N Tawfiq 1996).

While such cracking is considered likely in the bond-flexural failures, crack adjacent to the support could not be confirmed in all cases. Strand slip allows the cracks to open wider, thus increasing the curvature and flexural strain, which eventually leads to crushing of the concrete flange. In bond-flexural failure, crushing of the flange is preceded by -and partially attributed to- bond loss and strand slip. Examples of bond-flexural failure from the literature are listed in Table 3. In some instances bond-flexural behavior results in experimental flexural capacities up to 10% less than nominal flexural capacity (Barnes et al. 1999).

In addition to bond loss and strand slip, essential characteristics of bond-flexure failures include crushing of the top flange (or deck) and peak load that is less than the nominal flexural capacity. The latter criterion was used by Barnes et al. (1999) to distinguish "premature flexural failures due to inadequate bond capacity". Of the 120 specimens reviewed, 21 were characterized as bond-flexure, which all had *a/d* ratios of greater than 2.5. In programs where the nominal flexural capacity was not reported, timing of strand slip relative to peak capacity was used to distinguish bond-flexure and flexure-bond behavior (Deatherage et al. 1994).

Table 3. Examples of Bond-Flexure Failures

Reference	Specimen ID	Failure label in original reference
Deatherage et al. (1994)	5-1-EXT, 5-2-INT	Bond-flexure
Tawfiq (1996)	F8N, F12N	Bond-flexure

Flexure-bond

Representative crack patterns and structural behavior associated with flexure-bond failure are presented in Figure 2c. Flexure-bond failures are similar to typical flexural failures in most regards, the exception being that only a small degree of strand slip is observed near peak load in flexure-bond failure. The load-displacement response associated with flexure-bond is typically ductile and peak load corresponds to the flange crushing in compression. Bond loss and strand slip are only observed near to the load at which the concrete flange crushes. In some cases reported in the literature (Deatherage et al. 1994) strand slip was only observed after flange crushing and peak load. Deatherage et al. (1994) reported that flexure-bond failures occur when the load point is close to the development length. Flexure-bond failures only occurred when *a/d* was greater than 2.5. Because the strands are almost fully developed, the experimental capacity associated with flexure-bond failure is approximately equal to the nominal flexural capacity. There were four incidences of flexure-bond failure in the database, they are listed in Table 4.

Table 4. Examples of Flexure-Bond Failures

Reference	Specimen ID	Failure label in original reference
Deatherage et al. (1994)	5S-1-INT, 5S-3-EXT 5S-2-INT, 5-SWAI-WEST	Flexure-bond

Bond-shear/flexure

Bond-shear/flexure is a hybrid failure mode in which bond loss is primarily culpable for failure, but with both flexural and shear behaviors occurring subsequent to bond loss and strand slip (Kahn et al. 2002). Bond-shear/flexure failure initiates with the formation of inclined and/or flexural cracks in the web and bottom flange near the girder end (Figure 2d). These cracks disturb anchorage of the prestressing strands, leading to loss of strand-concrete bond and slipping of the strands relative to the concrete. As the load increases, the strands slip further, the cracks open wider, and the vertical displacement increases. The primary or widest crack that leads to bond-loss is typically an inclined crack; however flexural cracks can also be present. At peak load the flange crushes due to a combination of shear and flexure acting on the compression zone.

Of the 120 specimens in reviewed for this note (Table 1), fourteen specimens demonstrated bond-shear/flexure behavior. These specimens were loaded at *a/d* of 2.5 or less. Failures with bond-shear/flexure characteristics have also been called "slip-compression", and "flexure w/ slip" failures (Ross et al. 2011b; Barnes et al. 1999). Examples of bond-shear/flexure failures are listed in Table 5.

Table 5. Examples of Bond-Shear/Flexure

Reference	Specimen ID	Failure label in original reference
Meyer et al. (2002)	G1A-E	Flexure/shear-slip
Meyer et al. (2002)	G1C-E	Shear-slip/flexure
Ross et al. (2011b)	B5M-C, B5L-C	Slip-compression

Characterization of bond-loss failures

A flowchart for characterizing bond-loss failures is presented in Figure 3. Decision points in the flowchart are based on observations from the references presented in Table 1. The first decision point in the flowchart is regarding the *a/d*. Bond-loss failures were not reported for specimens loaded at *a/d* greater than 4.5; for *a/d* greater than 4.5 flexural failures were typically reported (Deatherage et al. 1994).

The second decision point in the flowchart is regarding the existence of cracking near the support, strand-concrete bond loss, and strand slip; these elements are common to each type of bond loss failure (Kahn et al. 2002; Ross et al. 2011a; Ross and Naji 2014). Failures not involving strand-concrete bond loss were also reported by test programs referenced in Table 1. These failures include web-crushing, lateral-splitting, shear-compression, horizontal-shear and flexural-shear.

The third decision point in the flowchart is based on crushing of the flange. This decision point separates bond-shear failure from the other bond-loss failure types. If the extreme compression fiber does not crush in flexure during load testing then failure is labeled bond-shear. On the other hand, crushing of the top concrete (e.g. deck or flange) occurs in bond-flexure, flexure-bond, and bond-shear/flexure failures. In some cases reported in the literature (Barnes et al. 1999) strand slip was observed but the test was stopped before crushing of the deck. Decision point number three considers tests where flexural crushing was imminent but not reached.

The fourth decision point in the flowchart is regarding *a/d*, and separates bond-shear/flexure failures from flexure-bond and bond-flexure failures. According to test

programs listed in Table 1, bond-flexure and flexure-bond failures were not reported for specimens loaded at *a/d* smaller than 2.5.

The fifth and final decision point in the flowchart differentiates between bond-flexure and flexure-bond failures. The distinction between these failure types is that bond-flexural failures have greater degrees of strand slip and, consequently, fail to reach nominal capacity. Thus comparison of experimental and nominal capacity is used as a criterion to separate flexure-bond and bond-flexure failures. The use of nominal capacity to assist in failure categorization follows the strategy employed by Barnes et al. (1999). Of the 120 specimens reviewed (Table 1), 25 are characterized as flexure-bond or bond-flexure according to the flowchart.

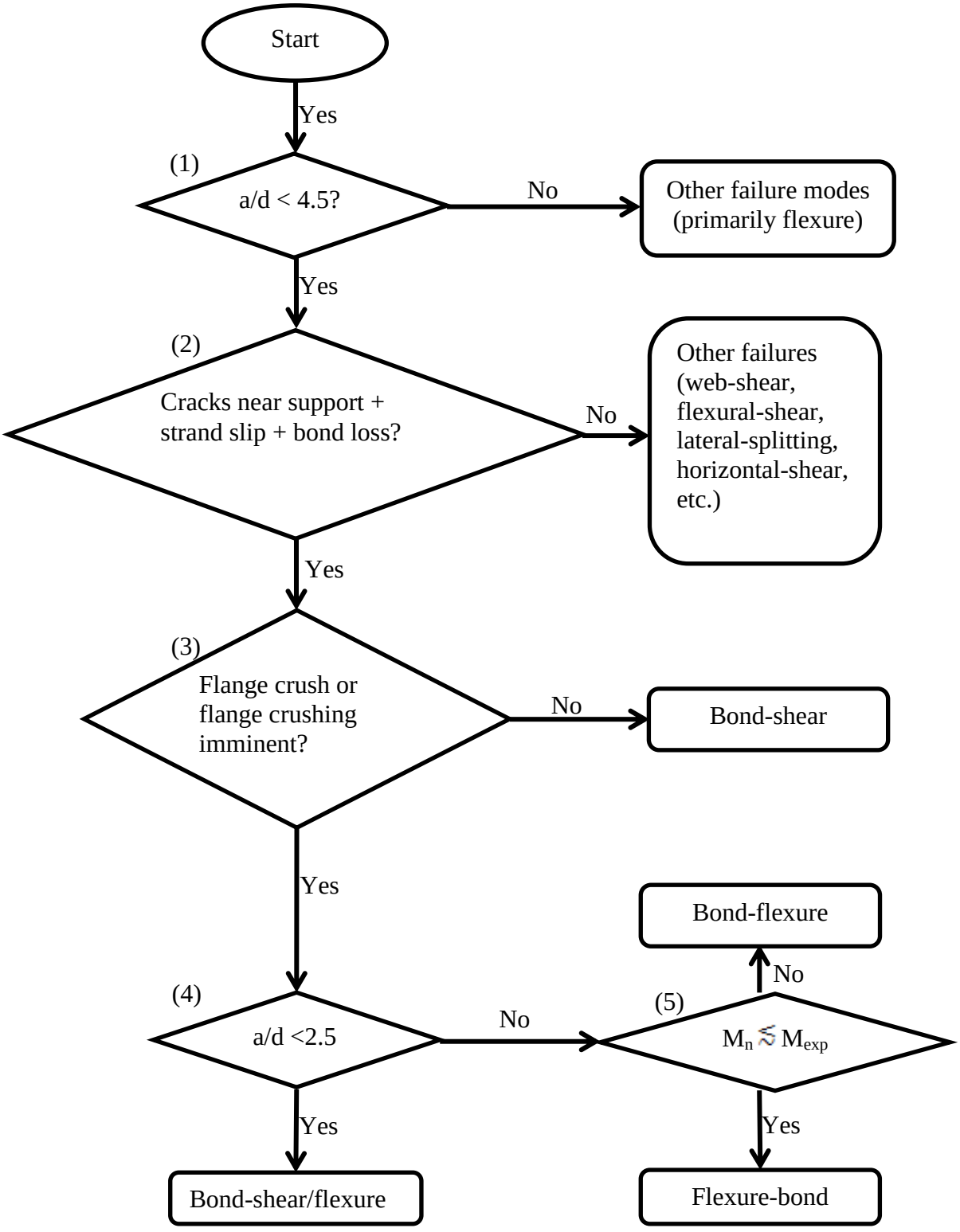

Fig. 3. Flowchart for characterizing types of bond-loss failure

Summary and Conclusion

A total of 327 unique tests of pretensioned girders from 22 different test programs were reviewed. Of these tests, 120 specimens experienced some type of bond-loss failure. Fifteen different terminologies were used by the researchers to describe these failures, and sometimes different terminologies were used to describe the same behavior.

In response to the inconsistent terminology used in the research literature, this technical note makes two contributions. First, four different types of failures involving strand-concrete bond loss were described and labels for each failure type were proposed. These four failure types encompass the fifteen labels given in the referenced test programs. Second, a flowchart for categorizing bond-loss failures was presented. Decision points in the flowchart were based on a synthesis of the reviewed literature. If accepted and utilized by the research community, the proposed labels and characterization scheme will engender much needed consistency in reporting and comparing bond-loss failures.

References

Abdalla, O. A., Ramirez, J. A., and Lee, R. H. (1993). "Strand debonding in pretensioned beams-precast prestressed concrete bridges with debonded strands." *Rep. No FHWA/ INDOT/ JHRP-92,* Indiana DOT, West Lafayette, IN.

Alshegeir, A., and Ramirez, J. A. (1992). "Strut-Tie approach in pretensioned deep beams." *ACI Struct. J.*, 89(3), 296-304.

Barnes, R. W., Burns, N. H., and Kreger, M. E. (1999). "Development length of 0.6-inch prestressing strand in standard I-shaped pretensioned concrete beams." *Rep. No. FHWA/TX-02/1388-1,* Texas DOT, Austin, TX.

Burkett, W. R., and Kose, M. M. (1999). "Development length of 0.6-inch (15-mm) diameter prestressing strand at 2-inch (50mm) grid spacing in standard I-shaped pretensioned concrete beams." *Rep. No. TX/98/1388-2,* Texas DOT, Austin, TX.

Dang, C. N., Floyd, R. W., Hale, W. M., and Marti-Vargas, J. R. (2016). "Measured Development Lengths of 0.7 in. (17.8 mm) Strands for Pretensioned Beams," *ACI Struct. J.*, 113(3), 525-535.

Deatherage, J. H., Burdette, E. G., and Chew, C. K. (1994). “Development length and lateral spacing requirements of prestressing strand for prestressed concrete bridge girders.” *PCI J.*, 39(1), 70-83.

Garber, D. B., Gallardo, J. M., Deschenes, D. J., and Bayrak O. (2016). “Nontraditional shear failures in bulb-t prestressed concrete bridge girders.” *J. of Bridge Eng.*, 10.1061/(ASCE)BE.1943-5592.0000890.

Hartmann, D. L., Breen, J. E., and Kreger, M. E. (1988). “Shear capacity of high strength prestressed concrete girders.” *Rep. No. FHWA/ TX-88+381-2*, Texas DOT, Austin, TX.

Jongpitaksseel, N. (2003). “Behavior of end zone of precast/pretensioned concrete bridge girders.” Ph.D. Dissertation, Univ. of Nebraska, Lincoln, NE.

Kahn, L. F., Dill, J. C., and C. G. Reutlinger, C. G. (2002). “Transfer and development length of 15-mm strand in high performance concrete girders.” *J. of Structural Eng.*, 10.1061/(ASCE)0733-9445, 913-921.

Kaufman, M. K., and Ramirez, J. A. (1988). “Re-evaluation of the ultimate strength behavior of high-strength concrete prestressed I-beams.” *ACI Struct. J.*, 85(3), 295-303.

Kuchma, D., Kim, K. S., Nagle, T. J., Sun, S., and Hawkins, N. M. (2008). "Shear tests on high-strength prestressed bulb-tee girders: strengths and key observations." *ACI Struct. J.*, 105(3), 358-367.

Labonte, T., and Hamilton, H. R. (2005). "Self-consolidating concrete (SCC) structural investigation." *Rep. No. BD545, RPWO# 21*, Florida DOT, Tallahassee, FL.

Ma, Z., Tadros, M. K., and Baishya, M. (2000). "Shear behavior of pretensioned high-strength concrete bridge I-girders." *ACI Struct. J.*, 97(1), 185-192.

Maruyama K., and Rizkalla, S. H. (1988). "Shear design consideration for pretensioned prestressed beams." *ACI Struct. J.*, 85(5), 492-498.

Meyer, K. F., Kahn, L. F., Lai, J. S., and Kurtis, K. E. (2002). "Behavior of high-strength/high-performance lightweight concrete prestressed girders." *Report No 2004*, Georgia DOT, Atlanta, GA.

Raymond, K. K., Bruce, R. N., and Roller, J. J. (2005). "Shear behavior of HPC bulb-tee girders." *ACI Special Publication* 228, 705-722.

Ross, B. E., Ansley, M. H., and Hamilton, H. R., III. (2011a). "Load testing of 30-year-old AASHTO Type III highway bridge girders." *PCI J.*, 56(4), 152-163.

Ross, B. E., Consolazio, G. R., and Hamilton, H. R. (2013). "End region detailing of pretensioned concrete bridge girders." *Rep. No. BDK-75-977-05*, Florida DOT, Tallahassee, FL.

Ross, B. E., Hamilton, H. R., and Consolazio, G. R. (2011b). "Experimental and analytical evaluations of confinement reinforcement in pretensioned concrete beams." *Transportation Research Record 2251*, Transportation Research Board, Washington, DC, 59-67.

Ross, B. E., Hamilton, H.R., and Consolazio, G. R. (2014). "Experimental study of end region detailing and shear behavior of concrete I-girders." *J. of Bridge Eng.*, 10.1061/(ASCE)BE.1943-5592.0000676.

Ross, B. E., Naji, B. (2014). "Model for nominal bond-shear capacity of pretensioned concrete girders." *Transportation Research Record 2406*, Transportation Research Board, Washington, DC, 79-86.

Shahawy, M. A., and Batchelor, B. (1996). “Shear behavior of full-scale prestressed concrete girders: comparison between AASHTO specifications and LRFD Code.” *PCI J.*, 41(3), 48-62.

Tawfiq, K. S. (1995). “Cracking and shear capacity of high strength concrete bridge girders.” *Rep. No. FL/DOT/RMC/612(1)-4269*, Florida DOT, Tallahassee, FL.

Tawfiq, K. S. (1996). “Cracking and shear capacity of high strength concrete bridge girders under fatigue loading.” *Rep. No. FL-DOT RMC*, Florida DOT, Tallahassee, FL.

CHAPTER THREE

A MODEL FOR NOMINAL BOND-SHEAR[1] CAPACITY OF PRETENSIONED CONCRETE GIRDERS

ABSTRACT: The 2010 AASHTO LRFD Bridge Design Specifications include requirements for proportioning flexural reinforcement at the end of pretensioned girders to carry longitudinal tie forces acting above the support. To prevent bond failure of the longitudinal tie AASHTO requires that "any lack of full development [of the tie] shall be accounted for." This paper proposes a model for calculating nominal bond-shear capacity, which is defined as the attendant shear force at bond capacity of the longitudinal tie. The model gives explicit consideration for tie development length. Variables in the model include: bearing and girder geometry, longitudinal and transverse reinforcement details, and inclination angle of cracking. Derivation of the model is presented and the model is compared to a database of experimental results compiled from the published literature. The proposed model can be used for designing girders that are resistant to bond-shear failure, particularly when partial strand debonding is employed. In some circumstances the model may justify exceedance of the AASHTO limits for partial strand debonding.

[1] This chapter refers to "bond-shear" capacity. The paper upon which this chapter is based, was published prior to the research presented in chapter 2. As such the labeling scheme presented in chapter 2 was not used for chapter 3. "Bond-shear" failure as discussed in chapter 3 should be considered synonymous with "bond-loss" failure used throughout the remainder of the dissertation.

INTRODUCTION

The end region of a pretensioned girder must fulfill two critical functions. First, it must facilitate transfer of prestress forces from the prestressing strands to the girder cross-section. Second, it must deliver shear forces from the girder to the support. Performance of these functions is directly affected by detailing of the end region reinforcement, prestressing, and bearing conditions (Ross et al. 2013a). This paper focuses on transfer of shear forces in the end region, and proposes a model for analyzing the end region bond-shear capacity. Bond-shear failure has been observed in numerous experimental studies (Barnes et al. 1998; Deatherage et al. 1994; Hawkins and Kuchma 2007; Kaufman and Ramirez 1988; Ma et al. 2000; Maruyama and Rizkalla 1988; Ross et al. 2011a; Ross et al. 2011b; Ross et al. 2013a; Shahway and Batchelor 1996) and occurs due to loss of strand-concrete bond. Bond-shear failure is problematic because it can affect capacities that are less than the calculated nominal shear strength. The proposed model will assist designers in selecting end region reinforcement and bearing conditions that reduce the likelihood of bond-shear failure. Because there is correlation between bond-shear capacity and partial strand debonding (Ross et al. 2013a; Shahway and Batchelor 1996), the proposed model will also provide an alternative to the prescriptive debonding requirements contained in the 2010 LRFD Bridge Design Specifications (hereafter "LFRD") (AASHTO 2010). In some circumstances the model may justify exceedance of the LRFD limits for partial strand debonding, thus facilitating reduced concrete stresses and improved serviceability.

BACKGROUND

Bond-shear failure initiates with the formation of cracks in the end region that reduce the available strand development length (FIGURE 1a). If the available development length is insufficient to transfer the attendant forces, then the strand-concrete bond will fail and the strands will slip relative to the concrete (FIGURE 1b). Strand slip allows the crack to open wider and causes additional rotation about the crack tip. If the slip and resulting rotation are sufficient, then the compression zone will fail due to combined shear and compression (FIGURE 1c). When transverse reinforcement is present, it acts to prevent opening of the crack and lends capacity and ductility to the bond-shear mechanism (FIGURE 1d).

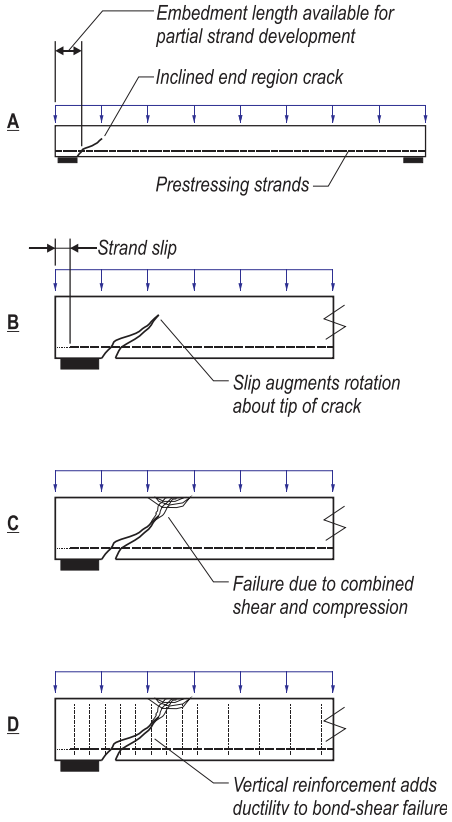

FIGURE 1 Mechanics of bond-shear failure.

For purposes of this paper, bond-shear failure is characterized by the formation of cracks within the strand development length, slipping of strands relative to the concrete, and failure of a member to reach nominal flexural capacity. Failures with these characteristics are sometimes called bond failures, slip failures, bond-compression failures, or bond-flexure failures. The term bond-shear failure is used here because the model derived in this paper is for calculating the shear force associated with bond loss between strands and concrete.

LRFD section 5.8.3.5 presents Equation 1 for proportioning flexural reinforcement to carry longitudinal tie forces at the inside edge of simple span supports. Equation 1 is based on the end region free body diagram shown in , and can be derived by taking moments about point 0. Forces causing moments about point 0 include the reaction force (V_u), prestressing forces (T and V_p), and force in the vertical reinforcement (V_s). Force from aggregate interlock*(V_a)* is assumed to have negligible moment about point 0. The offset between the lines of action for the factored shear force (V_u) and the vertical component of the prestressing force (V_p) is also assumed negligible. The bond-shear model proposed in this paper uses an approach similar to Equation 1 and . The primary author has previously used this approach to analyze bond-shear failure in experimental tests (Ross et al. 2011a).

Bond-shear failure is implicitly addressed in LRFD section 5.8.3, which requires that "any lack of full development length [of the longitudinal tie] shall be accounted for" when using Equation 1. One way of accounting for lack of full development is to select a stress in the prestressing strand (f_{ps}) that can be supported by the available strand

development length. LRFD section 5.11.4 contains provisions for determining a value of stress that is appropriate for the available embedment length. This section presents a bi-linear stress versus embedment length relationship which considers the strand diameter, member depth, prestress level, and transfer length.

Bond-shear failure is also implicitly addressed in the provisions of LRFD section 5.11.4.3 governing partial strand debonding. Commentary for this section references tests from the Florida Department of Transportation (FDOT) (Shahway and Batchelor 1996) which demonstrated the significant effect of strand anchorage -and consequently debonding- on end region shear capacity. FDOT test specimens with 40% of strands partially debonded had inadequate (less than nominal) shear capacity, with bond-shear failure being a primary cause of inadequacy. To prevent bond-shear failures LRFD limits the percentage of partially debonded strands to 25% of the strand total. LRFD also limits the number of strands in a given row that can be debonded (40%), and the number strands that can have debonding terminate at a given section (greater of 4 strands or 40% of debonded strands).

$$A_s f_y + A_{ps} f_{ps} \geq \left(\frac{V_u}{\phi_v} - 0.5V_s - V_p\right) cot\theta \qquad 1$$

Where:

A_s = area of non-prestressing tension steel

f_y = specified yield strength of reinforcement bars

A_{ps} = area of prestressing steel

f_{ps} = average stress in prestressing steel coincident with V_u

V_u = factored shear force

ϕ_v = resistance factor for shear

V_s = resistance provide by the vertical reinforcement

V_p = component of prestressing in direction of the shear force

θ = angle of inclination of diagonal compressive stresses

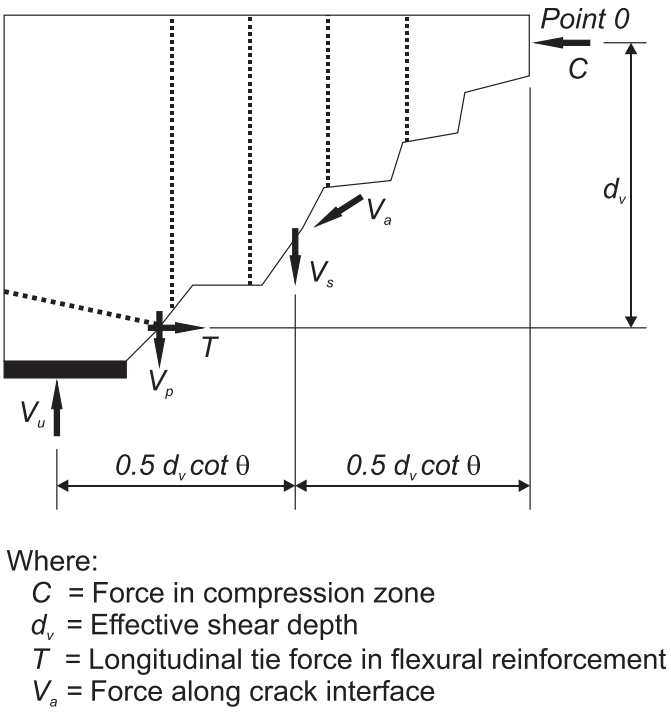

Where:
C = Force in compression zone
d_v = Effective shear depth
T = Longitudinal tie force in flexural reinforcement
V_a = Force along crack interface

FIGURE 2 Free body diagram of end region after LRFD (AASHTO 2010).

In addition to the FDOT project reference in LRFD commentary, the benefits and consequences of partial strand debonding have been studied by other researchers (Burgeno and Sun 2011; Csagoly 1991, Okumus and Oliva 2013; Ross et al. 2013b). It is generally accepted that partial strand debonding has serviceability benefits because of reduced end region stresses and cracking. The trade-off is that debonding limits the

number of strands available to act as a tie in the end region (), and thereby reduces resistance to bond-shear failure.

The model proposed in this paper is for calculating a girder's nominal bond-shear capacity. Using the model, a designer can quantify the number of fully bonded strands required to prevent bond-shear failure at factored loads. Strands not needed to prevent bond-shear failure can then reasonably be debonded, regardless of their overall percentage. By approaching end region detailing in this manner, designers can select strands patterns that leverage the benefits of partial strand debonding without creating undue risk of reduced capacity associated with bond-shear failure.

MODEL DERIVATION

The proposed model is for calculating nominal capacity of a pretensioned girder end region against bond-shear failure. The model was formulated to capture the multitude of variables that exist in pretensioned girders, but be practical enough for use by bridge designers. Variables in the model include girder and bearing geometry, longitudinal and vertical reinforcement, and the inclination angle of cracks.

Similar to the provisions of LRFD section 5.8.3.5, the proposed bond-shear model was based on moment equilibrium of the end region. The free body diagram used for the proposed model (FIGURE 3), however, has some key differences from the free body diagram used by LRFD (). These differences were introduced to make the model applicable to a wider range of girders, to facilitate analysis using strength design principles, and to simplify comparison with experimental data. Differences include:

- Reaction force was changed to the nominal bond-shear capacity (V_{nBV}) rather than the factored shear force (V_u).
- Harped strands were treated separately from the straight strands. A variable distance (d_h) was defined to describe the location of the harped strand forces.
- Resultant force from the vertical reinforcement was located at a variable location (X_s) to account for non-uniformly distributed reinforcement.
- Variables L_{dt} and L_{dh} were introduced to define the available development length of the tension tie and harped strands, respectively.
- The shear force acting at point 0 was included to complete the free body diagram.
- The variable θ_c was introduced to distinguish the angle of the inclined crack from the inclination angle of the compressive stress (θ). These variables can be used interchangeably in some circumstances as discussed in the Application to Design section of this paper.
- The flexural depth (d) was used in lieu of the effective shear depth (d_v).

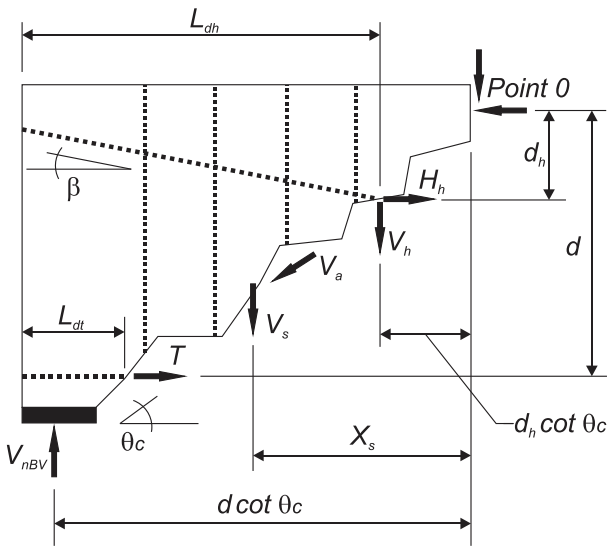

Where:

d = Flexural depth of tension tie
d_h = Depth of harped strands at crack interface
H_h = Horizontal force in harped strands
L_{dh} = Available embedment length of harped strands
L_{dt} = Available embedment length of tension tie
V_h = Vertical force in harped strands
V_{nBV} = Nominal bond-shear capacity
X_s = Horizontal distance to vertical steel centriod
β = Inclination angle of harped strands
θ_c = Inclination angle of crack

FIGURE 3 Free body diagram of end region for bond-shear model.

Equation 2 was derived by summing moments about point 0 from FIGURE 3. The compression zone shear force, compression force, and aggregate interlock act through point 0 and are not included in the equation. Summing moments results in:

$$\Sigma M_0 = -V_{nBV}(d\cot\theta_c) + T\,d + V_s\,x_s + V_h(d_h\cot\theta_c) + H_h d_h = 0 \qquad 2$$

Rearranging Equation 2 gives equation 3 for nominal bond-shear capacity:

$$V_{nBV} = \frac{T}{cot\theta_c} + \frac{V_s\,x_s}{d\cot\theta_c} + \frac{V_h d_h}{d} + \frac{H_h d_h}{d\cot\theta} \qquad 3$$

Equations 4 through 6 were derived for calculating the tension tie force (T). These equations include contributions to the tie from the mild reinforcement and prestressing strands. Stress in the reinforcement and strands were assumed to be linearly proportional to the ratio of the available and required embedment lengths. Embedment lengths are discussed in the next section.

$$T = A_s f_{sBV} + A_{ps} f_{pBV} \quad (4)$$

$$f_{sBV} = f_y \left(\frac{L_{dt}}{l_{db}}\right) < f_y \quad (5)$$

$$f_{pBV} = f_{pe} \left(\frac{L_{dt}}{l_t}\right) < f_{pe} \quad (6)$$

Where:

f_{sBV} = stress in reinforcement bars accounting for available development length

f_{pBV} = stress in prestressing strands accounting for available development length

l_{db} = required development length of reinforcement bars

f_{pe} = effective prestress in strands

l_t = required transfer length for prestressing strand

Equations 7 through 9 were developed for calculating forces H_h and V_h in the harped strands. Equation 9 for stress in the harped strands is similar to equation 6, but with embedment of the harped strands (L_{dh}) substituted in place of the tie embedment (L_{dt}).

$$H_h = A_{ph}\, f_{pBVh} \cos\beta \quad (7)$$

$$V_h = A_{ph}\, f_{pBVh} \sin\beta \quad (8)$$

$$f_{pBVh} = f_{pe}\left(\frac{L_{dh}}{l_t}\right) < f_{pe} \quad (9)$$

Where:

A_{ph} = area of harped prestressing strands

f_{pBVh} = stress in harped prestressing strands accounting for available development length

Equation 10 can be used to calculate force in the vertical reinforcement at bond-shear failure. An equation for calculating stress in the vertical steel (f_{sv}) was derived using an experimental database and is discussed later in this paper.

$$V_s = A_v\, f_{sv} \quad (10)$$

Where:

A_v = area of vertical reinforcement crossing crack interface

f_{sv} = stress in vertical reinforcement

REQUIRED AND AVAILABLE EMBEDMENT LENGTHS

LRFD provisions can be used in the proposed model for determining the required development length of reinforcing bars (l_{db}) and the transfer length of prestressing strands (l_t). LRFD section 5.11.2.1.1 applies to development of reinforcing bars. Section 5.11.4.2 applies to prestressing strands and states that the transfer length is equal to 60 times the strand diameter.

Once the transfer length is known, Equations 6 and 9 can be used to calculate stresses in straight and harped strands, respectively. Both equations assume that the

available development length is less than the required transfer length and that the strand stress is linear related to the ratio between the available and required lengths. Furthermore, Equations 6 and 9 limit stress in the strands to the effective prestress. This approach is conservative in situations where the available development length of the strands is greater than the transfer length.

Equations 11 and 12 can be used to calculate the available embedment length of the tension tie. These equations are based on the assumption that an inclined crack forms in front of the bearing and that the available embedment length of the tie is equal to the distance from the end of the girder to the inclined crack (FIGURE 4). This assumption is consistent with observations of cracks made in numerous load tests of specimens failing in bond-shear (Barnes et al. 1998; Hawkins and Kuchma 2007; Kaufman and Ramirez 1988; Ma et al. 2000; Ross et al. 2011a; Ross et al. 2011b; Ross et al. 2013a; Shahway and Batchelor 1996). Terms in these equations are graphically defined in FIGURE 4.

$$L_{dt} = x_{oh} + x_{brg} + x_t \quad (11)$$

$$x_t = (h - d)(\cot\theta_c) \quad (12)$$

Where:

h = depth of member

x_{oh} = overhang distance beyond bearing

x_{brg} = greater of bearing distance or bearing plate width (when present)

x_t = horizontal distance between front of bearing and intersection of crack and tie

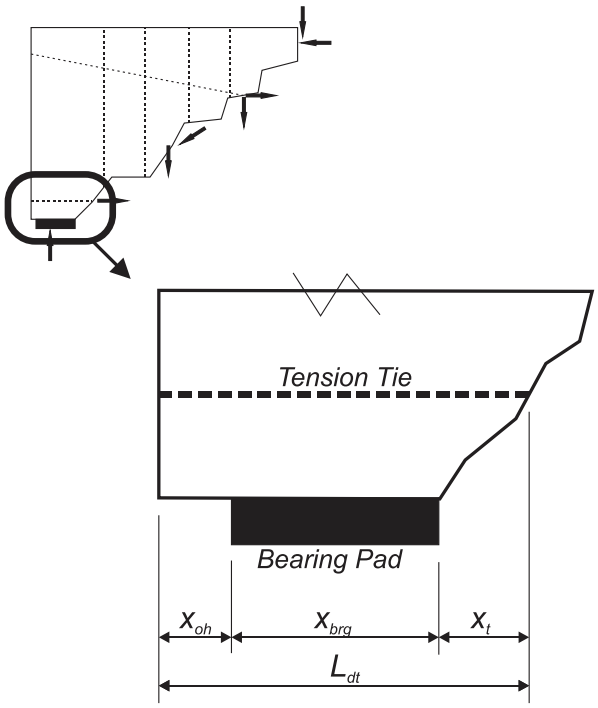

FIGURE 4 Definition of available development length variables.

BOND-SHEAR DATABASE

A database of experimental bond-shear failures was constructed for use in evaluating the proposed model. Data came from ten different test programs (Barnes et al. 1998; Deatherage et al. 1994; Hawkins and Kuchma 2007; Kaufman and Ramirez 1988; Ma et al. 2000; Maruyama and Rizkalla 1988; Ross et al. 2011a; Ross et al. 2011b; Ross et al. 2013a; Shahway and Batchelor 1996), having a total of 218 specimens. Of the 218 specimens, 84 failed in bond-shear and were included in the database. For purposes of compiling the database, failures were characterized as bond-shear where cracks occurred within the strand development length, strands slipped relative to the concrete, and the specimen failed to reach nominal flexural capacity.

As documented in FIGURE 5, specimens in the database have a range of variables. Approximately half of the specimens had compressive strengths greater than 50 MPa (7250 psi). Compressive strengths shown in FIGURE 5 are the tested strengths at the time each specimen was load tested. In cases where the tested strength was not reported, it was assumed to be 1.2 times the specified strength.

All of the database specimens had 1860 MPa (270 ksi) ultimate strength strands. Six of the specimens had harped strands, and the remaining 78 specimens had only straight strands. The area of prestressing shown in FIGURE 5 only includes the fully bonded straight strands. Many of the specimens also had partially debonded strands; however debonded strands cannot contribute to the tension tie and were not included in the data shown in the figure. Specified yield strength of the mild reinforcement was 415 MPa (60 ksi) in 80 of the specimens and 275 MPa (40ksi) in the remaining four.

Specimens in the database were simply supported and were load tested at shear span-to-depth (*a/d*) ratios ranging from 1.0 to 4.4. In five cases, the specimens were uniformly loaded and an effective *a/d* ratio was determined from the experimental slope of the inclined cracks. The vast majority of the specimens were built specifically for laboratory testing; however four specimens were girders salvaged from a bridge demolition project which were then tested in a laboratory.

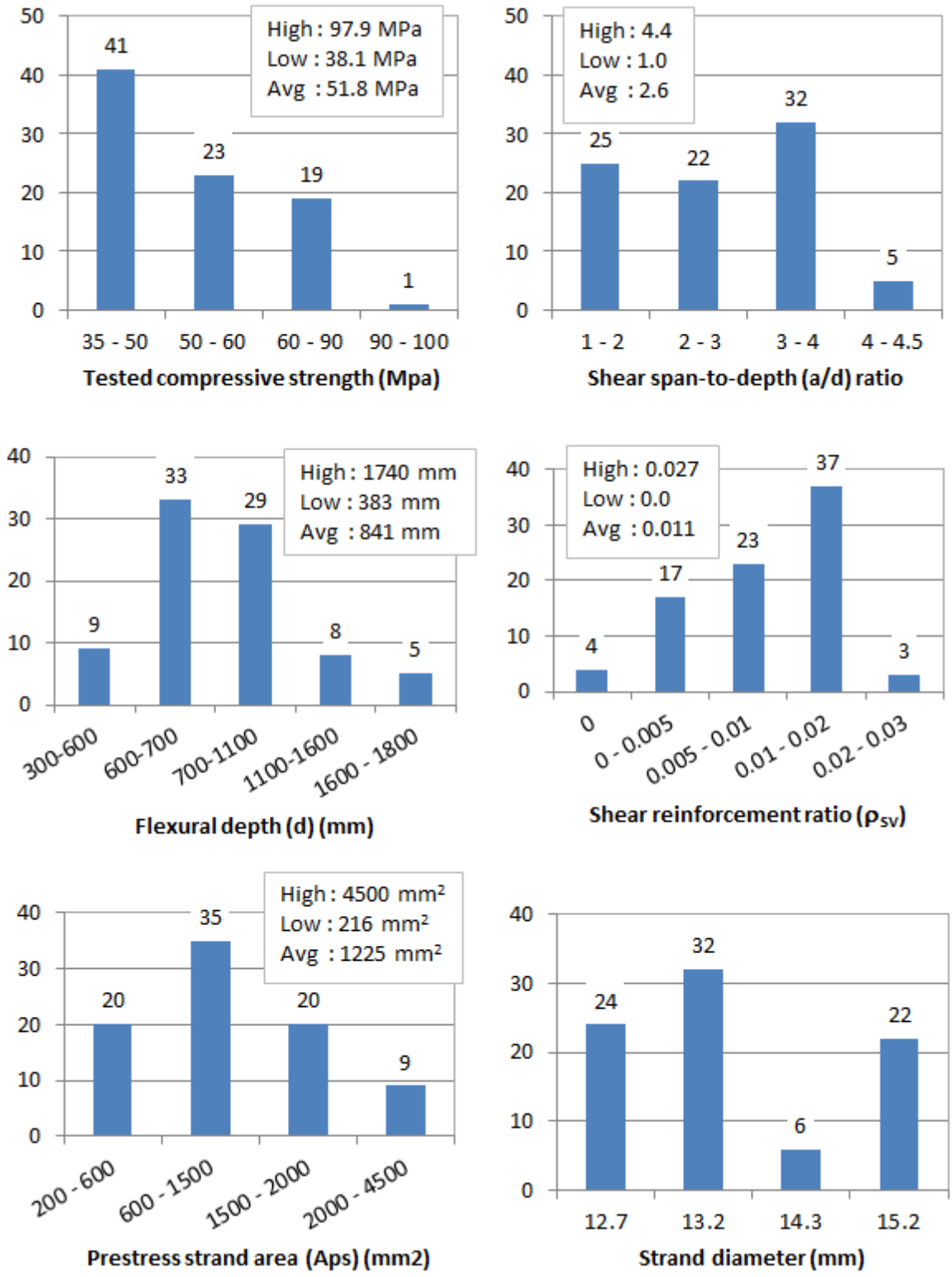

FIGURE 5 Details of specimens in bond-shear database.

VERTICAL REINFORCMENT STRESS AND DATABASE COMPARISON

Current LRFD provisions for the end region reinforcement (Equation 1) assume yielding of the vertical reinforcement. This assumption was tested using the bond-shear database by comparing the nominal and experimental bond-shear capacities. Nominal capacities were calculated using Equations 3 through 10. Stress in the vertical reinforcement was assumed to be the specified yield stress and the slope of the inclined crack ($cot\ \theta_c$) was assumed to equal the experimental *a/d* ratio. Using the *a/d* ratio as the slope of the inclined crack is consistent with experimentally observed crack patterns in the database specimens. Based on these assumptions, the calculated nominal capacities were 64% larger (unconservative) on average than the experimental capacities.

The conditions associated with the unconservative results are evaluated in FIGURE 6. This figure shows the nominal-to-experimental ratios of each database specimen plotted against the *a/d* and shear reinforcement ratios. The shear reinforcement ratio was calculated using Equation 13. FIGURE 6 shows a clear trend between the *a/d* ratio and the nominal-to-experimental ratio. For specimens with *a/d* ratios near 1.0 the nominal-to-experiment ratios were also near 1.0, indicating good agreement between the experimental data and the model. The model was not accurate for larger *a/d* ratios, where nominal capacities were up to 4.1 times greater than the experimental capacities. The relationship between the nominal-to-experimental ratio and shear reinforcement ratio was not as obvious as the relationship with *a/d*. The general trend, however, was that higher shear reinforcement ratios related to higher nominal-to-experimental capacity ratios and a greater degree of unconservitism.

Data in FIGURE 6 suggest that the assumptions for reinforcement stress and crack slope are reasonable for *a/d* less than approximately 2.5 and for shear reinforcement ratios less than approximately 0.015. Lack of agreement between model and the experimental results above these limits is attributed to larger amounts of vertical reinforcement. Where more reinforcement was present the load was spread over a greater reinforcement area and the stress decreased to levels less than yielding.

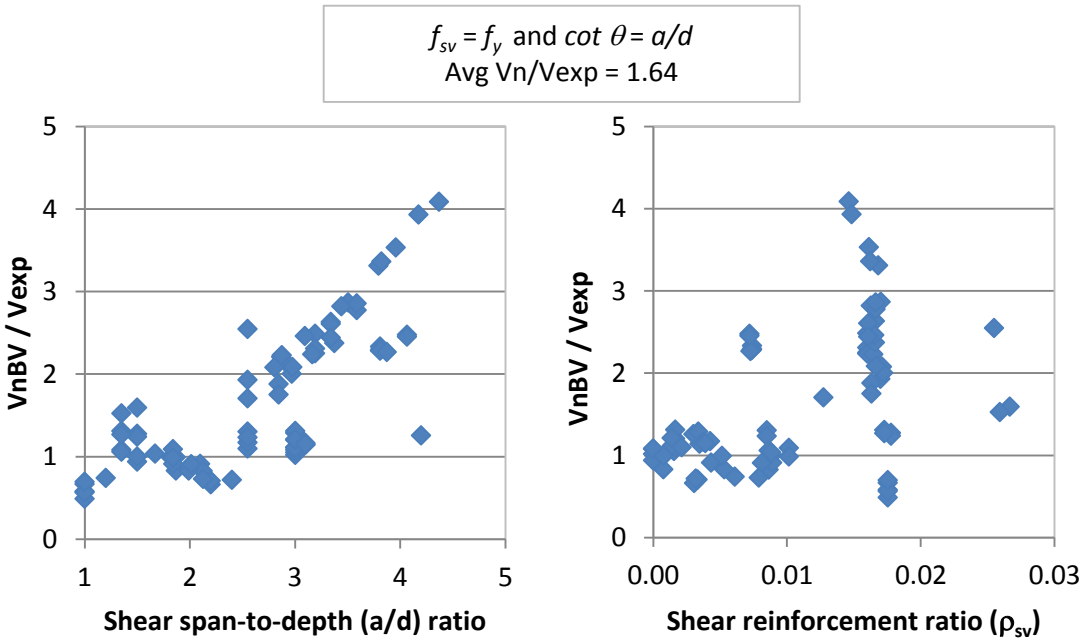

FIGURE 6 Nominal-to-experimental capacity ratio compared to specimen parameters ($f_{sv} = f_y$).

$$\rho_{sv} = \frac{A_v}{b_w d \cot\theta_c} \qquad 13$$

Where:

ρ_{sv} = shear reinforcement ratio

A_v = area of vertical reinforcement crossing assumed crack plane

b_w = web width

As an alternative to assuming that vertical reinforcement has yielded at bond-shear failure, Equation 14 can be used to calculate vertical reinforcement stress. This equation relates vertical reinforcement stress to the *a/d* ratio (expressed as $cot\ \theta_c$) and to the shear reinforcement ratio. When using Equation 14 larger *a/d* and shear reinforcement ratios affect lower stresses. Factors f_1, f_2, and κ_{sv} were empirically determined to provide a good fit with the bond-shear database. Nominal capacities calculated using equation 14 are compared to the database in FIGURE 7. As before, calculations assumed that slope of the inclined crack was equal to *a/d*. Using equation 14, the average nominal-to-experimental ratio was 0.99 with a standard deviation of 0.18. In contrast to comparisons made assuming the vertical reinforcement has yielded at bond-shear failure (FIGURE 6), the nominal-to-experimental ratios calculated using equation 14 do not vary as a function of the material, geometric, or detailing parameters (FIGURE 7).

Strain data from load tests gives another means of evaluating the reinforcement stress at bond-shear failure. Vertical reinforcement strain data has been reported by three researchers (Ma et al. 2000; Maruyama and Rizkalla 1988; Ross et al., 2013a) for nine of the database specimens. Reported strain in these specimens at bond-shear failure was always near or beyond yield strain. Each of these specimens had an *a/d* ratio or effective *a/d* ratio (slope of the inclined cracks) less than 2.1. Reinforcement stress calculated by equation 14 for these specimens was always within 27.6 MPa (4ksi) (7%) of yield stress. Based on the conservatism when compared with the available strain data, and on the

comparisons presented in FIGURE 7, it is concluded that equation 14 is a reasonable expression for calculating vertical reinforcement stress at bond-shear failure.

$$f_{sv} = (f_1 - f_2 \cot\theta_c)(1 - \kappa_{sv}\rho_{sv}) < f_y \quad (14)$$

Where:

f_{sv} = stress in vertical reinforcement

f_1 = empirical factor taken as 896 MPa (130 ksi)

f_2 = empirical factor taken as 193 MPa (28 ksi)

κ_{sv} = empirical factor taken as 26

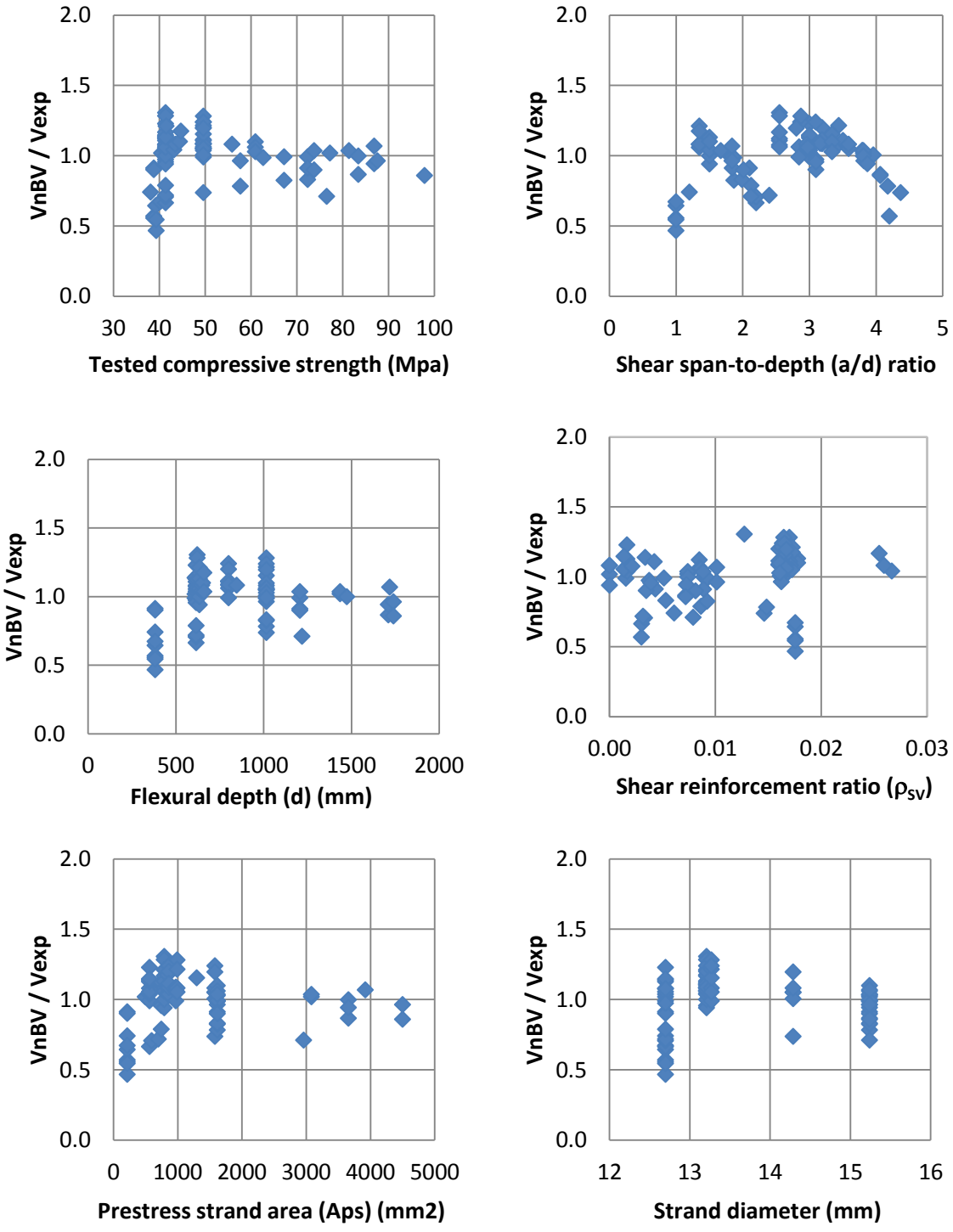

FIGURE 7 Nominal-to-experimental capacity ratios compared to specimen parameters (f_{sv} per Equation 14).

APPLICATION TO DESIGN

Nominal bond-shear capacity is highly dependent on the angle of the assumed end region crack, and care must be taken when determining an appropriate angle for use in the proposed model. In most design situations, it is recommended that the angle between the long axis of the girder and the direction of the principal compression stress in the web be used as the angle of the assumed crack. Procedures in LRFD 5.8.3.4.2 can be used to determine this angle. This approach is consistent with the current LRFD requirements of section 5.8.3.5 as presented in Equation 1 and . In situations where the proposed model is used to evaluate bond-shear capacity of existing pretensioned girders with cracks, then use of the observed crack angle is recommended. Recent work at Oregon State University has confirmed the validity of this approach for reinforced concrete bridge girders (Triska et al. 2013).

Calculated values presented in FIGURE 7 assumed that the crack slopes were equivalent to each experimental specimen's *a/d* ratio. This approach was consistent with crack orientations reported in the database literature and was deemed appropriate for the comparison. For design situations this approach is only recommended when point loads are applied at fixed *a/d* ratios such that the principal compression angle is driven by the shear force magnitude and load geometry. This is generally not the case in highway bridge girders.

A comprehensive reliability analysis is required to determine an appropriate strength reduction factor (ϕ) for the proposed model. In absence of such analysis, a possible strength reduction factor of 0.75 is suggested. As demonstrated in FIGURE 8 a

strength reduction factor of 0.75 gives design strength (ϕV_n) values that are less than experimental capacities of each specimen in the bond-shear database. Use of 0.75 as a strength reduction factor is consistent with the approach used in the ACI 318 code (ACI-318-11) for evaluating the capacity of sections occurring within the strand transfer length.

Equation 15 is presented to assist designers in selecting an appropriate number of fully bonded strands to prevent premature bond-shear failure. This equation was derived by substituting Equation 4 for the tie force in Equation 3 then rearranging to solve for the area of prestressing. Additionally, the factored shear force divided by the strength reduction factor (V_u/ϕ) was substituted for the nominal bond-shear capacity (V_{nBV}). The area of prestressing strands calculated by Equation 15 is the area of fully bonded strands recommended to prevent bond-shear failure. Strands in excess of this amount can be partially debonded without creating undue risk of bond-shear failure.

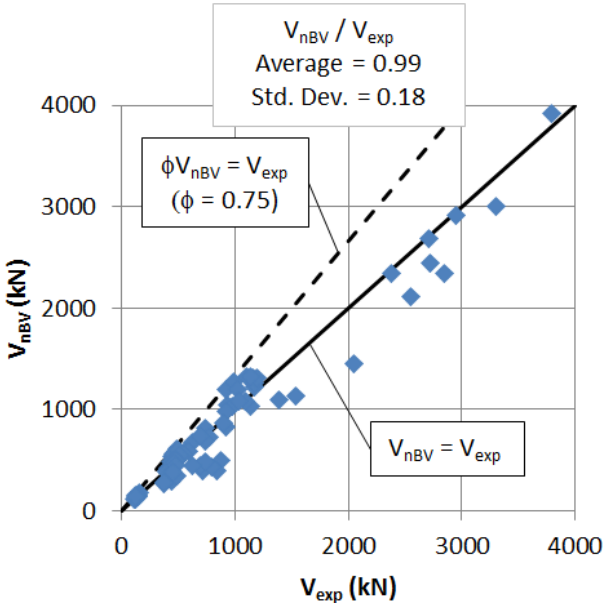

FIGURE 8 Model to experimental comparison (f_{sv} per Equation 14).

$$A_{ps,reqd} = \left[\left(\frac{V_u \cot\theta_c}{\phi} - \frac{V_s X_s}{d} - \frac{V_h d_h \cot\theta_c}{d} - \frac{H_h d_h}{d}\right) - A_s f_{sBV}\right]\left(\frac{1}{f_{pBV}}\right) \quad 15$$

Where:

$A_{ps,reqd}$ = Area of fully bonded prestressing required to prevent bond-shear failure

ϕ = strength reduction factor

Use of Equation 15 to select an area of prestressing will require an iterative design process. This is because the inclination angle of cracking (θ_c), stress in the strands (f_{pBV}), and stress in the vertical reinforced (f_{sv}) are a functions of prestressing quantity (A_{ps}). The flowchart is offered as a guide for iterative design (FIGURE 9). As an alternative to iterative design, a conservative value for the crack inclination angle could be assumed at the beginning of design and checked at the end.

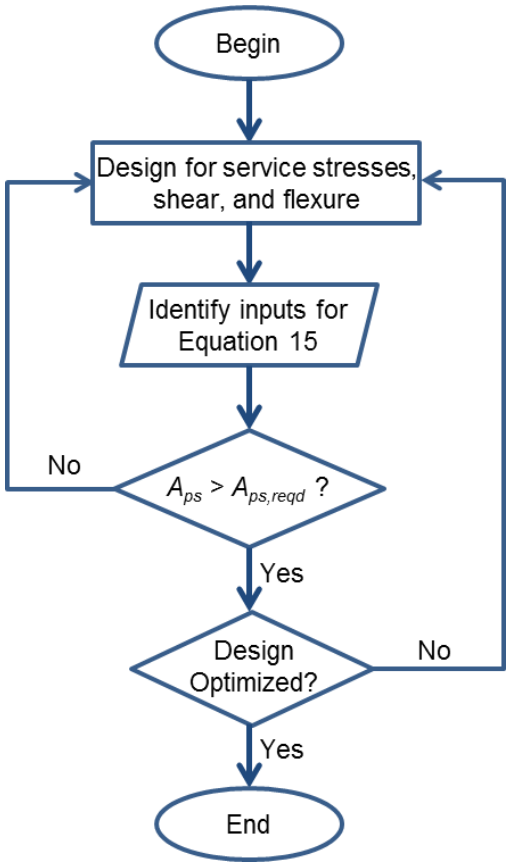

FIGURE 9 Bond-shear design flowchart.

SUMMARY AND CONCLUSION

A model for nominal bond-shear capacity of pretensioned concrete girders was presented. The model was derived from moment equilibrium of the end region and considers variables such as girder and bearing geometry, reinforcement and prestressing details, and inclination angle of end region cracking. Nominal capacities calculated by the model were compared to the experimental bond-shear capacities of 84 specimens from the literature. On average the nominal capacities calculated by the proposed model

were within 1% of the experimental capacities. The ratios of nominal-to-experimental capacity had a standard deviation of 18%.

The proposed model provides a direct method for calculating the quantity of fully bonded strands required to prevent bond-shear failure. Strands in excess of this amount can reasonably be debonded without creating undue risk of bond-shear failure. In some circumstances the model may justify exceedance of the AASHTO limits for partial strand debonding.

REFERENCES

AASHTO. (2010). *AASHTO LRFD Bridge Design Specifications,* 5th ed., Washington, D.C.

ACI 318-11. (2011). "Building code requirements for structural concrete and commentary." *American Concrete Institute (ACI).* Farmington Hills, MI.

Barnes, R. W., Burns, N. H., and Kreger, M. E. (1999). "Development length of 0.6-inch prestressing strand in standard I-shaped pretensioned concrete beams." *Rep. No. FHWA/TX-02/1388-1,* Texas DOT, Austin, TX.

Burgeno, R., and Sun, Y. (2011). "Effects of debonded strands on the production and performance of prestressed concrete beams." *Report CEE-RR-2011/01,* Michigan DOT, MI.

Csagoly, P. (1991). "A shear model for prestressed concrete beams." *Report 9900 1550,* Florida DOT, Tallahassee, FL.

Deatherage, J. H., Burdette, E. G., and Chew, C. K. (1994). "Development length and lateral spacing requirements of prestressing strand for prestressed concrete bridge girders." *PCI J.*, 39(1), 70-83.

Hawkins, N. M., and Kuchma, D. (2007). “Application of LRFD bridge design specifications to high-strength structural concrete: shear provisions.” *National Cooperative Highway Research Program report 579*. Transportation Research Board of the National Academies, Washington, D.C.

Kaufman, M. K., and Ramirez, J. A. (1988). “Re-evaluation of the ultimate strength behavior of high-strength concrete prestressed I-beams.” *ACI Struct. J.*, 85(3), 295-303.

Ma, Z., Tadros, M. K., and Baishya, M. (2000). “Shear behavior of pretensioned high-strength concrete bridge I-girders.” *ACI Struct. J.*, 97(1), 185-192.

Maruyama K., and Rizkalla, S. H. (1988). “Shear design consideration for pretensioned prestressed beams.” *ACI Struct. J.*, 85(5), 492-498.

Okumus, P., and Oliva, M. G. (2013). “Evaluation of crack control methods for end zone cracking in prestressed concrete bridge girders.” *PCI J.*, 58(2), 91-105.

Ross, B. E., Ansley, M. H., and Hamilton, H. R., III. (2011a). “Load testing of 30-year-old AASHTO Type III highway bridge girders.” *PCI J.*, 56(4), 152-163.

Ross, B. E., Hamilton, H. R., and Consolazio, G. R. (2011b). "Experimental and analytical evaluations of confinement reinforcement in pretensioned concrete beams." *Transportation Research Record 2251*, Transportation Research Board, Washington, DC, 59-67.

Ross, B. E., Consolazio, G. R., and Hamilton, H. R. (2013a). "End region detailing of pretensioned concrete bridge girders." *Rep. No. BDK-75-977-05*, Florida DOT, Tallahassee, FL

Ross, B., Consolazio, G. R., and Hamilton, H. R. (2013b). "Experimental evaluation of bottom flange splitting cracks in I-girders." *PCI Convention and National Bridge Conference*, Grapevine, TX.

Shahawy, M. A., and Batchelor, B. (1996). "Shear behavior of full-scale prestressed concrete girders: comparison between AASHTO specifications and LRFD Code." *PCI J.*, 41(3), 48-62.

Triska M. A., Goodall J. K., and Higgins C. (2013). "Flexural anchorage behavior in diagonally cracked girders: experiment." *ACI Struct. J.*, 110(2), 263-274.

CHAPTER FOUR

EVALUATION OF THE AASHTO LRFD STRAND DEBONDING LIMITATIONS IN THE CONTEXT OF BOND-LOSS FAILURE

Abstract: Debonding of select strands is an effective means of controlling stresses and cracking at the ends of pretensioned concrete girders, but can also have adverse effect on shear capacity due to loss of strand-concrete bond. To ensure sufficient shear capacity, the current AASHTO LRFD Bridge Design Specifications recommend that strand debonding be limited to no more that 25% of strands. This paper analytically evaluates the conservatism of the 25% debonding limitation with respect to shear failures involving loss of strand-concrete bond (i.e. bond-loss failure). This is accomplished by calculating the bond-loss capacity of six in-service bridge girders from different states and for varying levels of strand debonding. Calculations are based on a model previously published by the authors. It is determined that limiting strand debonding to 25% is conservative for all girders; however, the degree of conservatism is inconsistent. The demonstrated methodology can be used to balance the competing criteria of preventing bond loss failure and controlling end region cracking.

Introduction

End region cracks are horizontal and diagonal web cracks that form at the ends of pretensioned concrete I-girders during or soon after prestress transfer (Figure 1). The American Association of State Highway and Transportation Officials' *AASHTO LRFD*

Bridge Design Specifications (AASHTO 2014) (hereafter "LRFD") refers to this phenomenon as "splitting". End region splitting cracks have been studied for decades, and it has been suggested that splitting stresses causing end region cracks are larger in modern girders due to increased size, slenderness, and prestressing force (Gamble 2014).

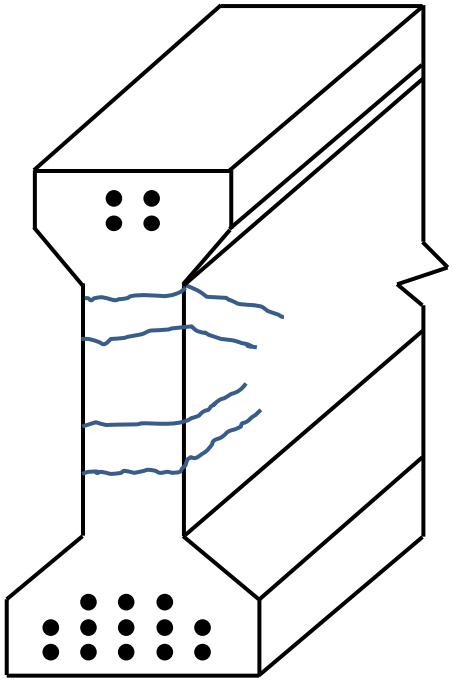

Figure 1. End-Region Cracking of I-Girder.

Splitting forces at the end of girders occur as eccentric pretension forces are transferred into the bottom flange then distributed to the rest of the cross-section (Figure 2(a)). Strand debonding is a common procedure used to reduce splitting stresses. Debonding is also used to control tensile stresses and cracking in the top flange within the end region, particularly prior to erection and placement of dead loads. The approach is to move the transfer length of select strands away from the girder end by placing plastic sheathing around the strand (Figure 2(b)). Because force transfer between

debonded strands and concrete occurs away from the girder end, splitting forces due to the debonded strands spread over a greater area of concrete; and thus, splitting cracks are mitigated. Fully bonded and partially debonded strands are commonly used together in the same girder; in this condition splitting forces are distributed over the end region, the attendant tensile stresses are reduced, and less cracking occurs (Burgeno and Sun 2011; Okumus and Oliva 2013; Ross et al. 2014).

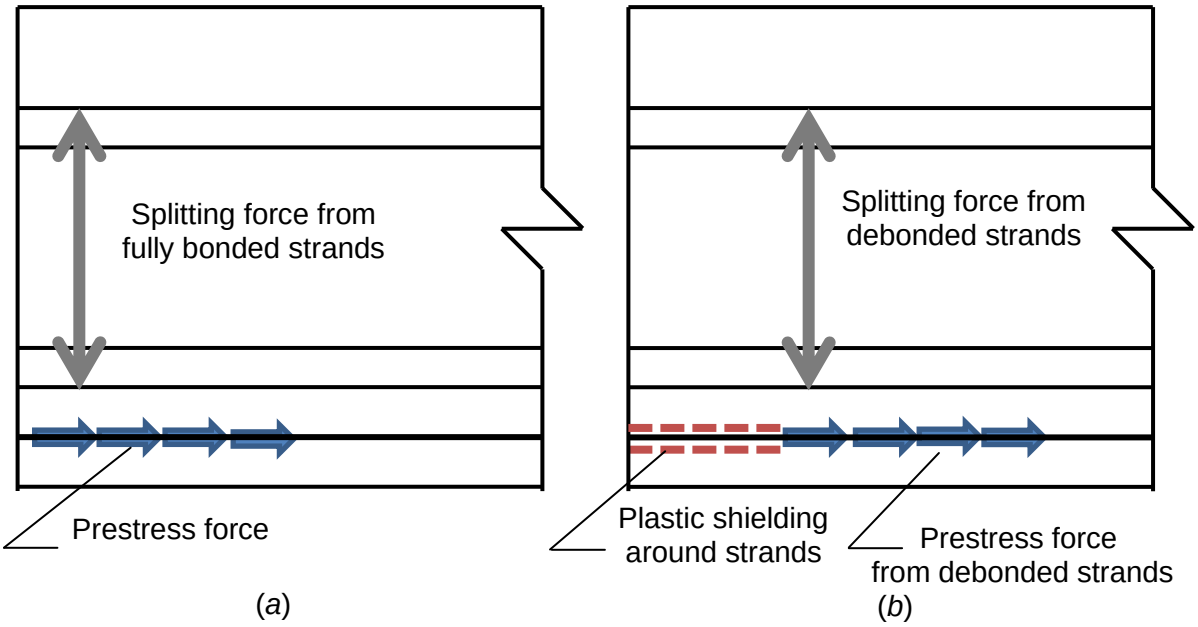

Figure 2. Splitting Force in End Region from Fully Bonded Strands (a) and Partially Debonded Strands (b).

While the use of debonded strands has a positive effect in reducing end region cracking and tensile stresses in the top flange, it also has a negative impact on the shear strength of the end region (Csagoly 1991; Ross et al. 2014). In particular, strand debonding affects a reduction in bond-loss capacity. Therefore, the durability and serviceability benefits of strand debonding must be balanced with the need for sufficient

resistance to bond-loss failure. These competing objectives are addressed by the strand debonding limitations of LRFD section 5.11.4.3. This section requires that the number of partially debonded strands may not exceed 25% of the total number of strands. According to LRFD commentary this limit is based on tests conducted by the Florida Department of Transportation (Shahawy and Batchelor 1991; Shahawy et al. 1993), which indicate that the anchored strength of the strands is one of the primary contributors to the shear resistance of prestressed concrete girder end regions. The commentary also states that shear resistance should be "meticulously investigated" when strands are debonded in excess of 25%. The purpose of this paper is to evaluate the level of conservatism inherent in the 25% limit. Is 25% debonding safe? Overly safe? Does this limit create a consistent level of safety?

Background

Bond-loss failures have been extensively observed in load tests of pretensioned concrete I-girders (Ross and Naji 2014). Many different terms have been used to label bond-loss failures, as these failures can exhibit subtly different types of structural behavior (Naji et al. 2016). The common feature of bond-loss failures is the formation of cracking near supports due to applied loads (Figure 3(a)). These cracks interrupt strand development. If the available development length between the end of the girder and the crack is less than the required development length, then the strands slip relative to the concrete and lose ability to transfer the attendant tie forces (Figure 3(b)). Strand slip allows cracks to lengthen, open wider, and causes rotation about the crack tip. If the slip, internal forces, and resulting rotation are sufficient, then the compression zone will fail

due to combined shear and compression. However, when transverse reinforcement is provided, it acts to prevent the crack from opening and lends capacity and ductility to the bond-loss failure mechanism.

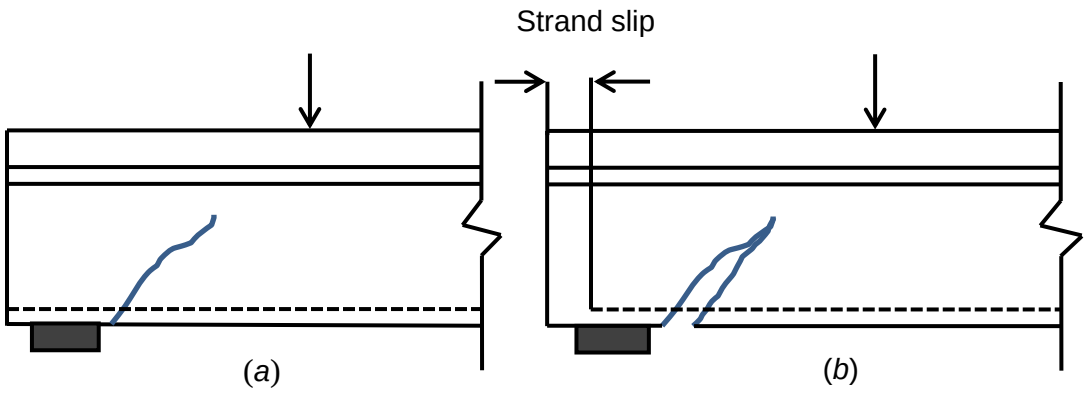

Figure 3. Formation of Cracks near Support (a) and Slippage of Strands Relative to the Concrete (b).

Strand debonding affects resistance to bond-loss failure. Because debonded strands are not anchored at the end of the girder, they cannot contribute to the strength of the end region after the formation of cracks near the support. Thus resistance to bond-loss failure is only provided by fully bonded strands. When a sufficient number of fully bonded strands are present, the strands are able to resist slipping even after cracks interrupt their development.

Currently, the National Cooperative Highway Research Program (NCHRP) is conducting a comprehensive study of partial debonding effects on the performance of pretensioned girders, NCHRP 12-91. According to the project synopsis provided by NCHRP (Shahrooz 2012), it is expected that the research will result in information regarding the integral role of strand anchorage on the shear performance of pretensioned

beams. The current paper is presented as a complimentary, albeit much smaller, study of strand anchorage and debonding.

Bond-Loss Database and Model

Ross and Naji (2014) presented a model for calculating nominal capacity of pretensioned girders against bond-loss failure (in the original paper the model was referred to as "bond-shear" model) and compared the model to a database of 84 published test specimens (Barnes et al. 1998; Deatherage et al. 1994; Hawkins and Kuchma 2007; Kaufman and Ramirez 1988; Ma et al. 2000; Maruyama and Rizkalla 1988; Ross et al. 2011a; Ross et al. 2011b; Ross et al. 2013; Shahway and Batchelor 1996). The model is highly correlated with the test data (R^2=0.94), having a coefficient of variation (COV) of 0.19. For comparison, The COV of code-based models for prestressed girder shear capacity ranges from 0.22 and 0.33 (Nakamura et al. 2013). Similar to the minimum flexural steel provisions of LRFD section 5.8.3.5, the bond-loss model (Figure 4) is based on moment equilibrium of the end region; however, the model relies on fewer simplifications and is consequently applicable to a wider range of girders. Equation (1) for nominal bond-loss capacity can be derived by the summation of moments about point 0 in Figure 4:

$$V_{nb} = \frac{T}{cot\theta} + \frac{V_s\, x_s}{d\cot\theta} + \frac{V_h d_h}{d} + \frac{H_h d_h}{d\cot\theta} \quad (1)$$

Where

V_{nb} = nominal bond-loss capacity

T = capacity of prestressing in the bottom tie, accounting for the available development length

θ = inclination angle of end region cracks; the inclination angle of principal compressive stress

V_s = shear resistance provided by the transverse reinforcement at the section under investigation

X_s = horizontal distance to vertical steel centroid

d = flexural depth of tension tie

V_h = vertical force in harped strand

d_h = depth of harped strands at crack interface

H_h = horizontal force in harped strand

L_{dt} = available embedment length of tension tie

L_{dh} = available embedment length of harped strand

a = shear span

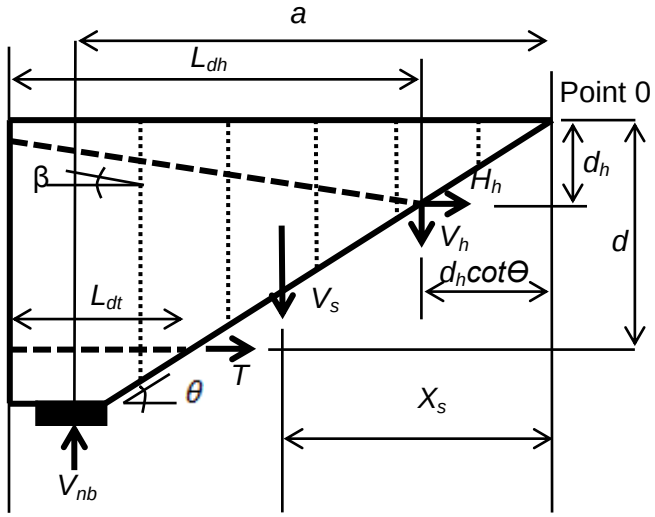

Figure 4. Free Body Diagram of End Region for Bond-Loss Model

Tension tie force (T) in Equation (1) includes contributions of prestressing strands and, when present, non-prestressed reinforcement. Force in the reinforcement and strands are assumed to be linearly proportional to the ratio of the available (l_{dt}) and required embedment length (l_t). The same approach is used for calculating force in the harped strands, terms V_h and H_h in Equation (1), but with different available embedment length (l_{dh}) than the tension tie. In this manner, the model follows the requirement from LRFD section 5.8.3.5 that "Any lack of full development length shall be accounted for". Note that in calculating tension tie force (T) in Equation (1), L_{dt} and L_{dh} were determined at the center of gravity of strand group.

Force in the vertical reinforcement (V_s) also contributes to the bond-loss capacity. Current LRFD provisions for end region reinforcement assume yielding of the vertical reinforcement. This assumption was tested by Ross and Naji and found to be inaccurate for girders with large shear span-to-depth ratios (a/d) and densely placed shear reinforcement. Equation (2) was proposed to account for circumstances where vertical reinforcement does not yield at bond-loss failure. The equation is used to calculate vertical reinforcement stress incident with bond-loss failure, and produces values less than yield stress for girders with large a/d and shear reinforcement ratios (ρ_{sv}). Equation (2) was empirically derived and factors f_1 , f_2, and k_{sv} were selected based on fit with the 84 tests specimens in the database (9). When combined with Equation (1), the resulting model produces consistent levels of accuracy for a range of variables such as girder size, shear reinforcement details, and material properties.

$$f_{sv} = (f_1 - f_2 \cot\theta)(1 - \kappa_{sv}\rho_{sv}) < f_y \quad (2)$$

Where

f_{sv} = stress in vertical reinforcement

f_y = yield stress in vertical reinforcement

f_1 = empirical factor taken as 896 MPa (130 ksi)

f_2 = empirical factor taken as 193 MPa (28 ksi)

k_{sv} = empirical factor taken as 26

ρ_{sv} = shear reinforcement ratio

In above equation, the shear reinforcement ratio is calculated as:

$$\rho_{sv} = \frac{A_V}{b_w d \cot\theta}$$

Where

A_v = area of vertical reinforcement crossing assumed crack plane

b_w = web width

Evaluation of 25% Debonding Limitation

Methodology

In this section, the bond-loss capacity model is used to evaluate the conservativeness of the 25% debonding limitation for six different in-service highway bridge girders. The approach is to compare the factored shear force on each girder to the nominal bond-loss capacity for different levels of debonding. Essential details of the in-service girders are presented in Table 1. Plans for the girders and associated bridges were obtained through email requests sent to state transportation departments. In this manner

the evaluations are based on realistic loads, girder sizes, strand quantities, and reinforcement details.

In addition to the six girders reported in Table 1, plans were also received for bridges in Nebraska, South Dakota, and Alaska. Plans from these states were not considered in the current study because the girders were detailed such that select strands were extended and anchored into cast-in-place concrete end diaphragms. Through this detail, strand-concrete bond capacity is improved as the anchored strands are fully developed through embedment in the diaphragm (Ma et al., 2000). The combination of strand debonding and anchoring in end diaphragms is mentioned here as a possible strategy for balancing end region serviceability and strength requirements; however, none of the specimens in the bond-loss database had this combination of variables, and the modeling approach used in the current study has not been validated for such girders. Thus, the current study focuses only on girders with strands that are not anchored in end diaphragms.

Table 1. Details of In-Service Girders Used in Evaluation.

State	Year built	Cross section	Span *L*, m.	Height *H*, m.	Total number of straight strands (% dedonded)	Girder spacing, m.	Total number of harped strands	Strand diameter, cm.
MD	2008	PCEF Bulb tee	33	1.4	51(0%)	2.7	21	1.27
FL	2010	FIB-54	37	1.4	39(25%)	3	0	1.5
AL	2012	AASHTO type II	18	0.9	22(15%)	2.4	0	1.27
AL	2012	Bulb tee	33	1.6	24(0%)	2.4	8	1.5
VT	2013	PCEF Bulb tee	48	2.2	42(0%)	2.6	10	1.5
AZ	2014	AASHTO type V	37	1.6	49(0%)	2.7	18	1.27

Factored loads for each in-service girder were calculated using a commercial bridge design software (Leap Bridge Enterprise 2013). Accuracy of the software results was verified in select cases through comparison with hand calculations. Once verified, the factored loads from the software were used for the remainder of the evaluation.

The nominal bond-loss capacity of each girder was calculated using Equation (1) and (2). To evaluate the effects of debonding, nominal bond capacity was calculated for four debonding levels (0, 15, 30, and 45 percent). Note that these levels of debonding are different from the in-service conditions reported in the table. Percent debonding was the

only variable in the evaluation; for purpose of calculations, the area of prestressing (A_{ps}) was adjusted in the equations based on the different levels of debonding. All other material and geometric properties were treated as constants and were obtained from the bridge plans provided by the state DOTs.

The angle of inclination of diagonal compressive stresses (θ) was determined as part of the calculations. This angle is different for each level of debonding because the quantity of fully bonded strands affects the level of prestress force, and hence the stress state and the crack angle in the end region. The angle was estimated using Equation (3). This equation comes from the shear design provisions of LRFD (1):

$$\theta = 29 + 3500\varepsilon_s \tag{3}$$

Where, ε_s is net longitudinal tensile strain in the section at the centroid of the tension reinforcement, and is calculated as:

$$\varepsilon_s = \frac{\left(\frac{|M_u|}{d_v} + 0.5N_u + |V_u - V_p| - A_{ps}f_{po}\right)}{E_sA_s + E_pA_{ps}} \tag{4}$$

Where:

A_{ps} = area of prestressing steel on the flexural tension side of the member

A_s = area of nonprestressed steel on the flexural tension side of the member

f_{po} = a parameter taken as modulus of elasticity of prestressing tendons multiplied by the locked-in difference in strain between the prestressing tendons and the surrounding concrete

N_u = factored axial force

M_u = absolute value of the factored moment

V_u = factored shear force

V_p = component in the direction of the applied shear of the effective prestressing force

d_v= effective shear depth

E_p = modulus of elasticity of prestressed steel

E_s = modulus of elasticity of nonprestressed steel

The inclination angle of the compressive stress was calculated for an assumed critical location at 1.2*d* from the face of the support. This location was selected because it is at or near the location where critical cracks formed in experimental tests contained in the bond-loss failure database (9). The bond-loss model (Figure 4) assumes that the inclination angle of the compressive stress is the angle of the inclined crack that leads to failure.

LRFD section 5.8.3.4.2 requires that if the value of ε_s, calculated from Equation (4) is negative, then it should be taken as zero or the value of ε_s should be recalculated (as was done in this research) by adding the stiffness of the concrete in the precompressed tensile zone (E_cA_{ct}) to the denominator of the equation. However, ε_s should not be taken as less than -0.004. Based on this lower limit for strain, the minimum value of θ is 27.6 degrees. Additionally, LRFD requires that ε_s should not be taken greater than 0.006, resulting in a maximum value of θ equal to 50 degrees.

Capacities calculated from the bond-loss model were then compared to the factored shear loads from the structural analysis of the bridges. These calculations were repeated for each of the six in-service girders and for each level of debonding.

Results and Discussion

Figure 5 presents the results of the evaluation in terms of the strength-to-load ratio, V_{nb} / V_u. As seen in the figure, nominal bond-loss capacity decreases approximately linearly as the percentage of debonding increases. This reduction in bond capacity is attributed to the decrease in the quantity of fully-bonded strands available to act in the tension tie. At the LRFD limit of 25% debonding the strength-to-load ratio (factor of safety) is between 1.8 and 2.7, meaning that the girders have 80% to 170% more bond-loss capacity than the factored load requires. This result indicates that the LRFD 25% debonding limitation produces conservative bond-loss capacities for each of the in-service girders. The limitation, however, does not create a uniform level of conservatism in the girder sample.

When all strands are fully bonded the strength-to-load ratio is between 2.3 and 3.1. These are the largest values in the evaluation, and are attributed to the positive effect of fully bonded strands on bond-loss capacity. The lowest strength-to-load ratios correspond to the FIB-54 girder from Florida and the largest correspond to the girder from Maryland; however, the nominal bond-loss capacity was conservative for all girders and all levels of debonding considered.

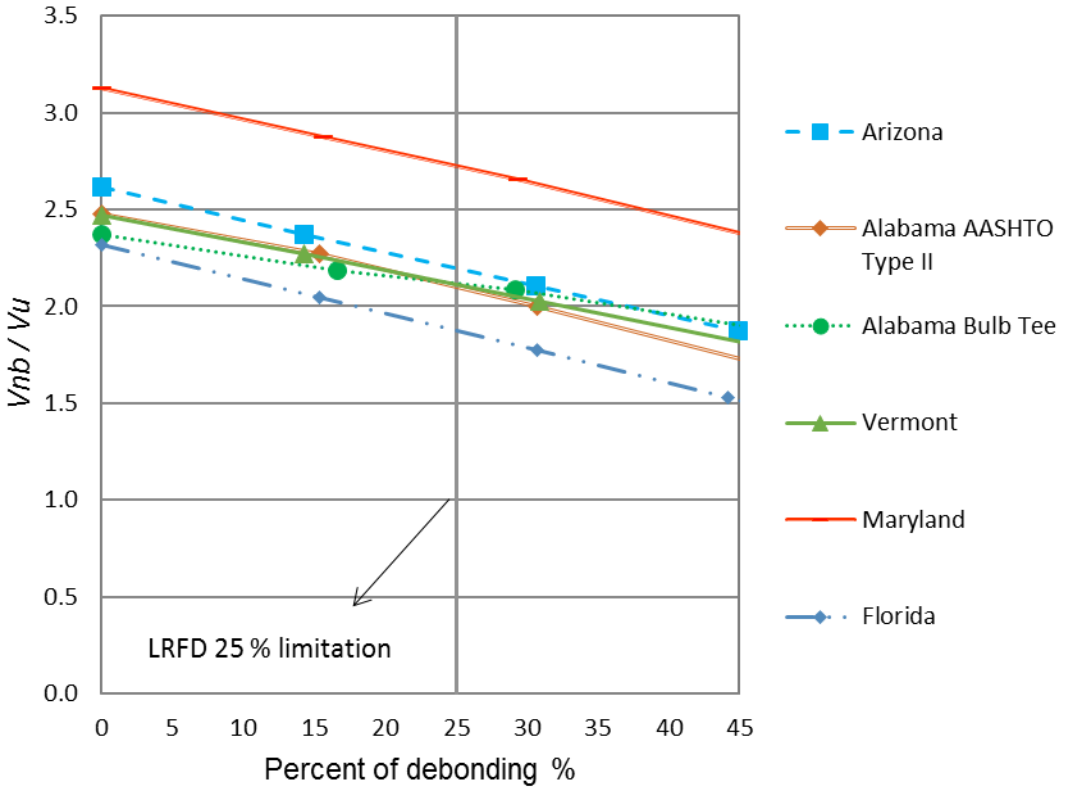

Figure 5. Nominal Bond-Loss Capacity-to-Factored Shear Load Ratio at Different Strand Debonding Levels for Six In-Service Girders.

Many factors impact the strength-to-load ratios shown in Figure 5. Spacing and span length impact the factored shear force in the denominator. Girder details, specifically flexural and transverse reinforcement quantities, impact the nominal bond-loss capacity in the numerator. Variations in these parameters are the reason for the differences between girders observed in Figure 5. To explore the effects of these variations, Figure 6 shows the contributions to bond-loss resistance of flexural reinforcement (First term in Equation (1)), transverse reinforcement (Second term in Equation (1)), and harped strands (third and fourth terms in Equation (1)) for each girder.

Results in the figure are normalized by the factored shear force and indicate the relative contribution of flexural, transverse, and harped reinforcement to bond-loss resistance. A relatively high value in the figure indicates a larger contribution. The information shown in the Figure 6 corresponds to 0% level of debonding. This level of debonding was selected for the comparison, because it was the most common percentage in the sample girders.

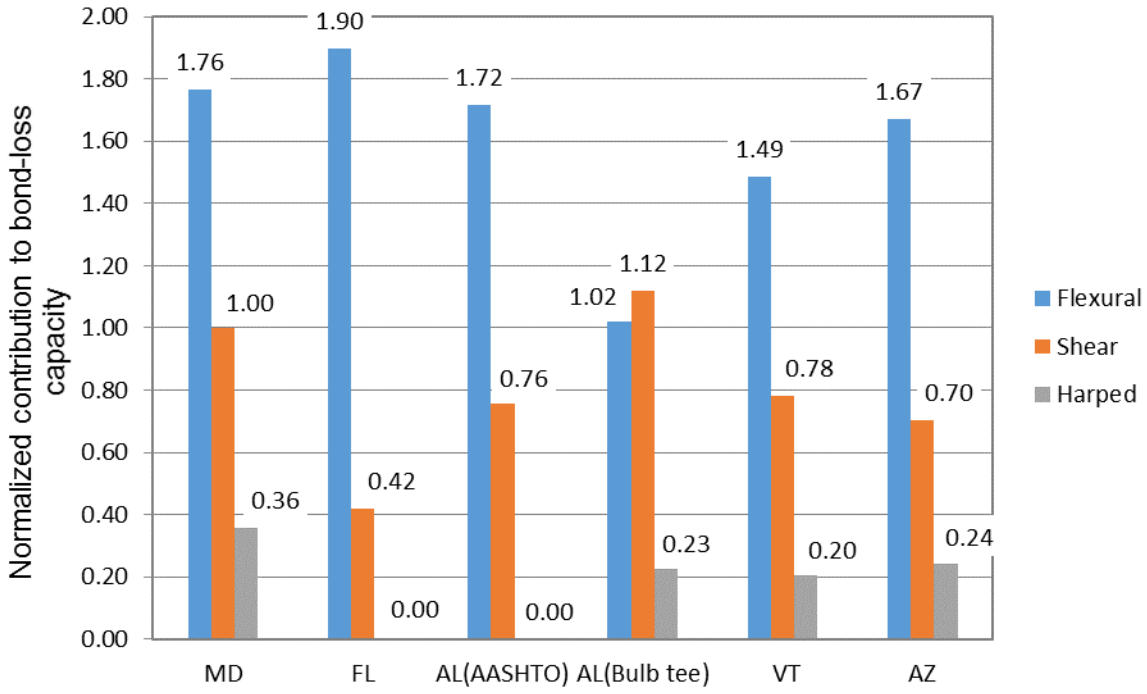

Figure 6. Normalized Contribution to Bond-Loss Capacity for 0% Debonding Level.

The values presented in Figure 6 provide a means of comparing the differences between girders observed in Figure 5. Maryland had the highest strength ratio overall. The large strength-to-load ratio of the girder from Maryland is attributed to the relatively large flexural, transverse, and harped reinforcement contributions, having normalized values of 1.76, 1.0, and 0.36, respectively. The Florida girder had the lowest overall

strength ratio, and is attributed to the low contribution of transverse reinforcement and absence of harped strands. Although the Florida girder had the lowest overall strength ratio, it had the highest relative contribution from the flexural reinforcement. The FIB cross section used for the Florida girder allows for large quantities of prestressing strands to be placed low in the cross section, thus leading to the large contribution of bond loss resistance from flexural reinforcement.

To provide context for assessing bond-loss resistance for the girders, bond-loss and shear capacities are compared in Figure 7. Shear capacities for each in-service girder for all debonding levels (0 , 15, 30, and 45 %) were calculated using shear design provisions of LRFD section 5.8.3.3 (Equations (5.8.3.3-1) and (5.8.3.3-2)). As seen in Figure 7, as percent of debonding increases, girders move towards bond-loss controlling; bond-loss governs for all cases in the analysis when percentage of debonding is greater than 45%. On the contrary, shear becomes the controlling factor in capacity as percent of debonding decreases. Shear governs for all cases in the analysis when percent of debonding is less than 15 %. At LRFD 25% debonding level, shear is the controlling factor in three girders (MD, AL AASHTO, and AZ girders), and bond-loss governs in the remaining girders (VT, AL bulb tee, and FL girders). Additionally, as can be interpreted from Figure 7 and Table 1, shear governs for in-service conditions of all girders except the Florida girder.

Increased levels of debonding lead to lower levels of prestressing and thus to lower concrete shear contribution and lower shear strength. As demonstrated in Figure 5, increased debonding also leads to lower bond-loss capacity. The relative effects of

debonding are greater on bond-loss capacity than on shear capacity, as demonstrated by the downward trends shown in Figure 7.

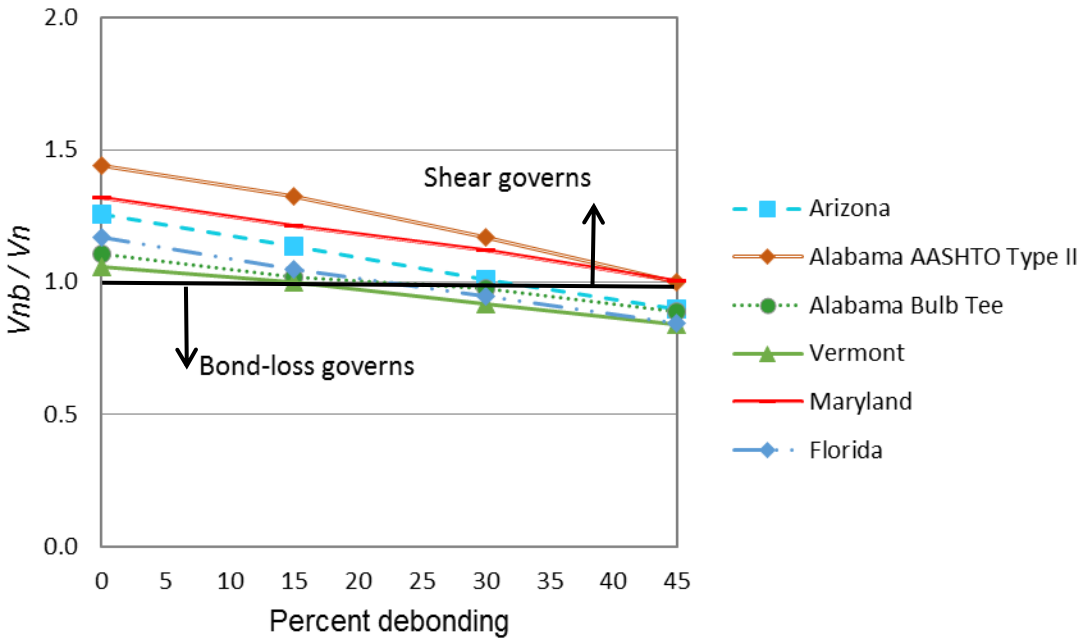

Figure 7. Bond Loss-to-Shear Capacity Ratio for In-Service Girders. Bond Loss Capacity Calculated by Earlier Model (Ross and Naji, 2014). Shear Capacity Calculated by AASHTO LRFD.

Minimum Number of Strands

Based on the model, each of the six girders could have maintained bond-loss resistance while also taking advantage of the serviceability and durability benefits of exceeding the LRFD debonding limitation. As a guide for balancing the strength benfits of fully bonded strands with the serviceability benefits of debonding, the minimum quantity of fully bonded strands needed to resist bond-loss failure can be directly calculated using Equation (5). This equation was derived by rearranging Equation (1)

and substituting the term $n_b A_{ps1} f_{pb} + A_s f_{sb}$ for the force in the tension tie, T. Additionally, the factored shear force divided by the strength reduction factor (V_u / ϕ) was substituted for the nominal bond capacity (V_{nb}) . Strands in excess of n_b, according to the model, may be debonded without compromising the required bond-loss resistance. A reliability analysis of the model has not been conducted and an appropriate value for the strength reduction factor has not been determined; such an analysis is suggested as a natural extension of the current research. In absence of a rigorously determined strength reduction factor, a factor of 0.75 has been suggested to match the value used for shear design in LRFD (9).

$$n_b = \left[\left(\frac{V_u \cot\theta_c}{\phi} - \frac{V_s X_s}{d} - \frac{V_h d_h \cot\theta_c}{d} - \frac{H_h d_h}{d}\right) - A_s f_{sb}\right]\left(\frac{1}{A_{ps1} f_{pb}}\right) \quad (5)$$

Where

n_b = number of fully bonded strands required to provide bond resistance

ϕ = strength reduction factor for bond-loss failure

f_{sb} = stress in reinforcement bars accounting for available development length

f_{pb} = stress in prestressing strands accounting for available development length

A_{ps1} = area of single prestressing strand

Theoretically it is possible for Equation (5) to result in a number of bonded strands less than zero; this circumstance could occur in girders with large amounts of transverse reinforcement or in girders with non-prestressed flexural reinforcement. Complete absence of fully bonded strands however, is strongly discouraged and is outside of the bounds of the dataset from which the model was derived. As a conservative

alternative to Equation (5), Equation (6) replaces the factored shear force divided by the strength reduction factor (V_u/ϕ) with nominal shear capacity (V_n). Equation (6) provides the number of fully bonded strands required such that bond-loss resistance is at least equal to the shear resistance.

$$n_{bv} = \left[\left(V_n \cot\theta_c - \frac{V_s X_s}{d} - \frac{V_h d_h \cot\theta_c}{d} - \frac{H_h d_h}{d}\right) - A_s f_{sb}\right]\left(\frac{1}{A_{ps1} f_{pb}}\right) \quad (6)$$

Where

n_{bv}= number of fully bonded strands required to provide bond-loss resistance equal to shear resistance

V_n = nominal shear capacity

The percentage of debonding associated with equal bond-loss and shear capacities can be calculated from Equation (7).

$$\%\ debonded\ strands = \frac{n_s - n_{bv}}{n_s} \times 100 \quad (7)$$

Where

n_s = total number of strands

Equations (6) and (7) were applied to the in-service girders, and maximum percent of debonding, in order for shear to still be the controlling factor in capacity, was determined. Results are presented in Table 2. These results correspond to the debonding percent in Figure 7 where the lines for each girder cross the $\frac{V_{nb}}{V_n} = 1$ line. For the analyzed girders, between 10% (Vermont) and 45% (Maryland) of strands could be debonded while still maintaining shear as the governing capacity.

Table 2. Maximum Percent of Strand Debonding while Shear Controls the Capacity.

State	Debond percentage for shear to control	As-built debond percentage
Arizona	32%	0%
Alabama AASHTO Type II	44%	15%
Alabama Bulb Tee	22%	0%
Vermont	10%	0%
Maryland	45%	0%
Florida	19%	25%

Conclusion

Conservatism of the AASHTO LRFD 25% debonding limitation was evaluated using a previously published model for bond-loss capacity. The nominal bond-loss capacity was calculated for six different bridge girders and at varying levels of strand debonding. Girder details were taken from plans of in-service bridges to ensure that the calculations were based on practical girder sizes, strand quantities, and reinforcement. The bridge plans were also used as the basis of a structural analysis to calculate factored loads on the girders. The level of conservatism was determined by comparing the factored shear force with nominal bond-loss capacity of each girder and debonding percentage. Comparisons were also made between bond-loss capacity and shear capacity.

The following conclusions were made:

- The nominal bond-loss capacity decreases approximately linearly as the percentage of debonding increases. In other words, the quantity of fully-bonded strands is proportional to the bond-loss capacity.
- The 25% debonding limitation of LRFD is conservative with respect to bond-loss capacity of each of the analyzed girders and debonding levels. The LRFD limitation however, does not produce a uniform degree of conservatism. At the 25% debonding level, the bond-loss capacities of the analyzed girders were 1.8 to 2.7 times greater than the factor loads.
- The model utilized in this paper provides a means of directly calculating the number of fully bonded strands required for resistance to bond-loss failure. The model can also be used to design such that shear–rather than bond-loss- is the limiting capacity. In this manner the model can assist engineers in determining the level of conservatism in their girder designs and to "meticulously analyze" designs that exceed the LRFD 25% limit.

Strand debonding is an established means of mitigating cracking and controlling tensile stresses in the end region of pretensioned I-girders. Experimental testing, however, has shown that excessive debonding can lead to premature shear failures, specifically bond-loss failures. The model and evaluations presented in this paper provide a way to balance the serviceability and durability benefits of strand debonding with the necessity of providing resistance to bond-loss failure.

References

AASHTO. (2014). *AASHTO LRFD Bridge Design Specifications*, 7th ed., Washington, D.C.

Barnes, R. W., Burns, N. H., and Kreger, M. E. (1999). "Development length of 0.6-inch prestressing strand in standard I-shaped pretensioned concrete beams." *Rep. No. FHWA/TX-02/1388-1*, Texas DOT, Austin, TX.

Burgeno, R., and Sun, Y. (2011). "Effects of debonded strands on the production and performance of prestressed concrete beams." *Report CEE-RR-2011/01*, Michigan DOT, East Lansing, MI.

Csagoly, P. (1991). "A shear moment model for prestressed concrete beams." *Report 9900 1550*, Florida DOT, FL.

Deatherage, J. H., Burdette, E. G., and Chew, C. K. (1994). "Development length and lateral spacing requirements of prestressing strand for prestressed concrete bridge girders." *PCI J.*, 39(1), 70-83.

Gamble, W. L. (2014). "Discussion on comparison of details for controlling end-region cracks in pretensioned concrete I-girders." *PCI J. Discussion*, 134-136.

Hawkins, N. M., and Kuchma, D. (2007). "Application of LRFD bridge design specifications to high-strength structural concrete: shear provisions." *National Cooperative Highway Research Program report 579*, Transportation Research Board of the National Academies, Washington, D.C.

Kaufman, M. K., and Ramirez, J. A. (1988). "Re-evaluation of the ultimate strength behavior of high-strength concrete prestressed I-beams." *ACI Struct. J.*, 85(3), 295-303.

LEAP Bridge Enterprise (V8i), Bentley Systems Incorporated, 2013, Exton, PA.

Ma, Z., Tadros, M. K., and Baishya, M. (2000). "Shear behavior of pretensioned high-strength concrete bridge I-girders." *ACI Struct. J.*, 97(1), 185-192.

Maruyama K., and Rizkalla, S. H. (1988). "Shear design consideration for pretensioned prestressed beams." *ACI Struct. J.*, 85(5), 492-498.

Naji, B., Ross, B. E., and Floyd, R. W. (2016). "Characterization of bond-loss failures in pretensioned concrete girders." *Accepted in ASCE J. of Bridge Engineering*.

Nakamura, E., Avendaño, A. R., and Bayrak, O. (2013). "Shear database for prestressed concrete members." *ACI Struct. J.*, 110(6), 909-918.

Okumus, P., and Oliva, M. G. (2013). “Evaluation of crack control methods for end zone cracking in prestressed concrete bridge girders.” *PCI J.*, 58(2), 91-105.

Ross, B. E., Ansley, M. H., and Hamilton, H. R., III. (2011a). “Load testing of 30-year-old AASHTO Type III highway bridge girders.” *PCI J.*, 56(4), 152-163.

Ross, B. E., Hamilton, H. R., and Consolazio, G. R. (2011b). “Experimental and analytical evaluations of confinement reinforcement in pretensioned concrete beams.” *Transportation Research Record 2251*, Transportation Research Board, Washington, DC, 59-67.

Ross, B. E., Consolazio, G. R., and Hamilton, H. R. (2013). “End region detailing of pretensioned concrete bridge girders.” *Rep. No. BDK-75-977-05*, Florida DOT, Tallahassee, FL.

Ross, B. E., and Naji, B. (2014). “Model for nominal bond-shear capacity of pretensioned concrete girders.” *Transportation Research Record 2406*, Transportation Research Board, Washington, DC, 79-86.

Ross, B. E., Willis, M. D., Hamilton, H. R., and Consolazio, G. R. (2014). “Comparison of details for controlling end-region cracks in precast, pretensioned concrete I-girders.” *PCI J.*, 59(2), 96-108.

Shahawy, M. A., and Batchelor, B. (1991). “Bond and shear behavior of prestressed AASHTO type II beams.” Florida DOT, FL.

Shahawy, M. A., and Batchelor, B. (1996). “Shear behavior of full-scale prestressed concrete girders: comparison between AASHTO specifications and LRFD Code.” *PCI J.*, 41(3), 48-62.

Shahawy, M. A., Robinson, B., and Batchelor, B. (1993). “An investigation of shear strength of prestressed concrete AASHTO type II girders.” Florida DOT, FL.

Shahrooz, B. M. (2012). “Strand debonding of pretensioned girders.” *National Cooperative Highway Research Program (research in progress NCHRP 12-91)*. Transportation Research Board of the National Academies, Washington, D.C.

CHAPTER FIVE

ANALYSIS OF BOND-LOSS RESISTANCE MODELS FOR PRETENSIONED I-GIRDERS

Abstract: Bond-loss failures have been widely observed in load tests of precast-pretensioned concrete I-girders. This type of failure is associated with shear cracking near the support that interrupts anchorage of the strands, leading to loss of bond and slipping of the strands relative to the concrete. This paper presents a database of bond-loss failures that are documented in the research literature, and uses the database to create a bond-loss failure model. The database and model are expansions and refinements of the authors' previous work on the subject. The refined model is created through linear regression and least squares analyses, and is demonstrated to have superior accuracy when compared to the end-region model in section 5.8.3.5-2 of the 2014 AASHTO LRFD Bridge Design Specifications. One of the key insights accounted for in the refined model is that stress in transverse reinforcement attendant with bond-loss failure is often less than yield stress.

Introduction

The end-region of a pretensioned girder must perform two critical functions. It must facilitate transfer of forces from the prestressing strands to the concrete and it must carry shear forces from the girder to the support. This paper focuses on transfer of shear forces in the end region, and aims to refine a previously proposed model for end region bond-loss resistance (Ross and Naji 2014). The refined model is compared to the AASHTO LRFD Bridge Design Specifications (AASHTO 2014) (hereafter 'LRFD')

requirements for proportioning flexural reinforcement in the end region; the comparison demonstrates that the refined model provides improved accuracy and conservatism relative to LRFD.

Failures involving loss of strand-concrete bond have been observed in many load tests of precast pretensioned concrete I-girders (Deatherage et al. 1994; Shahway and Batchelor 1996). Bond-loss failure is characterized by the formation of cracks in the end region due to applied loads (**Fig. 1_left**). These cracks interrupt anchorage of strands, leading to loss of bond and slipping of strands relative to the concrete (Abdalla et al. 1993) (**Fig. 1_right**). Strand slip allows the crack to open wider and causes rotation about the crack tip. Once the slip and resulting rotation are sufficient, then the beam will fail as the compression zone crushes under a combination of shear and flexural actions. The specifics of bond-loss behavior can vary from specimen to specimen; the terminology and mechanics associated with different types of bond-loss failures are described in detail by Naji et al. (2016).

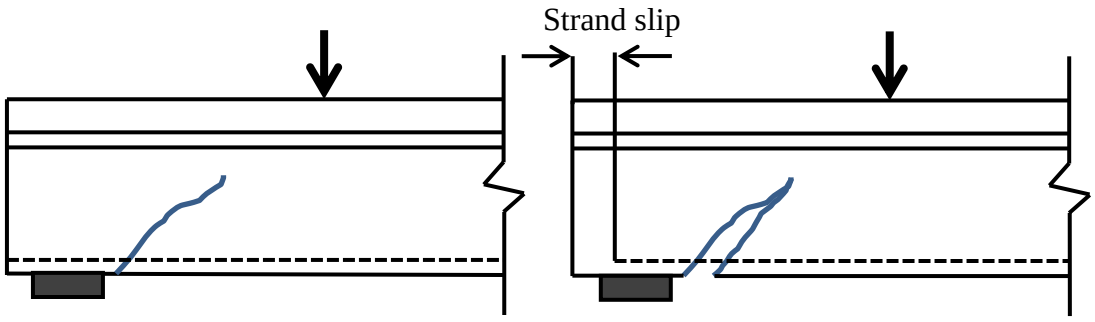

Figure 1. Basic description of bond-loss failure; crack forms near support (left) and crack leads to bond loss and strand slip (right)

It has been experimentally observed that failure due to loss of strand-concrete bond can lead to capacities that are less than nominal shear and nominal flexural strength (Ross et al. 2011a; Shahway and Batchelor 1996). Because bond loss can be the controlling factor in capacity (Garber et al. 2016; Ross et al. 2014), it is critical that bond-loss resistance be considered when designing I-girder end regions. Towards the goal of understanding and designing for this failure mode, the first part of this paper presents a database consisting of 120 specimens experiencing bond-loss failure. This database provides a means of exploring the mechanisms and variables that contribute to bond-loss failures. The second part of this paper presents a refined model for calculating the nominal bond-loss resistance of pretensioned I-girders. Quantitative methods including the least squares method and linear regression were used in developing the model. The database and model presented in this paper are expanded and refined from the authors' previous work (Ross and Naji 2014). The third and final part of this paper includes an example calculation to demonstrate the bond-loss resistance model. It is intended that the database, refined model, and example calculation will contribute to the design of safe and efficient precast-pretensioned I-girders. As will be shown, the refined model is more accurate than LRFD, as it corrects some potentially unconservative scenarios with the LRFD code.

Background

AASHTO LRFD

Although "bond-loss resistance" is not directly mentioned in LRFD, the concept is implicitly addressed in LRFD equation 5.8.3.5-2 (Eq. [1]). This equation is used for

proportioning flexural reinforcement to carry longitudinal tie forces at the inside edge of simple span supports. This equation is based on equilibrium of the end region and can be derived through the summation of moments about point 0 as shown in **Fig. 2**. The end region considered by LRFD in Fig. 2 is similar to the girder portion that is adjacent to the support in a bond-loss failure (Fig. 1); in both cases a crack separates the end region from the remainder of the girder.

$$A_s f_y + A_{ps} f_{ps} \geq \left(\frac{V_u}{\phi_v} - 0.5V_s - V_p\right) cot\theta \qquad (1)$$

where

A_s = area of non-prestressing tension steel

f_y = specified yield strength of reinforcement bars

A_{ps} = area of prestressing steel

f_{ps} = average stress in prestressing steel coincident with V_u

V_u = factored shear force

ϕ_v = resistance factor for shear

V_s = resistance provided by the vertical reinforcement

V_p = component of prestressing in direction of the shear force

θ = angle of inclination of diagonal compressive stresses

C = force in compression zone

d_v = effective shear depth

T = longitudinal tie force in flexural reinforcement

V_a = force along crack interface

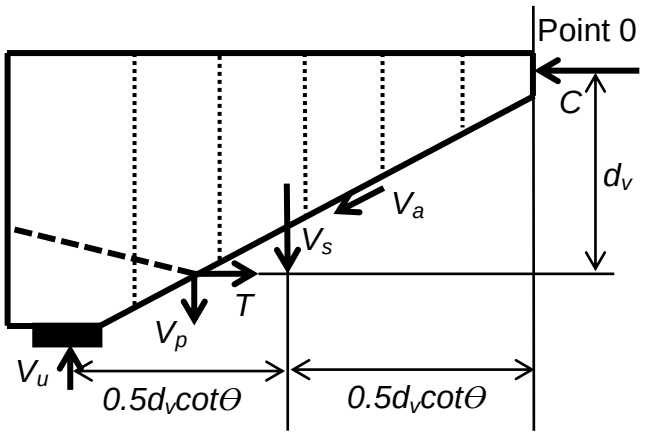

Figure 2. Free body diagram of end region (based on AASHTO LRFD 2014)

The intent of the code provision is to ensure that sufficient transverse and longitudinal reinforcement are present to maintain equilibrium in the end region. Bond-loss failure is implicitly addressed in LRFD section 5.8.3.5, which requires that "any lack of full development length [of the longitudinal tie] shall be accounted for" when using Eq. (1). However, explicit requirements are not given for how to account for lack of full development. In lieu of explicit requirements, multiple authors (Garber et al. 2016; Ross et al. 2014; Ross and Naji 2014) have suggested a reduced strand capacity can be calculated on the basis of strand embedment length between the end of the girder and the assumed inclined cracks. The transfer and development length provisions of LRFD section 5.11.4 are used by these authors to calculate the reduced strand capacity.

Assuming that bond-loss of the flexural reinforcement controls end region capacity, Eq. (1) can be rearranged to the form shown in Eq. (2) to calculate nominal bond-loss capacity. This approach has been used by multiple authors (Garber et al. 2016; Ross et al. 2011a) in order to modify the LRFD equation for use in calculating bond-loss capacity.

$$\frac{V_u}{\phi_v} \leq V_{nb} = \frac{A_s f_y + A_{ps} f_{psb}}{cot\theta} + 0.5V_s + V_p \quad (2)$$

where

V_{nb} = nominal bond capacity

f_{psb} = stress in prestressing strand coincident with bond-loss failure

Original Bond-Loss Model

Ross and Naji (2014) previously proposed a model for calculating nominal capacity of a pretensioned I-girder end region against bond-loss failure and compared the model to a database of 84 experimental tests. The previously proposed model will be referred to as the "original model" in the current paper. Similar to the provisions of LRFD section 5.8.3.5, the original model (**Fig. 3**) is also based on moment equilibrium of the end region; however, the model relies on fewer simplifications and is consequently applicable to a wider range of girders.

Key differences between the original model (Fig. 3) and free body diagram used by LRFD (Fig. 2) include: 1) Harped strands are treated separately from the straight strands. 2) Non-uniformly distributed reinforcement is considered by locating the resultant force from vertical reinforcement at a variable location (X_s). 3) Available development length of the tension tie and harped strands are explicitly considered by introducing variables L_{dt} and L_{dh}, respectively. 4) And finally, the flexural depth (d) was used in lieu of the effective shear depth (dv).

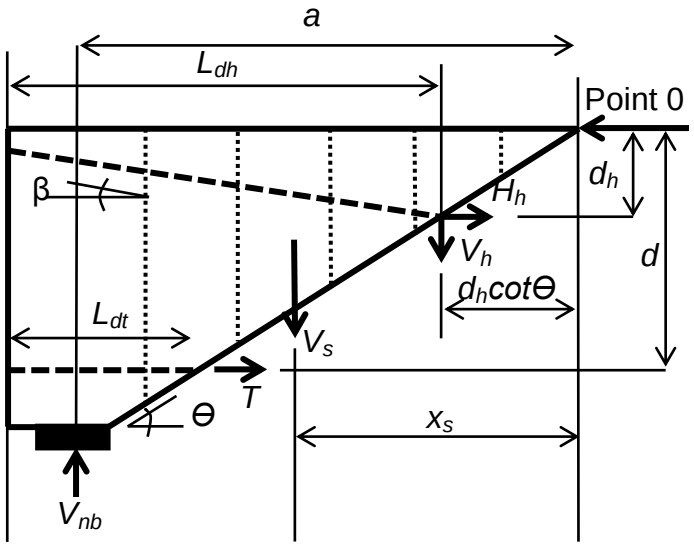

Figure 3. Free body diagram of end region for original model

Equation (3) for nominal bond-loss resistance can be derived by summing moments about point 0 in Fig. 3:

$$V_{nb} = \frac{V_s\, x_s}{d\cot\theta} + \frac{T}{cot\theta} + \frac{V_h d_h}{d} + \frac{H_h d_h}{d\cot\theta} \qquad (3)$$

where

x_s = horizontal distance to vertical steel centroid

d = flexural depth of tension tie

a = shear span

V_h = vertical force in harped strand

d_h = depth of harped strands at crack interface

H_h = horizontal force in harped strand

L_{dh} = available embedment length of harped strand

β = inclination angle of harped strands

When applying the above equation to analyze test specimens, shear span-to-depth ratio (*a/d*) is assumed to equal $\cot\theta$. This is based on the observation that inclined cracks in tests are often oriented along a line between the support and load point (Ross and Naji 2014).

Longitudinal tie force is calculated as:

$$T = A_s f_y + A_{ps} f_{pe} \left(\frac{L_{dt}}{L_t}\right) \quad (4)$$

$$V_s = A_v f_y \quad (5)$$

where

f_{pe} = effective stress in prestressing steel

L_{dt} = available embedment length of tension tie

L_t = required transfer length

A_v = area of vertical reinforcement crossing assumed crack plane

Equation (4) follows the same approach as LRFD section 5.11.4; force in the strands calculated as being linearly proportional to the available length of embedment (L_{dt}). Maximum possible force in the strands is taken as the effective prestress force, which occurs at the transfer length (L_t).When harped strands are present, the same approach is used to calculate forces V_h and H_h, but with a different available development length (L_{dh}). In this manner, the original model addresses the LRFD section 5.8.3.5 requirement of accounting for lack of full development length.

One key insight taken from development of the original model is that transverse reinforcement does not necessarily yield prior to or during bond-loss failure. The original

model uses Eq. (6) to account for this circumstance. The equation is used to calculate stress in transverse reinforcement that is attendant at bond-loss failure. Equation (6) was constructed empirically and factors (f_1, f_2, and K_{sv}) were selected using a guess-and-check approach in order to fit the original model with the 84 specimens in the bond-loss database.

$$f_{sv} = (f_1 - f_2 \cot\theta)(1 - \kappa_{sv}\rho_{sv}) \leq f_y \quad (6)$$

where

f_{sv} = stress in vertical reinforcement (ksi)

f_1 = empirical factor taken as 130 ksi

f_2 = empirical factor taken as 28 ksi

k_{sv} = empirical factor taken as 26

ρ_{sv} = shear reinforcement ratio

In above equation, the shear reinforcement ratio is calculated as:

$$\rho_{sv} = \frac{A_v}{b_w d \cot\theta} \quad (7)$$

where

b_w= web width

The current paper improves the original study by expanding and refining the database, and by using statistical linear regression analysis and the least squares method to identify best-fit equations with the experimental data.

Expanded Bond-Loss Database

The original bond-loss database included 84 specimens from ten different sources (Barnes et al. 1998; Deatherage et al. 1994; Hawkins and Kuchma 2007; Kaufman and

Ramirez 1988; Ma et al. 2000; Maruyama and Rizkalla 1988; Ross et al. 2011a; Ross et al. 2011b; Ross et al. 2013; Shahway and Batchelor 1996). In the current study, 44 specimens from eleven different test programs (Abdalla et al. 1993; Alshegeir and Ramirez 1992; Garber et al. 2016; Hartmann et al. 1988; Jongpitaksseel 2003; Kahn et al. 2002; Labonte and Hamilton 2005; Meyer et al. 2002; Raymond et al. 2005; Tawfiq 1995; Tawfiq 1996) are added. Additionally, eight specimens from Barnes et al. (1999) are removed because they only experienced bond loss and strand slip in shielded (i.e., partially debonded) strands. Thus, all specimens in the expanded database experienced strand slip in fully bonded strands and failed according to the mechanics and models described in the previous sections. A summary of the expanded database including 120 specimens is presented in **Fig. 4**; individual specimens are listed in Appendix A.

As shown in the figure, specimens in the expanded database cover a range of variables. Approximately half of the specimens had concrete with tested compressive strength greater than 7200 psi at the time of load testing. All of the database specimens had 270 ksi ultimate strength strands. Nine of the specimens had both harped and straight strands; the remaining 111 specimens had only straight strands. The area of prestressing shown in Fig. 4 only includes fully bonded straight strands; debonded strands cannot contribute to the tension tie and bond-loss resistance. Specified yield strength of the mild reinforcement was 60 ksi in 114 of the specimens and 40 ksi in the remaining six. All specimens in the database were simply supported and were load tested at a/d ratio ranging from 1.0 to 4.4.

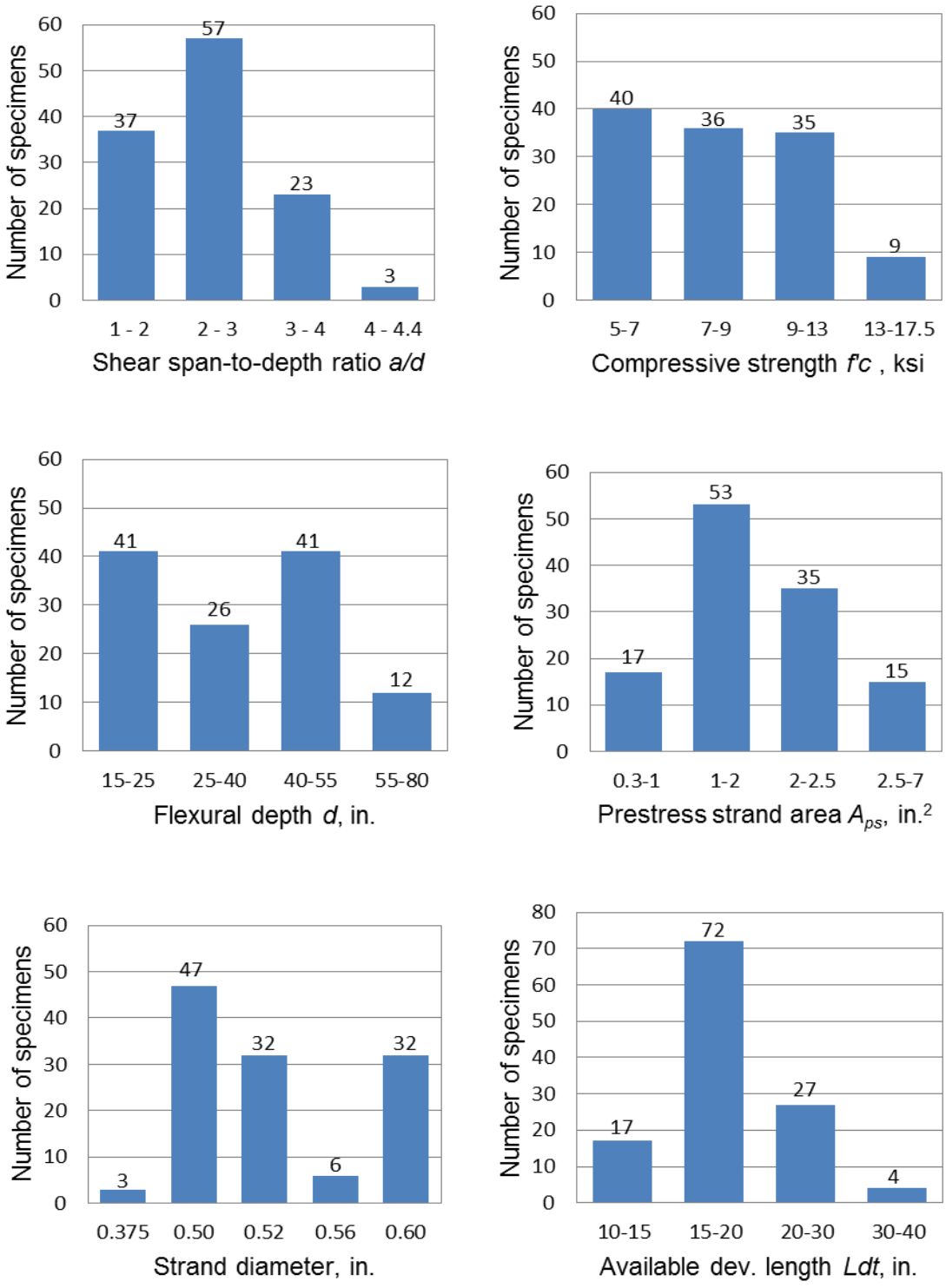

Figure 4. Distribution of the variables in expanded database. Note: 1 in. = 25.4 mm; 1ksi = 6.89 MPa

Development of Refined Bond-Loss Model

To begin, the expanded bond-loss database, including 120 specimens, was used to calculate bond-loss capacity given by Eq. (3) through Eq. (5). Results are presented in **Fig. 5** according to the 'strength ratio' (V_{nb}/V_{exp}). The figure shows the strength ratio of each database specimen plotted against six different variables. A strength ratio greater than one indicates that the calculated result is unconservative (larger) relative to the experimental result. As seen in Fig. 5, Eq. (3) through (5) in their current form are not an accurate representation of bond-loss capacity of pretensioned I-girders. Using these equations to design can result in understrength members. If the model were ideal all the points would fall at strength ratio of 1.0; however, the calculated strength ratios are typically greater than 1.0 (unconservative). The average of strength ratio is 1.47 (i.e., model over predicted experimental strength by 47% on average) with coefficient of variation (CoV) of 0.51.

Referring to **Fig. 5_upper left,** there is an apparent trend between *a/d* ratio and strength ratio. For specimens with *a/d* ratios less than 2.0 the strengths ratios are typically near 1.0; however, as *a/d* ratio increases, the strength ratios also increase and the model becomes more-and-more unconservative. The highest strength ratio is over 4.0, and corresponds to the largest *a/d* ratio. Trends can also be observed for concrete compressive strength (*f'c*), flexural depth (*d*), and prestress strand area (A_{ps}). As these variables increase, the strength ratio decreases, which indicates a higher level of conservatism for these conditions.

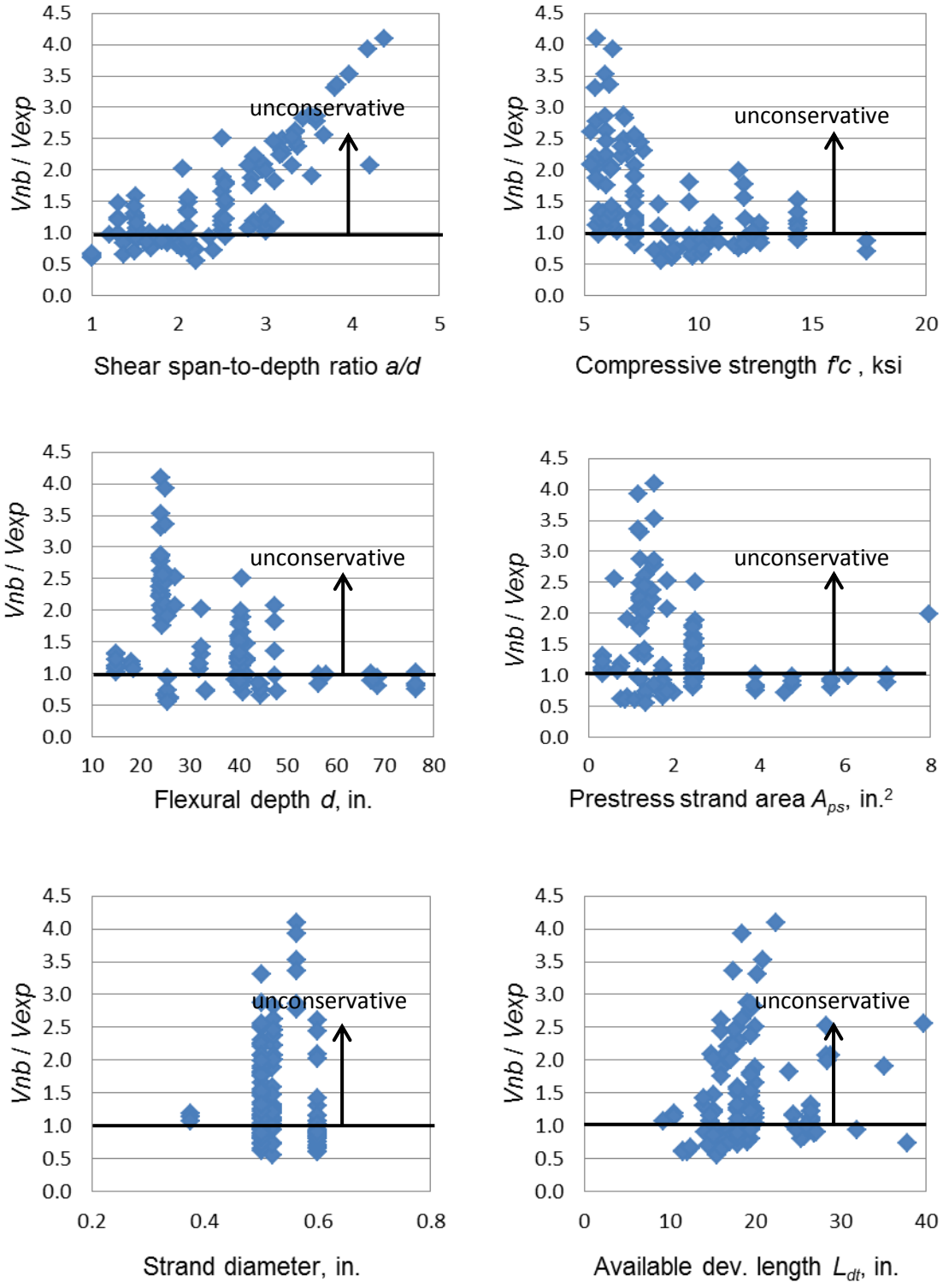

Figure 5. Strength ratios for original model compared to specimen parameters

The relationship between the nominal-to-experimental ratio and strand diameter and available development length are not as obvious as the relationships observed for the other variables. In order to statistically identify whether the strength ratio has a significant correlation with the six independent abovementioned variables, a linear regression model was developed for each variable (Hines et al. 2003). This approach elucidates if the value of the strength ratio changes when any one variable changes and the others are held fixed.

Table 1 shows the results of the regression analysis for each variable, where a low p-value ($p < 0.05$) indicates that changes in a variable results in significant changes in the strength ratio. Conversely, a large p-value suggests that changes in the variable do not significantly result in changes in the response. Results obtained from the regression analysis confirm observations made from Fig. 5 that changes in *a/d* ratio, $f'c$, d , and A_{ps} are significantly related to changes in the strength ratio. Results also indicate that there is no clear trend between the strength ratio and the other variables.

Table 1. Results of linear regression analysis

Variables	P-value	Significant trend
a/d	7.26×10^{-25}	Yes
$f'c$	4.52×10^{-9}	Yes
L_{dt}	0.254	No
A_{ps}	0.004	Yes
Flexural depth, *d*	8.18×10^{-6}	Yes

Strand diameter	0.327	No

While regression analyses are helpful for identifying important variables, it is also important to consider the physical phenomena that are underpinning the statistical results. Why is the accuracy of the model affected by these variables? The two most significant variables according to regression analysis are *a/d* ratio and *f'c*. The phenomena behind these observations are discussed in the paragraph below. The trends observed for *d* and A_{ps}, while falling below the 0.05 p-value threshold, are less significant than the trends of *a/d* and *f'c*.

The effects of concrete compressive strength (*f'c*) are considered first. Referring to Eq. (3), we see that bond-loss capacity consists of four different terms. The first term is based on transverse reinforcement and the remaining three terms are based primarily on contributions from prestressing strands. Recent research from Ramirez et al. (2015) suggests that *f'c* likely has insignificant effect on the prestressing strand contribution of the database specimens. They found that transfer length, a critical parameter when calculating contribution of the prestress strand, is generally independent of concrete strength for *f'c* greater than 5ksi. All of the specimens in the database had concrete compressive strength greater than 5 ksi, and it is reasoned that the observed trend with *f'c is* not associated with the prestressing strand contribution to bond-loss capacity. This leaves the first term of Eq. (3) as the term affected by *f'c*. The results presented in Fig. 5 and Table 1 assume yielding of the transverse reinforcement ($f_{sv} = f_y$). This assumption is also made in the end-region provisions in LRFD section 5.8.3.5. The regression results

suggest, however, that vertical reinforcement stress attendant with bond-loss failure is often less than yielding. Recalling that peak-load of bond-loss failures is often based on failure of the compression zone (Naji et al. 2016), it is reasoned that as *f'c* decreases, strength of the compression zone decreases, and peak capacity of the bond-loss mechanism occurs at lower loads. Because lower *f'c* leads to reduced bond-loss capacity, attendant stress in the transverse reinforcement is limited by the concrete strength; i.e., the concrete compression zone fails while the transverse reinforcement stress is less than yield. Hence, transverse reinforcement stress at ultimate load was likely less than yield stress ($f_{sv} \leq f_y$) in the database specimens with lower concrete compressive strengths.

The strongest trend observed in Fig. 5 and Table 1 involves the *a/d* ratio. As with *f'c*, it is reasoned that *a/d* ratio effects the contribution of the transverse reinforcement. As *a/d* ratio increases, inclined cracks cross greater amounts of reinforcement, and consequently stress in the reinforcement decreases. In other words, more bars carry the force and stress in the bars is reduced.

Similar phenomena were considered by Ross and Naji (2014) in the development of Eq. (6). While Eq. (6) was developed using a guess-and-check approach, the following section aims to create an equation for vertical reinforcement stress that is based on rigorous statistical formulation and analysis.

Evaluation of Database Using Least Squares Method

The method of least squares is a standard approach in regression analysis that minimizes the sum of the squares of the errors between a model and experimental data. More specifically in this case, the least squares method provides the best fit that

minimizes the errors between nominal capacities (V_{nb}) and experimental capacities (V_{exp}) in 120 specimens of the database. The method is mathematically described as:

$$Min \sum_{j=1}^{120} \left({V_{nb}}^{j} - {V_{exp}}^{j} \right)^2 \tag{8}$$

where *j* is the index for each of the 120 specimens. This definition is expanded by substituting Eq. (3) into Eq. (8):

$$Min \sum_{j=1}^{120} \left(\frac{{V_s}^j \, {x_s}^j}{d^j cot\theta^j} + \frac{T^j}{cot\theta^j} + \frac{{V_h}^j \, {d_h}^j}{d^j} + \frac{{H_h}^j \, {d_h}^j}{d^j \, cot\, \theta^j} - {V_{exp}}^j \right)^2 \tag{9}$$

As illustrated before, strength ratio is inversely related to *f'c*, and directly related to *a/d*. It was also argued that both variables affect the stress in the transverse reinforcement. To account for these relationships, Eq. (10) is created which includes *f'c* in the numerator and *a/d* in the denominator of the first term. As already discussed *a/d* is expressed as *cot* θ. A variable alpha (α) was also included in the first term for calibration purposes:

$$Min \sum_{j=1}^{120} \left(\frac{{V_s}^j \, {x_s}^j \alpha {f'c}^j}{d^j cot^2 \theta^j} + \frac{T^j}{cot\theta^j} + \frac{{V_h}^j \, {d_h}^j}{d^j} + \frac{{H_h}^j \, {d_h}^j}{d^j \, cot\, \theta^j} - {V_{exp}}^j \right)^2 \tag{10}$$

The least squares method was used to minimize the sum of the squares of the errors between nominal capacities and experimental capacities by solving for variable alpha (α), while also considering variables *f'c* and *a/d* (expressed as *cot* θ) in the first term. Variable *T* in Eq. (10) was calculated for each specimen using Eq. (4). By solving Eq. (10) for 120 specimens, alpha was determined to be 0.16; and hence, the refined bond-loss capacity equation takes the form:

$$V_{nb} = \frac{0.16\, V_s\, x_s f'c}{d\cot^2\theta} + \frac{T}{cot\theta} + \frac{V_h d_h}{d} + \frac{H_h d_h}{d\cot\theta} \quad (11)$$

In absence of the harped strands, the equation can be written as:

$$V_{nb} = \frac{0.16\, V_s\, x_s f'c}{d\cot^2\theta} + \frac{T}{cot\theta} \quad (12)$$

Recalling that compresive strength and shear span ratio affect stress in the transverse reinforcement, it is convinient to express Eq. (11) in the following format:

$$V_{nb} = \frac{V_{sb}\, x_s}{dcot\theta} + \frac{T}{cot\theta} + \frac{V_h d_h}{d} + \frac{H_h d_h}{d\cot\theta} \quad (13)$$

where

$V_{sb} = A_v f_{sb}$

$$f_{sb} = f_y\left(\frac{0.16 f'c}{cot\theta}\right) \leq f_y \quad (14)$$

and

V_{sb} = force in transverse reinforcment conincident with bond-loss failure

f_{sb} = stress in transverse reinforcment conincident with bond-loss failure

This approach relates transverse reinforcement stress to the shear span ratio (expressed as $cot\theta$) and compressive strength of the concrete. When using Eq. (14), the concrete compressive strength must be input with ksi units.

Validation of Refined Model

Nominal bond-loss capacity, calculated using the refined model, Eq. (11), was compared to experimental capacity of each database specimen. As was done in Fig. 5, **Fig. 6** uses the strength ratio to compare the calculated and expeirmental results against

six different variables. When performing the calculations, lack of full development length was accounted for using Eq. (4).

Refferring to Fig. 6, the strength ratios appear to be uniformly distributed around 1.0, indicating good agreement between the experimental data and the refined model. The average strength ratio was 0.98 with a coefficient of variation of 0.20. For comparison, the strength ratio and coefficient of variation for the first analysis were 1.47 and 0.51, respectively. Observations made from Fig. 6 are confirmed by results of a linear regression analysis as shown in **Table 2**. Large p-values (greater than 0.05) for all six variables indicate that the refined model provides a robust estimation over the range of all independent variables. To express it differently, the refined bond-loss capacity model (Eq. [11]) produces a uniform degree of accuracy and conservatism across the range of each considered variable.

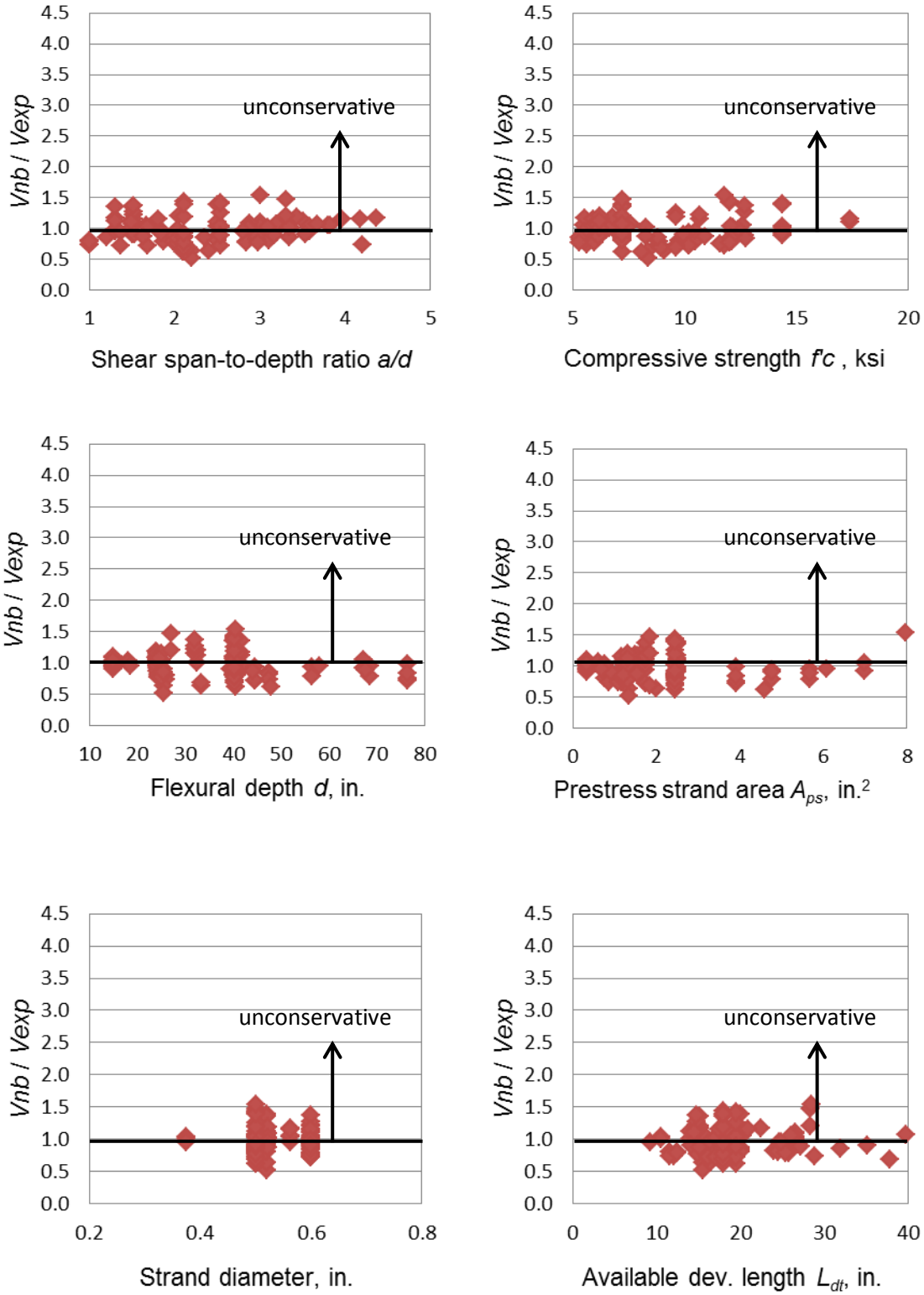

Figure 6. Strength ratios from refined model compared to specimen parameters

Table 2. Results of linear regression analysis for the refined model

	Single regression analysis	
Variables	P-value	Significant trend
a/d	0.217	No
$f'c$	0.192	No
L_{dt}	0.651	No
A_{sp}	0.683	No
Flexural depth, *d*	0.161	No
Strand diameter	0.726	No

The earlier analysis presented in in Table 1, indicated that the values from the original model are significantly related with the *a/d* ratio, *f'c*, *d*, and A_{ps}. However, after considering *f'c* and *a/d* ratio in the refined model, there is no longer a significant trend between the model results and *d* and A_{ps}. This is evident from the large (greater than 0.05) p-values associated with *d* and A_{ps} (Table 2). Thus, the refinements based on *a/d* and *f'c* were sufficient to create a robust model.

Additionally, **Fig. 7** uses the strength ratio to compare the calculated and expeirmental results against stress in transverese reinforcement (f_{sb}), calculated using Eq. (14). Refferring to Fig. 7, the strength ratios appear to be uniformly distributed around 1.0, indicating good agreement between the experimental data and the refined model. Observations made from Fig. 7 are confirmed by result of a linear regression analysis.

Large p-value (0.764) associated with the independent variable indicates that the refined model provides a robust estimation over the range of the variable.

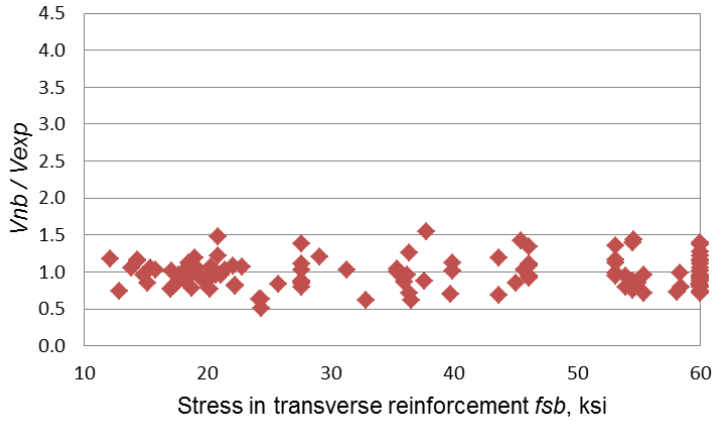

Figure 7. Strength ratios from refined model compared to stress in transverse reinforcement

Comparison of Model with AASHTO LRFD

Strength ratios of all 120 specimens are calculated using both the refined model (Eq. [11]) and the LRFD provisions (Eq. [2]), and are compared in **Fig. 8**. In both cases the effects of reduced development of the tension tie were considered using Eq. (4). The LRFD end-region equilibrium model, which assumes yielding of the vertical reinforcement, resulted in calculated capacities that were 48% larger (unconservative) on average than the experimental capacities. The coefficient of variation of strength ratio for the LRFD was 0.51, approximately twice that of the refined model. Thus, the refined model produces results that are more accurate and have less scatter than the current AASHTO LRFD provisions. The refined model also has the added benefit of producing results that have relatively consistent levels of conservatism and accuracy for the ranges of the considered variables.

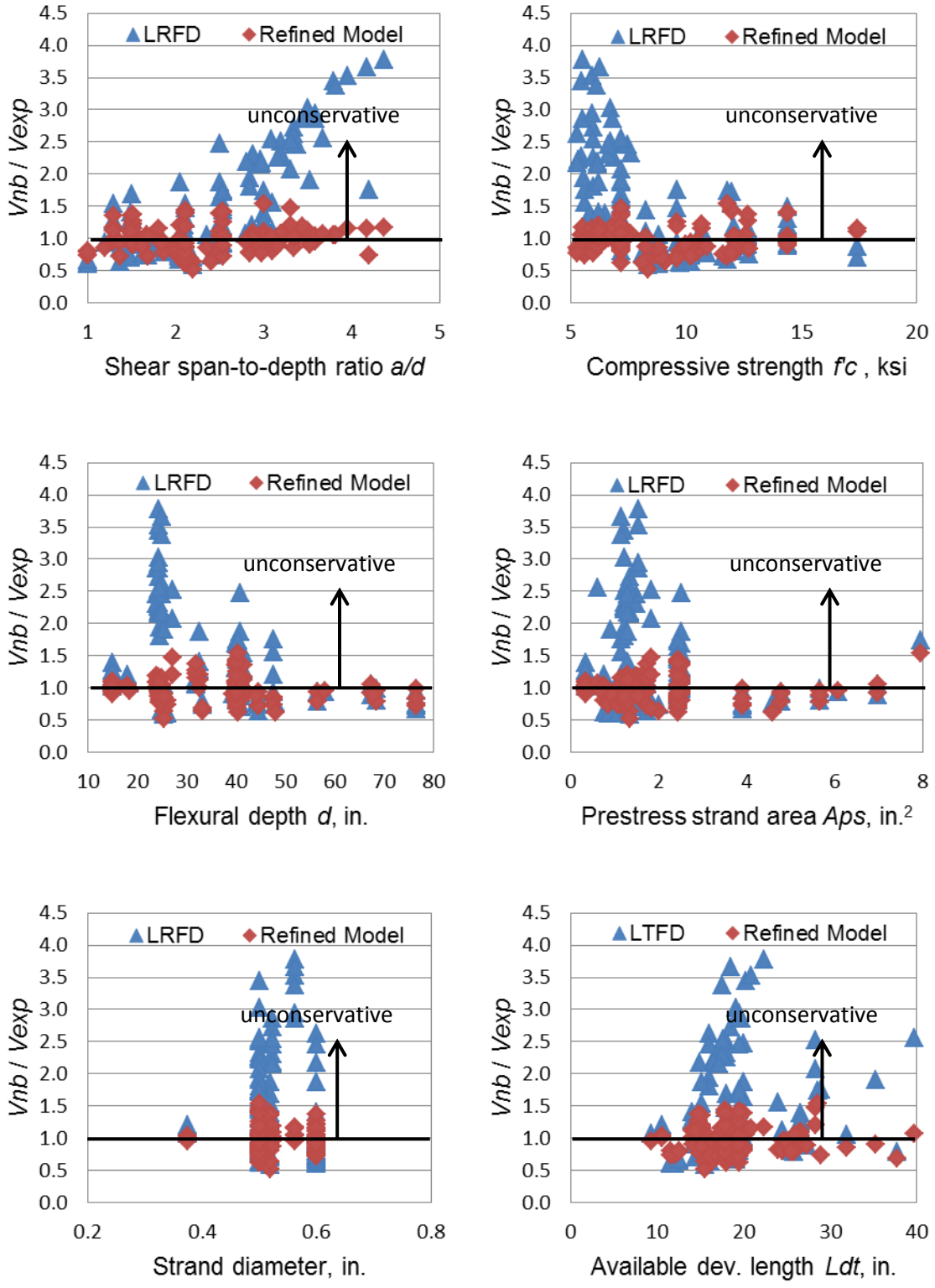

Figure 8. Comparison of strength ratios from LRFD and refined models

Example Calculation

To aide in application of the refined model, this section of the paper presents an example calculation for an AASHTO Type III girder. Girder parameters are summarized in **Table 3** and are based on specimen *G1* from a program by Ross et al.; specimen details and drawings are available in the Fall 2011 issue of PCI Journal (Ross et al. 2011a).

Table 3. Specimen parameters of girder *G1*

Item	Value	Notes
A_{ps}	1.152 in.^{2}	(8) 1/2 in. strands
f_{pe}	162 ksi	
A_s	0.6 in.^{2}	(3) No. 4 bars
$f'c$	5.63 ksi	Tested compressive strength
d	47.5 in.	
a	4.75 ft.	Based on load and support geometry.
$a/d \approx \cot\theta$	1.2	
A_v	4.88 in.^{2}	(12) No. 4 bars, (8) No. 5 bars
X_s	32.4 in.	Specimen G1 had non-uniform distribution of transverse reinforcement. This value is the centroid of the transverse bars that cross the assumed crack (see Fig. 8).
f_y	60 ksi	
H	52 in.	Height of precast girder and deck
X_{brg}	8 in.	Bearing distance
X_{oh}	2 in.	Overhang distance

$X_t=(H-d).\cot\theta$	5.4 in.	See Fig. 8
$L_{dt}=X_{brg}+X_{oh}+X_t$	15.4 in.	See Fig. 8
A_{ph}	0.864 in.^{2}	(6) 1/2 in. strands
B	4.5 degree	See Fig. 8
L_{dh}	45.3 in.	
L_t	30 in.	Taken as 60 strands diameter per LRFD section 5.11.4
d_h	22.6 in.	

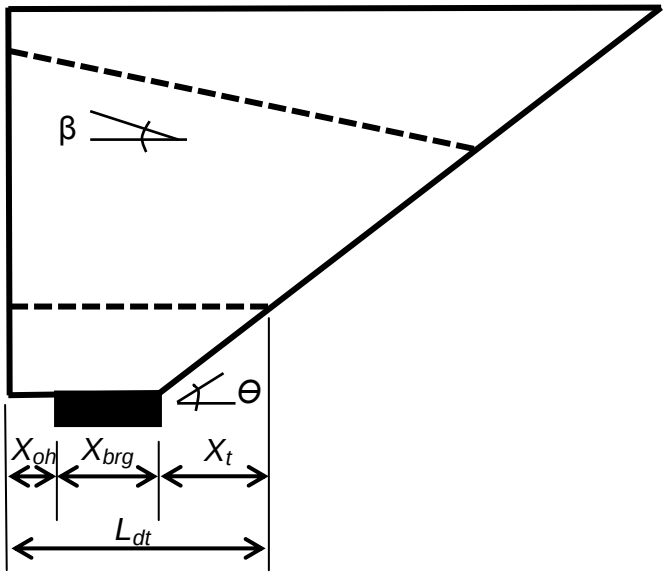

Figure 9. Definition of select geometric parameters

Calculation of Force in Harped Strands:

$F_h=A_{ph}f_{pe}(L_{dh}/L_t)< A_{ph}.f_{pe}$

$F_h=A_{ph}f_{pe}=$ 140 kips

$H_h=F_h.cos\ \beta=$139.5 kips

$V_h=F_h.sin\ \beta=$11 kips

Calculation of Tension Tie Force:

$T=A_s f_y+A_{ps} f_{pe}(L_{dt}/L_t)< A_s f_y+A_{ps} f_{pe}$

$T=A_s f_y+A_{ps} f_{pe}(L_{dt}/L_t)$=132 kips

Calculation Force in Transverse Reinforcement (Eq. [14]):

$$f_{sb} = f_y\left(\frac{0.16f'c}{cot\theta}\right) = 45\ ksi \leq f_y$$

$V_{sb} = A_v f_{sb}$= 220 kips

Calculation of Bond-Loss Capacity (Eq. [13]):

$$V_{nb} = \frac{V_{sb}\ x_s}{dcot\theta} + \frac{T}{cot\theta} + \frac{V_h d_h}{d} + \frac{H_h d_h}{d\cot\theta} = 295 \text{ kips}$$

Summary and Conclusions

A previously published database of test specimens was expanded and then used to create a refined model for bond-loss resistance of pretensioned I-girders. The refined model was constructed using the least squares method and linear regression analysis. Salient conclusions are as follows:

- Results from regression analysis indicate that stress in the transverse reinforcement attendant at bond-loss failure is related to the shear span-to-depth ratio (*a/d*) and concrete compressive strength (*f'c*). With regard to shear span ratio, this result is attributed to the increased number of bars that are engaged as the ratio becomes larger; as more bars are engaged the stress in the bars is decreased. With regard to concrete strength, this result is attributed to the effect of concrete on the peak capacity of the bond-loss mechanism. Lower concrete strength results in earlier failure of the compression zone, which is often the event

that controls peak capacity in bond-loss failures; because the compression zone fails earlier, stress in the vertical reinforcement at failure is often less than yield.

- By considering the effects of concrete compressive strength and shear span-to-depth ratio, the refined model is a more accurate representation of bond-loss behavior. When compared to specimens in the bond-loss database, the average strength ratio (calculated-to-experimental capacity) was 0.98 with a coefficient of variation of 0.2. Additionally, large p-values (greater than 0.05) in a regression analysis of the refined model indicate that the model provides a robust estimate over the range of each variable. In other words, the accuracy and conservatism of the refined model are consistent over the considered ranges of the independent variables.
- The refined model is a significant improvement in terms of accuracy and scatter when compared to the current AASHTO LRFD end-region equilibrium model. The LRFD model resulted in calculated capacities that were 48% larger (unconservative) on average than the experimental capacities. The coefficient of variation of strength ratio for the LRFD model was 0.51, more than twice that of the refined model. The unconservative results from the LRFD model may be attributed to the assumption that vertical reinforcement always reaches yield stress.

References

American Association of State Highway and Transportation Officials (AASHTO). (2014). *AASHTO LRFD Bridge Design Specifications*. 7th ed. Washington, DC.

Abdalla, O. A., Ramirez, J. A., and Lee, R. H. (1993). "Strand debonding in pretensioned beams-precast prestressed concrete bridges with debonded strands." *Rep. No FHWA/ INDOT/ JHRP-92*, Indiana DOT, West Lafayette, IN.

Alshegeir, A., and Ramirez, J. A. (1992). "Strut-Tie approach in pretensioned deep beams." *ACI Struct. J.*, 89(3), 296-304.

Barnes, R. W., Burns, N. H., and Kreger, M. E. (1999). "Development length of 0.6-inch prestressing strand in standard I-shaped pretensioned concrete beams." *Rep. No. FHWA/TX-02/1388-1*, Texas DOT, Austin, TX.

Deatherage, J. H., Burdette, E. G., and Chew, C. K. (1994). "Development length and lateral spacing requirements of prestressing strand for prestressed concrete bridge girders." *PCI J.*, 39(1), 70-83.

Garber, D. B., Gallardo, J. M., Deschenes, D. J., and Bayrak O. (2016). "Nontraditional shear failures in bulb-t prestressed concrete bridge girders." *J. of Bridge Eng.*, 10.1061/(ASCE)BE.1943-5592.0000890.

Hartmann, D. L., Breen, J. E., and Kreger, M. E. (1988). "Shear capacity of high strength prestressed concrete girders." *Rep. No. FHWA/ TX-88+381-2*, Texas DOT, Austin, TX.

Hawkins, N. M., and Kuchma, D. A. (2007). "Application of LRFD bridge design specifications to high-strength structural concrete: shear provisions." *National Cooperative Highway Research Program report 579*, Transportation Research Board, Washington, DC.

Hines, W. W., Montgomery, D. C., Goldsman, D. M., and Borror, C. M. (2003). *Probability and Statistics in Engineering*. New York, NY: John Wiley and Sons, pp. 447-452.

Jongpitaksseel, N. (2003). "Behavior of end zone of precast/pretensioned concrete bridge girders." Ph.D. Dissertation, Univ. of Nebraska, Lincoln, NE.

Kahn, L. F., Dill, J. C., and C. G. Reutlinger, C. G. (2002). "Transfer and development length of 15-mm strand in high performance concrete girders." *J. of Structural Eng.*, 10.1061/(ASCE)0733-9445, 913-921.

Kaufman, M. K., and Ramirez, J. A. (1988). "Re-evaluation of the ultimate strength behavior of high-strength concrete prestressed I-beams." *ACI Struct. J.*, 85(3), 295-303.

Labonte, T., and Hamilton, H. R. (2005). "Self-consolidating concrete (SCC) structural investigation." *Rep. No. BD545, RPWO# 21*, Florida DOT, Tallahassee, FL.

Ma, Z., Tadros, M. K., and Baishya, M. (2000). "Shear behavior of pretensioned high-strength concrete bridge I-girders." *ACI Struct. J.*, 97(1), 185-192.

Maruyama K., and Rizkalla, S. H. (1988). "Shear design consideration for pretensioned prestressed beams." *ACI Struct. J.*, 85(5), 492-498.

Meyer, K. F., Kahn, L. F., Lai, J. S., and Kurtis, K. E. (2002). "Behavior of high-strength/high-performance lightweight concrete prestressed girders." *Report No 2004*, Georgia DOT, Atlanta, GA

Naji, B., Ross, B. E., and Floyd, R. W. (2016). "Characterization of bond-loss failures in pretensioned concrete girders." *Accepted in ASCE J. of Bridge Eng.*

Ramirez-Garcia, A. T., Floyd, R. W., Hale, W. M., and Marti-Vargas, J. R. (2015). "Effect of concrete compressive strength on transfer length." In *Structures* 5, 131-140.

Raymond, K. K., Bruce, R. N., and Roller, J. J. (2005). "Shear behavior of HPC bulb-tee girders." *ACI Special Publication* 228, 705-722.

Ross, B. E., Ansley, M. H., and Hamilton, H. R., III. (2011a). "Load testing of 30-year-old AASHTO Type III highway bridge girders." *PCI J.*, 56(4), 152-163.

Ross, B. E., Consolazio, G. R., and Hamilton, H. R. (2013). "End region detailing of pretensioned concrete bridge girders." *Rep. No. BDK-75-977-05*, Florida DOT, Tallahassee, FL.

Ross, B. E., Hamilton, H. R., and Consolazio, G. R. (2011b). "Experimental and analytical evaluations of confinement reinforcement in pretensioned concrete beams." *Transportation Research Record 2251*, Transportation Research Board, Washington, DC, 59-67.

Ross, B. E., Hamilton, H.R., and Consolazio, G. R. (2014). "Experimental study of end region detailing and shear behavior of concrete I-girders." *J. of Bridge Eng.*, 10.1061/(ASCE)BE.1943-5592.0000676.

Ross, B. E., and Naji, B. (2014). “Model for nominal bond-shear capacity of pretensioned concrete girders.” *Transportation Research Record 2406*, Transportation Research Board, Washington, DC, 79-86.

Shahawy, M. A., and Batchelor, B. (1996). “Shear behavior of full-scale prestressed concrete girders: comparison between AASHTO specifications and LRFD Code.” *PCI J.*, 41(3), 48-62.

Tawfiq, K. S. (1995). “Cracking and shear capacity of high strength concrete bridge girders.” *Rep. No. FL/DOT/RMC/612(1)-4269*, Florida DOT, Tallahassee, FL

Tawfiq, K. S. (1996). “Cracking and shear capacity of high strength concrete bridge girders under fatigue loading.” *Rep. No. FL-DOT RMC*, Florida DOT, Tallahassee, FL.

Notations

a = shear span

a/d = shear span-to-depth ratio

A_{ph} = area of harped strands

A_{ps} = area of prestressing steel

A_s = area of non-prestressing tension steel

A_v = area of vertical reinforcement crossing assumed crack plane

b_w = web width

C = force in compression zone

d = flexural depth of tension tie

d_h = depth of harped strands at crack interface

d_v = effective shear depth

f_1 = empirical factor taken as 130 ksi

f_2 = empirical factor taken as 28 ksi

$f'c$ = concrete compressive strength

f_{pe} = effective stress in prestressing steel

f_{ps} = average stress in prestressing steel coincident with V_u

f_{psb} = stress in prestressing strand coincident with bond-loss failure

f_{sb} = stress in vertical reinforcment conincident with bond-loss failure

f_{sv} = stress in vertical reinforcement (ksi)

f_y = specified yield strength of reinforcement bars

F_h = total force in harped strands

H = height of precast girder and deck

H_h = horizontal force in harped strand

k_{sv} = empirical factor taken as 26

L_{dh} = available embedment length of harped strand

L_{dt} = available embedment length of tension tie

L_t = required transfer length

T = longitudinal tie force in flexural reinforcement

V_a = force along crack interface

V_{exp} = experimental bond capacity

V_h = vertical force in harped strand

V_{nb} = nominal bond capacity

V_p = component of prestressing in direction of the shear force

V_s = resistance provided by the vertical reinforcement

V_{sb} = force in vertical reinforcment conincident with bond-loss failure

V_u = factored shear force

X_{brg} = bearing distance

X_{oh} = overhang distance

x_s = horizontal distance to vertical steel centroid

X_t = horizontal distance between front of bearing and intersection of crack and tie

β = inclination angle of harped strands

θ = angle of inclination of diagonal compressive stresses

ρ_{sv} = shear reinforcement ratio

ϕ_v = resistance factor for shear

Appendix A

Table 4. List of specimens (V_{nb} calculated from model in chapter 5).

Specimen number	Reference	Specimen ID	Vnb	Vexp	Vnb/Vexp
1	Ross et al. 2011a	G1	291.9	344.0	0.848
2		G2	211.9	255.0	0.831
3		G3	171.7	207.0	0.829
4		G4-2	147.5	198.0	0.745
5	Ross et al. 2011b	B5M-C	130.4	162.0	0.805
6		B5L-C	144.9	179.0	0.809
7		B6S-C	122.1	165.0	0.740
8		B6M-C	131.3	180.0	0.730
9		B6L-C	148.4	188.0	0.789
10	Maruyama and Rizkalla 1988	PS1-0	27.7	27.2	1.018
11		PS2-S6M	30.5	34.0	0.898
12		PS3-D2	33.9	35.1	0.965
13		PS4-M2	30.7	32.9	0.935
14		PS5-0	27.7	25.7	1.080
15		PS6-WD	29.9	31.3	0.955
16		PS7-WSH	30.4	30.2	1.007
17		PS8-WS	30.4	27.7	1.100
18		PS9-WDH	30.0	28.8	1.043
19	Kaufman and Ramirez 1988	I-3	63.4	100.0	0.634
20		I-4	56.4	110.0	0.513
21		II-1	89.3	140.0	0.638
22	Shahway and Batchelor 1996	A0-00-R-N	193.2	313.0	0.617
23		A1-00-M-N	123.7	141.0	0.877
24		A1-00-M-S	137.7	168.0	0.819
25		A1-00-R/2-N	141.7	166.0	0.853
26		A1-00-R/2-S	138.9	173.0	0.803
27		A1-00-R-N	177.6	210.0	0.846
28		A1-00-3R/2-N	213.5	207.0	1.031
29		B0-00-R-N	175.9	220.0	0.799
30		B0-00-2R-N	247.7	223.0	1.111
31		B0-00-3R-N	319.6	231.0	1.383
32		B1-00-0R-N	156.1	166.0	0.940
33		B1-00-0R-S	152.1	155.0	0.981
34		B1-00-R-N	223.2	245.0	0.911

35		B1-00-R-S	219.9	232.0	0.948
36		B1-00-2R-N	290.4	262.0	1.108
37		B1-00-2R-S	287.8	247.0	1.165
38		B1-00-3R-N	355.7	264.0	1.347
39		B1-00-3R-S	355.6	263.0	1.352
40		B1-00-2R2-N	289.1	268.0	1.079
41		B1-00-2R2-S	287.8	255.0	1.129
42	Deatherage et al. 1994	5-1-EXT	95.8	91.2	1.050
43		5-1-INT	97.9	107.0	0.915
44		5-2-EXT	111.0	104.0	1.067
45		5-2-INT	110.5	98.1	1.127
46		5-3-INT	112.2	115.0	0.976
47		5-4-INT	120.3	112.0	1.074
48		5-SWAI-WEST	98.0	125.0	0.784
49		5-UWR-EAST	101.9	115.0	0.886
50		5-UWR-WEST	102.8	134.0	0.767
51		5-FWC-EAST	95.3	117.0	0.815
52		5S-1-EXT	118.3	109.0	1.085
53		5S-1-INT	116.8	117.0	0.998
54		5S-2-INT	118.5	100.0	1.185
55		5S-3-EXT	103.8	103.0	1.008
56		5S-3-INT	104.4	103.0	1.014
57		5S-4-EXT	107.4	112.0	0.959
58		5S-4-INT	106.9	122.0	0.876
59		916-1-EXT	98.7	83.9	1.176
60		916-1-INT	101.0	105.0	0.962
61		916-2-EXT	104.5	90.0	1.162
62		916-2-INT	105.3	102.0	1.033
63		916-3-EXT	95.3	90.1	1.057
64		916-4-EXT	95.5	82.9	1.152
65		6-2-EXT	87.9	103.0	0.854
66		6-2-INT	88.7	116.0	0.765
67		6-3-EXT	112.7	110.0	1.024
68	Ross et al. 2013	WN	503.8	534.0	0.944
69		WB	503.8	639.0	0.788
70		SL	582.6	609.0	0.957
71	Hawkins and Kuchma 2007	G1E	453.0	572.0	0.792
72		G1W	631.5	662.0	0.954
73		G2E	680.0	743.0	0.915

74		G2W	892.5	852.0	1.048
75		G6W	548.0	612.0	0.895
76	Ma et al. 2000	AVW14608Y	285.0	460.0	0.620
77	Barnes et al. 1998	L0B-B-72	210.8	175.6	1.200
78		L0B-D-54	238.4	236.2	1.009
79		L0B-C-54H	270.5	240.8	1.123
80		M0B-D-54	352.3	305.1	1.155
81		M0B-C-54H	384.0	314.3	1.222
82		H0B-D-54	394.8	308.8	1.278
83		H0B-C-54H	426.4	311.9	1.367
84	Meyer et al. 2002	G1A-E	340.8	362.8	0.939
85		G1B-E	224.6	312.2	0.719
86		G1C-E	209.9	289.2	0.726
87	Kahn et al. 2002	G2BS	297.8	292.9	1.017
88		G4BS	363.3	328.9	1.105
89		G4AS	294.0	254.1	1.157
90	Raymond et al. 2005	BT6-Live End	423.7	592.0	0.716
91		BT6-Dead End	419.5	557.0	0.753
92		BT7-Live End	608.1	614.0	0.990
93		BT7-Dead End	505.9	605.0	0.836
94	Abdalla et al. 1993	2B	134.5	110.9	1.214
95		2D	88.8	98.3	0.903
96		3B	134.5	91.4	1.472
97		3D	71.8	67.4	1.065
98	Alshegeir and Ramirez 1992	II-1A	154.1	222.0	0.694
99		I-3A	97.8	113.5	0.861
100	Jongpitaksseel 2003	B4E2	353.9	387.7	0.913
101	Labonte and Hamilton 2005	SS2-SCCF2	195.4	222.9	0.876
102	Tawfiq 1996	F8N	184.8	180.0	1.026
103		F8S	195.0	222.0	0.878
104		F12N	222.9	216.0	1.032
105		F12S	233.0	275.0	0.847
106	Hartmann et al. 1988	3--1	65.5	63.2	1.036
107		3--2	65.5	65.2	1.004
108		3--3	39.3	41.0	0.958
109	Tawfiq 1995	R-8-North	198.1	277.0	0.715
110		R-8- South	208.3	302.0	0.690

111		2R-8-North	294.5	235.0	1.253
112		2R-8-South	304.4	256.0	1.189
113		R-10-South	232.3	299.0	0.777
114		2R-10-North	342.6	240.0	1.428
115		2R-10-South	352.5	245.0	1.439
116		R-12-North	246.3	279.0	0.883
117		R-12-South	256.4	276.0	0.929
118		2R-12-North	390.8	279.0	1.401
119		2R-12-South	400.5	287.0	1.396
120	Garber et al. 2016	Q-8	836.3	543.0	1.540

CHAPTER SIX

CONTRIBUTION OF STUDY

Bond-loss database

As a first contribution, a database of specimens failing in bond-loss was constructed. For purpose of this research, bond-loss failure is characterized by the formation of cracks in the end region due to applied loads. These cracks interrupt anchorage of strands, leading to loss of bond and slipping of strands relative to the concrete. Based on the available published data, all specimens in the database experienced bond-loss failure. At the first phase of data gathering, data were collected from 10 different test programs, having a total of 218 specimens. Of the 218 specimens, 84 failed in bond-loss failure and were added to the database. At the final phase of data collecting, 36 more specimens from eleven different test programs were added to the bond-loss failure database. In total, load tests of 327 different pretensioned girders were reviewed, of which bond-loss failure was reported as a primary failure in 120 specimens. This database provides an essential resource for developing and testing models for assessing bond-loss capacity.

Characterization of bond-loss failures

Through a review of 22 different test programs, fifteen different terminologies were identified to describe failures associated with bond loss. In many cases, researchers used different terms to describe same failure behavior. To provide clarity and

consistency in the language used to discuss this topic, the fifteen different labels were condensed into four primary behaviors, namely bond-shear, flexure-bond, bond-flexure and bond-shear/flexure. These failure types encompass all of the fifteen labels given in the referenced test programs. Additionally, a flowchart for categorizing bond-loss failures was presented. Decision points in the flowchart were based on a synthesis of the reviewed literature. The proposed flowchart will assist future researchers in characterizing and labeling bond-loss failures.

Model for bond-loss resistance

As a third contribution, a model for calculating bond-loss resistance of pretensioned concrete I-girders was proposed. The accuracy of the model was tested using the bond-loss database by comparing the nominal (from the proposed model) and experimental (from the database) bond-loss capacities. Note that, two models were created. The initial or original model was described in chapter 3 and was developed/evaluated by the 84 specimens collected during phase one of the data gathering. A refined model was described in chapter 5 and was developed/evaluated suing the 120 specimens from the expanded database. The refined model improves the original model by using the expanded database, and by using statistical linear regression analysis and the least squares method to identify best-fit equations with the experimental data.

Evaluation of the AASHTO LRFD strand debonding limitations

It is generally accepted that partial strand debonding has serviceability benefits because of reduced end region stresses and cracking. However, the drawback is that

debonding results in reduced horizontal tie force capacity at the support, and thereby reduces resistance to bond-loss failure. Therefore, the benefits of strand debonding must be balanced with the requirement to provide sufficient strength against bond-loss failure. Balancing these competing objectives was the essence of the final contribution of this proposal (**Fig. 1**).

To balance these competing objectives of serviceability and strength, AASHTO LRFD limits debonding to no more than 25% of the total number of strands. As a fourth contribution, the conservativeness of the 25% debonding limitation with respect to shear failures involving loss of strand-concrete bond was evaluated. This was accomplished by calculating the bond-loss capacity of six in-service bridge girders from different states and for varying levels of strand debonding. Capacities were compared to the factored shear force of girder in the in-service bridges. Calculations of bond-loss capacity were based on the original model described in chapter 3. It was also determined if the 25% debonding limitation produces a uniform degree of conservatism for all girders. Additionally, the possibility of debonding more than 25% while maintaining sufficient bond-loss capacity was investigated; and finally, a model that provides a means of directly calculating the number of fully bonded strands required for sufficient bond-loss resistance was proposed.

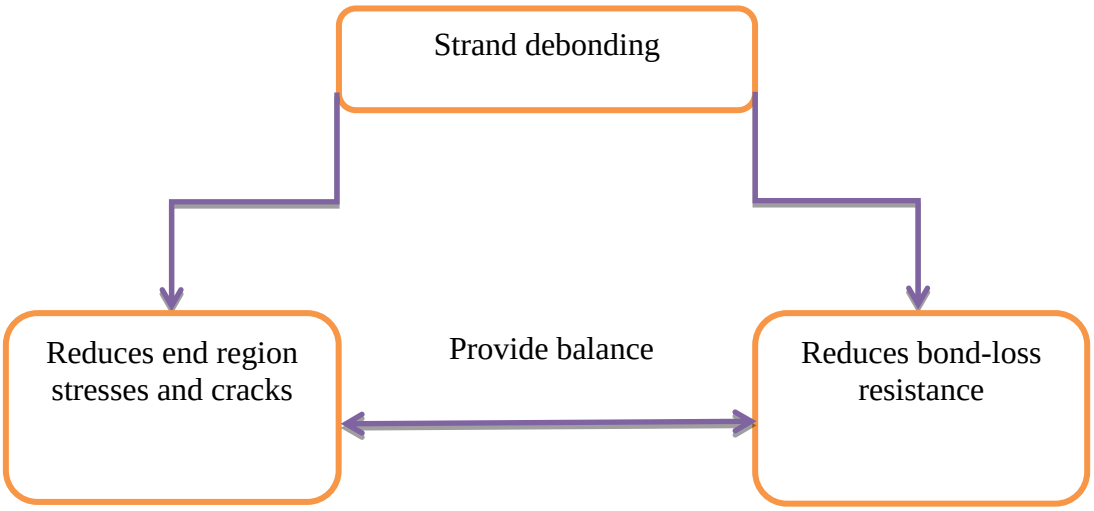

Figure 1. Strand debonding flowchart

In conclusion, this research helps engineers understand bond-loss behavior. This study also provided clarity and consistency in the language used to discuss failures associated with bond loss by proposing the bond-loss characterization flowchart. Additionally, this research proposed two models for calculating bond-loss resistance of pretensioned concrete I-girders. Proposed models will help designers/engineers determine bond-loss capacity of pretensioned concrete I-girders. This research also investigated the effect of debonding on bond-loss capacity, and provided a means of balancing strength (reduced horizontal tie force capacity) and serviceability (reduced end region stresses and cracking) by proposing a model that directly calculate the number of fully bonded strands required for sufficient bond-loss resistance. It is the intention that these contributions will lead to safe and serviceable girders.